ON NONLINEAR COUPLING EFFECTS IN IMPERFECT ELASTIC PLATES IN THE POSTBUCKLING RANGE

A THESIS

Presented to

The Faculty of the Division of Graduate

Studies and Research

by

Edward Michael Dombourian

In Partial Fulfillment
of the Requirements for the Degree
Doctor of Philosophy
in the School of Aerospace Engineering

Georgia Institute of Technology

June 1974

ERRATA

1) Page 9, Eq. (II-11b)

$\bar{v} = \mu y$ on $x = \pm b$ should read $\bar{v} = -\mu y$ on $\bar{x} = \pm b$

2) Page 24, line 8

x_{io} should read x_{ik}

3) Page 75, line 8

$D_4\left[\frac{h^2}{a^2 h^2} \frac{\partial^2 w}{\partial x^2} \frac{\partial^2 w}{\partial y^2}\right.$ should read $D_4\left[\frac{h^2}{a^2 b^2} \frac{\partial^2 w}{\partial x^2} \frac{\partial^2 w}{\partial y^2}\right.$

4) Page 102, line 4

the aspect as $r = \frac{a}{b}$ should read the aspect ratio as $r = \frac{a}{b}$

5) Page 105, Eq. (G-3)

$\nabla^4 w - \frac{1}{D}\left[N_x \frac{\partial^2 w}{\partial x^2} + \frac{\partial^2 w}{\partial y^2} + 2N_{xy} \frac{\partial^2 w}{\partial x \partial y}\right]$ should read

$$\nabla^4 w = \frac{1}{D}\left[N_x \frac{\partial^2 w}{\partial x^2} + N_y \frac{\partial^2 w}{\partial y^2} + 2N_{xy} \frac{\partial^2 w}{\partial x \partial y}\right]$$

6) Page 107, line 1

$\frac{\partial P_2}{\partial y} = \frac{2Q_2}{\partial x}$ 0) should read $\frac{\partial P_2}{\partial y} = \frac{\partial Q_2}{\partial x}$)

ON NONLINEAR COUPLING EFFECTS IN IMPERFECT

ELASTIC PLATES IN THE POSTBUCKLING RANGE

Approved:

Robert L. Carlson, Chairman

C. Virgil Smith, Jr.

G. Alvin Pierce

Date approved by Chairman: June 10, 1974

ACKNOWLEDGMENTS

I wish to express my deepest gratitude to Dr. Robert L. Carlson, an individual who is both my thesis advisor and a very inspiring teacher. It was through his skillful guidance, infinite patience and penetrating perception that this work reached its successful conclusion. I shall always feel indebted to him for all the knowledge and precious advice he has given me.

I would very much like to thank Dr. C. V. Smith, Jr. for his meticulous reading of the final manuscript, also for his availability to discuss and answer related questions. To Drs. G. Alvin Pierce, J. T. S. Wang and C.E.S. Ueng who served as the other members of the reading committee, I express my appreciation for their many suggestions.

I would also like to take this opportunity to thank my other professors at Georgia Tech, especially Drs. Edward R. Wood, G. Alvin Pierce and M. P. Stallybrass who helped me so generously.

To Mrs. Ruth Shaw, who patiently deciphered and typed page after page of "solid equations", I express my appreciation.

My wife, Loretta, proofread the entire manuscript and my daughter, Sona, in her own fashion contributed a lot, and I thank them both.

Finally, I am very grateful to my parents. Their love and devotion made this difficult task possible. With affection I dedicate this work to them.

TABLE OF CONTENTS

LIST OF FIGURES

Figure | Page

NOMENCLATURE

$\bar{A}$	a real matrix
a	one half the length of plate
a_i	coefficients associated with the in-plane displacement u
$\bar{B}$	a column matrix
b	one half the width of plate
b_i	coefficients associated with the in-plane displacement v
c_{ij}, c_{ijk}	coefficients used in the nonlinear equations
$c_{ijk\ell}$	coefficients used in the nonlinear equations
c_i	coefficients associated with the out-of-plane displacement w
D	flexural rigidity of the plate
d_i	coefficients associated with the initial out-of-plane imperfection
E	Young's modulus
$\bar{e}$, e_i	constants
F_i	a real function
f_i	a real function
G_i	function of x_5 and x_6
$\bar{g}$, g_i	constants
H_n	a critical load parameter
h	thickness of the plate

i	an integer
j	an integer
$\bar{k}_i$, k_i	constants
k	an integer
ℓ	an integer
M_x, M_y	bending moments
m	an integer
$\bar{N}_x^o$, N_x^o	in-plane normal stresses in the x direction
$\bar{N}_y^o$, N_y^o	in-plane normal stresses in the y direction
$\bar{N}_{xy}^o$, N_{xy}^o	in-plane shear stresses
$\bar{p}$, p_i	constants
p	an integer
q	an integer
r	aspect ratio of plate
U^o	strain energy due to in-plane forces
U_B	strain energy due to bending and twisting moments
$\bar{u}$, u	displacements in the x direction
u_1	out-of-plane displacement
u_2	out-of-plane displacement
$\bar{v}$, v, v^*	displacements in the y direction
$\bar{w}$, w	displacements in the z direction

w_o	initial imperfection
$\bar{X}$	column matrix of the unknowns
$\bar{x}$, x	coordinate axis
x_i	coefficients of the displacement functions
$\bar{y}$, y	coordinate axis
$\bar{z}$, z	vertical coordinate axis
α_{ik}	coefficients used in perturbation method
γ_i	coefficients
γ_{xy}	shear strain
δ_{ij}	Kronecker delta
ϵ	a perturbation parameter
$\bar{\epsilon}_x$, ϵ_x	normal strain quantities
$\bar{\epsilon}_y$, ϵ_y	normal strain quantities
η	a nondimentionalization parameter associated with $\bar{v}$
Λ_o	a point about which an expansion is made
Λ	prescribed end loading
λ	incremental loading
μ	strain in the direction of loading
ν	Poisson's ratio
Ξ	solution vector
ξ_i	elements of solution vector
Π	total potential energy

σ_x , σ_y	normal stresses
Φ	Airy-Stress function
ϕ_i	deflection functions associated with w
χ_i	deflection functions associated with u
Ψ_i	deflection functions associated with v
Ω	potential of external loads

SUMMARY

The objective of the investigation was to study the effect of imperfection on the coupling behavior of a compressed elastic plate which develops moderately large deflections. The procedure used was to form the associated total potential energy functional for this problem and to then use the Ritz method to obtain a system of nonlinear algebraic equations. A perturbation solution procedure was then used to solve the algebraic equations.

Results for different initial imperfection configurations and plate length to width ratios were used to examine changes in waveform of plates in the postbuckling range.

CHAPTER I

INTRODUCTION

Thin plates have been used as structural elements in the hulls of ships, the outer skins of airplane wings, and many other systems because of their many unique properties. They can, serve their intended purpose well even after buckling has occurred. Unlike some other structural members, the inevitable initial imperfections that are inherent with man-made products do not reduce the ability of the plate to carry continuously increasing loads. This is a quality which is technically referred to as imperfection-insensitivity.

The elastic stability of plates has been studied very thoroughly since about 1890. Early work was concerned with determinations of the buckling load of plates with various types of loads and boundary conditions. The behavior of plates for loads exceeding the buckling load — the so called postbuckling range — has only been examined in detail during the past forty years. Recently a number of researchers have made detailed studies of the nonlinear postbuckling problem. Notable among these investigators are Koiter [1,2,3], Stein [4,5], Hlavacek [6], Augusti [7], Chilver [8] and Supple [9,10,11,12].

Koiter [1,2] was one of the earliest investigators who formulated a general theory of the stability of nonlinear structural systems. However, his work remained dormant for some time because it was originally written in Dutch and was published during the Second World War.

Stein [4] sought to explain the phenomenon of changes in the buckle pattern by choosing as his model a symmetric, three-element column restrained by nonlinear springs. The springs simulate the nonlinear characteristics of plates in the postbuckling range. He then studied the stability of this system for both the controlled-loading and controlled-end shortening types of load application. He concluded that for initially perfect specimens, intersections between curves for various equilibrium configurations lead to changes in buckle patterns, and that the load at which a change in buckle pattern occurs is independent of the type of loading, i.e., rigid or soft systems.

Augusti [7] and Hlavacek [6] made postbuckling behavior studies of various structural systems and their work was published only a decade ago.

Chilver [8] later studied a model with two degrees of freedom and concluded that when eigenvalues corresponding to two modes of buckling are equal, or nearly so, elastic postbuckling of the system can involve coupling between the modes. Supple's studies [11,12] were based on the assumption that the behavior of a plate can be approximated as a two-degree-of-freedom system. He categorized structural systems according to the type of coupled and uncoupled postbuckling modal behavior which could be developed. He also included the effect of imperfection in his work.

In one of his papers Supple [12] analyzed a rectangular plate with constant in-plane compressive forces at the opposite ends. He used von Karman's large deflection equations involving the out-of-plane deflection function of position $w(x,y)$, and initial imperfection

$w_o(x,y)$ and a stress function $\Phi(x,y)$. Using two-degrees-of-freedom for w, he developed an approximate solution of these equations through a Galerkin solution procedure. He obtained two nonlinear algebraic equations, and these, he solved by an elimination technique.

In the present work a rectangular plate is loaded with a prescribed end displacement, and the unknowns are taken as the three displacement functions $u(x,y)$, $v(x,y)$, $w(x,y)$ (the imperfection function $w_o(x,y)$ being prescribed). An approximate solution is then initiated by the selection of six displacement functions (two each for u, v, w) which satisfy all the prescribed boundary conditions. These functions, which provide six degrees of freedom, are used as a basis for a direct variational solution; i.e., the total potential energy functional is minimized, as in the Ritz procedure, and a system of nonlinear algebraic equations is obtained. A perturbation method is then developed and used to obtain solutions for various imperfections and aspect ratios; i.e., the length to width ratios of plate.

A comparison of methods indicates that in Supple's procedure, the stress function, $\Phi(x,y)$, must be computed after the solution for $w(x,y)$. In the present work the solution for u, v and w are obtained simultaneously. Further, the algebraic procedure of Supple would become difficult to use if the number of degrees of freedom or approximation functions were increased. The difficulty of the perturbation procedure developed here, on the other hand, would not computationally increase appreciably.

Finally, in using von Karman equations in Supple's approach to obtain stresses, $\Phi(x,y)$ must be differentiated twice. They may introduce some problems with accuracy. In the present formulation the stress and strain quantities are computed by differentiating the displacement functions once.

The objective of this thesis was to develop the solution technique outlined above and to use it to investigate postbuckling behavior in plates. Particular emphasis is placed on an investigation of the behavior patterns developed for various combinations of initial imperfection and plate aspect ratios.

CHAPTER II

FORMULATION OF THE PROBLEM

The problem of buckling and postbuckling of a plate may be formulated in terms of the middle surface displacement functions. In Cartesian coordinates these may be represented as u, v and w for displacements in the x, y and z directions, respectively. Each displacement function depends on the independent variables x and y. One method of determining u, v and w is to develop a solution procedure which makes use of a functional whose extremum yields the governing differential equations of the problem. The appropriate functional for the given problem can be identified as the total potential energy which will be designated as Π in this thesis.

Π is composed of two parts. One part is the internal potential or the strain energy, U, of the plate, and it is developed by the in-plane membrane stresses, the internal bending moments, and the twisting moments.

The second part of the functional Π is the external potential, Ω, which is associated with the applied edge tractions or the so called prescribed edge loadings. The two potential functions are related to Π through the expression $\pi = U + \Omega$. However, in the present work edge displacements rather than edge tractions are specified so the external potential $\Omega = 0$.

The component of U due to the middle surface stretching may be expressed in terms of the membrane stresses $\bar{N}_x^o$, $\bar{N}_y^o$ and $\bar{N}_{xy}^o$, and the middle surface strain components $\bar{\epsilon}_x^o$, $\bar{\epsilon}_y^o$ and $\bar{\gamma}_{xy}^o$. These in turn may be defined through the strain displacement relations given in Vol'mir [13] as

$$\bar{\epsilon}_x^o = \frac{\partial \bar{u}}{\partial \bar{x}} + \frac{1}{2}\left[\frac{\partial}{\partial \bar{x}}\left(\bar{w}_o + \bar{w}\right)\right]^2 - \frac{1}{2}\left(\frac{\partial \bar{w}_o}{\partial \bar{x}}\right)^2 \tag{II-1}$$

$$\bar{\epsilon}_y^o = \frac{\partial \bar{v}}{\partial \bar{y}} + \frac{1}{2}\left[\frac{\partial}{\partial \bar{y}}\left(\bar{w}_o + \bar{w}\right)\right]^2 - \frac{1}{2}\left(\frac{\partial \bar{w}_o}{\partial \bar{y}}\right)^2 \tag{II-2}$$

$$\bar{\gamma}_{xy}^o = \frac{\partial \bar{u}}{\partial \bar{y}} + \frac{\partial \bar{v}}{\partial \bar{x}} + \frac{\partial}{\partial \bar{x}}\left(\bar{w}_o + \bar{w}\right) . \frac{\partial}{\partial \bar{y}}\left(\bar{w}_o + \bar{w}\right) \tag{II-3}$$

$$- \frac{\partial \bar{w}_o}{\partial \bar{x}} . \frac{\partial \bar{w}_o}{\partial \bar{y}}$$

where the function $\bar{w}_o$ is the initial out-of-plane imperfection and $\bar{w}$ is the additional elastic deflection as seen in Figure II-1.

The membrane strain energy developed in the linearly elastic isotropic, homogeneous plate according to [14] may be written as

$$U^o = \frac{1}{2} \int_{-\frac{b}{2}}^{+\frac{b}{2}} \int_{-\frac{a}{2}}^{+\frac{a}{2}} \left(\bar{N}_x^o \, \bar{\epsilon}_x^o + \bar{N}_y^o \, \bar{\epsilon}_y^o + \bar{N}_{xy}^o \, \bar{\gamma}_{xy}^o\right) d\bar{x} d\bar{y} \tag{II-4}$$

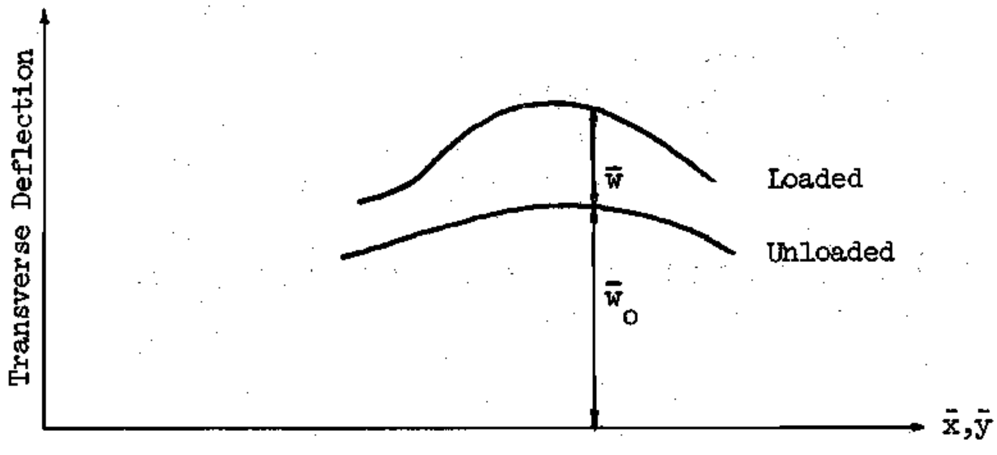

Figure II-1. Deflected Configuration

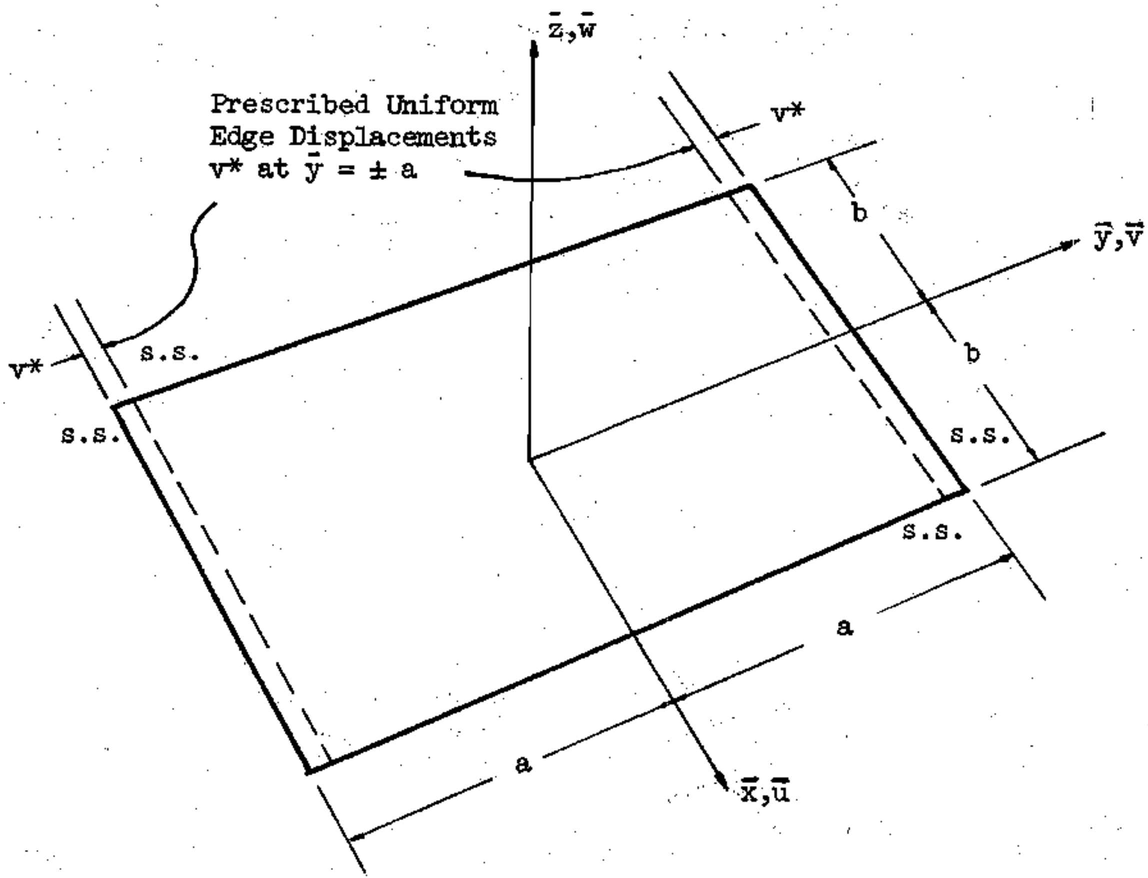

Figure II-2. The Rectangular Plate

where

$$\bar{N}_x^o = \frac{Eh}{1-\nu^2}\left(\bar{\epsilon}_x^o + \nu\bar{\epsilon}_y^o\right) \tag{II-5}$$

$$\bar{N}_y^o = \frac{Eh}{1-\nu^2}\left(\bar{\epsilon}_y^o + \nu\bar{\epsilon}_x^o\right) \tag{II-6}$$

$$\bar{N}_{xy}^o = \frac{Eh}{2(1+\nu)}\bar{\gamma}_{xy}^o \tag{II-7}$$

The strain energy due to bending and twisting of the plate in Figure II-2 is, according to [14]

$$U_B = \frac{D}{2}\int_{-\frac{b}{2}}^{+\frac{b}{2}}\int_{-\frac{a}{2}}^{+\frac{a}{2}}\left\{\left(\frac{\partial^2\bar{w}}{\partial\bar{x}^2} + \frac{\partial^2\bar{w}}{\partial\bar{y}^2}\right)^2 \right. \tag{II-8}$$

$$\left. - 2(1-\nu)\left[\frac{\partial^2\bar{w}}{\partial\bar{x}^2}\frac{\partial^2\bar{w}}{\partial\bar{y}^2} - \left(\frac{\partial^2\bar{w}}{\partial\bar{x}\partial\bar{y}}\right)^2\right]\right\}d\bar{x}d\bar{y}$$

where

$$D = \frac{Eh^3}{12(1-\nu^2)} \tag{II-9}$$

The total potential energy is then

$$\Pi = U^o + U_B \tag{II-10}$$

The equation for Π must, of course, be expressed in terms of u, v and w. This is accomplished by use of Hooke's law and the strain displacement relations in Equation (II-4). (See Appendix A for the form of Π.)

The first variation of the total potential energy functional Π gives the static equilibrium equations of an imperfect plate subject to the in-plane edge displacements for moderately large transverse deflections. The problem selected for analysis here is shown in the Figure II-2. The boundary conditions are as follows: The plate is simply supported on all edges so that

$$\bar{w} = 0 \;, \quad M_x = D\left(\frac{\partial^2 \bar{w}}{\partial \bar{x}^2} + \nu \frac{\partial^2 \bar{w}}{\partial \bar{y}^2}\right) = 0 \quad \text{at} \quad \bar{x} = \pm b$$

$$\bar{w} = 0 \;, \quad M_y = D\left(\frac{\partial^2 \bar{w}}{\partial \bar{y}^2} + \nu \frac{\partial^2 \bar{w}}{\partial \bar{x}^2}\right) = 0 \quad \text{at} \quad \bar{y} = \pm a \qquad \text{(II-11a)}$$

In addition

$$\bar{v} = -\,\mu a \quad \text{on} \quad \bar{y} = +\,a$$

$$\bar{v} = +\,\mu a \quad \text{on} \quad \bar{y} = -\,a$$

$$\bar{u} = 0 \quad \text{on} \quad \bar{y} = \pm\, a \qquad \text{(II-11b)}$$

$$\bar{v} = \mu y \quad \text{on} \quad \bar{x} = \pm\, b$$

$$\bar{u} = 0 \quad \text{on} \quad \bar{x} = \pm\, b$$

Note that $\bar{u} = 0$ on $\bar{y} = \pm a$ is not the only possible condition. $\bar{N}^{o}_{xy} = 0$ at $\bar{y} = \pm a$ is another possibility. As seen from the relation

$\bar{N}^{o}_{xy} = \frac{Eh}{2(1+\nu)} \bar{\gamma}^{o}_{xy}$ evaluated at $\bar{y} = \pm a$

$$\bar{N}^{o}_{xy}\Big|_{\bar{y} = \pm a} = \frac{Eh}{2(1+\nu)} \left[\frac{\partial\bar{u}}{\partial\bar{y}} + \frac{\partial\bar{v}}{\partial\bar{x}} + \frac{\partial}{\partial\bar{x}}\left(\bar{w}_o + \bar{w}\right)\frac{\partial}{\partial\bar{y}}\left(\bar{w}_o + \bar{w}\right) - \frac{\partial\bar{w}_o}{\partial\bar{x}}\frac{\partial\bar{w}_o}{\partial\bar{y}}\right]\Big|_{\bar{y} = \pm a} = 0$$

where

$$\frac{\partial\bar{v}}{\partial\bar{x}} = \frac{\partial\bar{w}_o}{\partial\bar{x}} = \frac{\partial\bar{w}}{\partial\bar{x}} = 0 \quad \text{at} \quad \bar{y} = \pm a$$

Note that

$$\frac{\partial\bar{u}}{\partial\bar{y}}\Big|_{\bar{y} = \pm a} = 0$$

would be a consequence of $\bar{N}^{o}_{xy} = 0$.

This alternative set of conditions could be expected to provide results different from those presented in this investigation.

For convenience the variables in the problem have been non-dimensionalized in accordance with the following definitions:

$$x = \frac{\bar{x}}{b}, \quad y = \frac{\bar{y}}{a}, \quad w = \frac{\bar{w}}{h}, \quad u = \frac{\bar{u}}{\eta}, \quad v = \frac{\bar{v}}{\eta}$$

where η was later decided to equal "a" for convenience.

If the plate has a prescribed initial imperfection, which is symmetric with respect to the $\bar{x}$ and the $\bar{y}$ axis, then at the early stages of the application of a loading symmetric with respect to the $\bar{x}$ and the $\bar{y}$ axis, the plate would be expected to deflect in such a way as to preserve the general shape of the initial imperfection. This is illustrated in Figure II-3.

However, if the plate has a prescribed initial imperfection, which is symmetric with respect to the $\bar{y}$ axis and antisymmetric with respect to the $\bar{x}$ axis as seen in Figure II-4, then upon the application of symmetric loading, it would begin to deflect in the same shape as the initial imperfection with increasing amplitude.

When the plate deflects, two symmetrically equidistant points from the $\bar{y}$ axis will initially move in opposite directions parallel to the $\bar{x}$ axis. Therefore, u must be an odd function of x and an even function of y so as to be compatible with the deformation of the symmetric structure under the symmetric loading. However, u is also allowed to possess a second component which is odd in y to account for the possible deformation of the structure of Figure II-4.

Likewise, two equidistant points from the $\bar{x}$ axis will move in opposite directions parallel to the $\bar{y}$ axis upon the application of symmetric loading on the structure. Thus, the v displacement is chosen such that it is odd in y and even in x.

Finally, the functions representing the transverse displacements $\bar{w}$ are chosen to represent the deflection configurations as depicted in Figures II-3 and II-4.

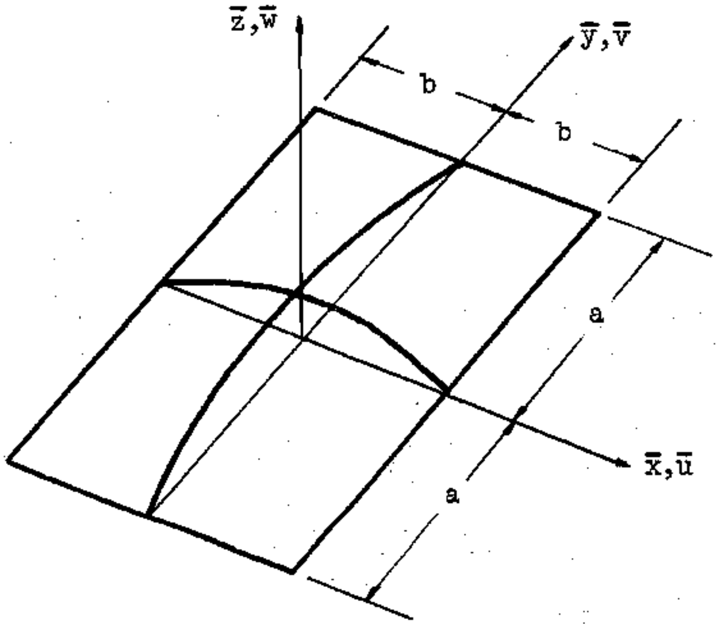

Figure II-3. A Symmetric Mode

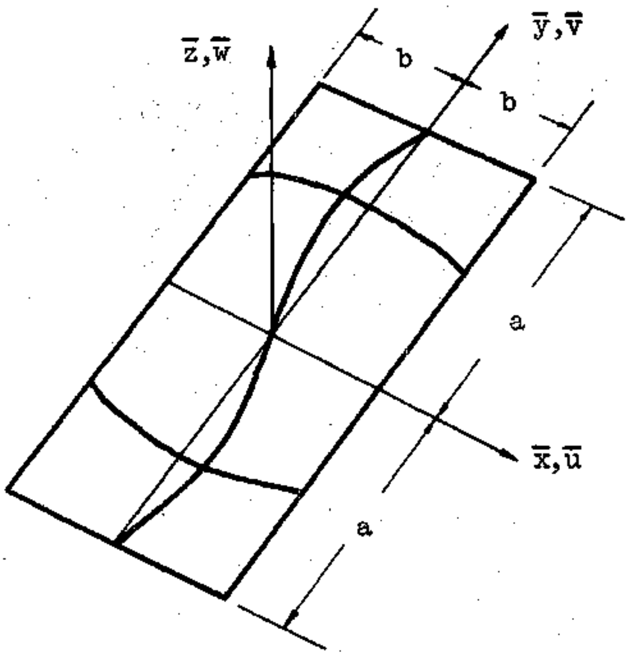

Figure II-4. An Antisymmetric Mode

For direct variational solution procedure functions, u, v and w can now be chosen as follows.

$$u(x,y) = \sum_i a_i \chi_i(x,y) \tag{II-12}$$

$$= a_1 \sin \pi x \cos \frac{\pi y}{2} + a_2 \sin \pi x \sin \pi y$$

$$v(x,y) = \sum_i b_i \psi_i(x,y) - \mu y \tag{II-13}$$

$$= b_1 \cos \frac{\pi x}{2} \sin \pi y + b_2 \cos \frac{\pi x}{2} \sin 2 \pi y - \mu y$$

$$w(x,y) = \sum_i c_i \phi_i (x,y) \tag{II-14}$$

$$= c_1 \cos \frac{\pi x}{2} \cos \frac{\pi y}{2} + c_2 \cos \frac{\pi x}{2} \sin \pi y$$

$$w_o(x,y) = \sum_i d_i \phi_i (x,y) \tag{II-15}$$

$$= d_1 \cos \frac{\pi x}{2} \cos \frac{\pi y}{2} + d_2 \cos \frac{\pi x}{2} \sin \pi y$$

In Equation (II-13), $\mu = \frac{v^*}{a}$ is the constant compressive strain in the y direction, and a_i, b_i and c_i are nondimensionalized.

An approximate solution may now be developed by use of the Ritz procedure. This is accomplished by rendering the functional Π stationary with respect to the coefficients of the expressions for u, v and w (see Appendix B). This operation produces a system of nonlinear algebraic equations in the coefficients a_1, a_2, b_1, b_2, c_1 and c_2. It may be noted here that the latter are redefined in terms of the quantities x_1, x_2, x_3, x_4, x_5 and x_6 respectively, for convenience in the computer programming (see results in Appendix C).

CHAPTER III

NUMERICAL METHODS OF SOLUTION

Introduction

There is a wide variety of problems in mechanics for which elementary methods of solution are not applicable. Difficulties arise, for example, for problems in which the governing equations are nonlinear in nature, or the variables are intertwined such that a coupled or an implicit form of representation is encountered.

Recently, some numerical techniques that were suggested several decades ago have been applied with a certain measure of success due to great advances made in the high speed computers. An example involves the use of iterative schemes of solution wherein an attempt is made to develop a scheme in which trial solutions are systematically improved in successive application. Naturally, some assurance that the end result is converging to the correct solution is required.

Iterative schemes have been used to develop solutions to systems of nonlinear algebraic equations, so it was logical to consider an application in the studies described here. The results of an evaluation of this method are presented in the section which follows.

An alternative method for developing solutions to nonlinear equations of the type encountered here can be based on the use of perturbation techniques. An application of this method yields a system of linear simultaneous equations whose solution may be obtained by elementary methods. The development of a perturbation method for the problem of interest in this dissertation is described in this chapter.

Let the system of nonlinear Equations (C-1) to (C-6) of Appendix C be represented by

$$\begin{aligned} f_1(x_1, x_2, ----, x_6) &= 0 \\ f_2(x_1, ------, x_6) &= 0 \\ f_3(x_1, ------, x_6) &= 0 \\ f_4(x_1, ------, x_6) &= 0 \\ f_5(x_1, ------, x_6) &= 0 \\ f_6(x_1, ------, x_6) &= 0 \end{aligned} \qquad \text{(III-1)}$$

involving six real functions of the six real variables x_1, x_2, x_3, x_4, x_5, x_6. Using the notation

$$X = \left[x_1, x_2, ---, x_6\right]^T \qquad \text{(III-2)}$$

let us write

$$f_i(X) = f_i(x_1, x_2, ---, x_6), \qquad i = 1, 2, \dots 6 \qquad \text{(III-3)}$$

Now let

$$\Xi = \left[\xi_1, \xi_2, --- \xi_6\right]^T \tag{III-4}$$

be a solution of (III-1); that is

$$f_i(\Xi) = 0 \tag{III-5}$$

Now rearrange the original system (III-1) such that

$$x_i = F_i(X) \tag{III-6}$$

implies

$$f_j(X) = 0, \quad j = 1, 2, \ldots , 6 \tag{III-7}$$

In particular, let

$$\xi_i = F_i(\Xi).$$

Starting with the vector

$$X_o = \left[x_{10}, x_{20}, x_{30}, --- x_{60}\right]^T \tag{III-8}$$

as a first approximation to Ξ, and substituting it into $F_1(X)$, we find a new x_{11} from (III-6) which leads to the new vector $\left[x_{11}, x_{20}, x_{30}, x_{40}, x_{60}\right]^T$. Substituting this new vector into $F_2(X)$

we get the vector

$$\left[x_{11},\ x_{21},\ x_{30},\ \ldots,\ x_{60}\right]^T.$$

This procedure may be continued until

$$X_{01} = \left[x_{11},\ x_{21},\ x_{31},\ x_{41},\ x_{51},\ x_{61}\right]^T$$

is obtained. That is, the most recently computed elements of the solution vector are always used in evaluating the F_i.

A sufficient condition for convergence [15] is that, if there exists a region R described by

$$|x_j - \xi_j| \leq \gamma \ ,$$

and for X in R, there is a positive number $\zeta < 1$, such that

$$\sum_{j=1}^{6} \left| \frac{\partial F_i(X)}{\partial x_j} \right| \leq \zeta < 1 \quad , \qquad \text{(III-9)}$$

then, if the starting vector X_o lies in R, this method converges to the solution of the system (III-1); that is

$$\lim_{k \to \infty} X_k = \Xi \qquad \text{(III-10)}$$

The particular system of Equations (III-1) is such that some of the coefficients of the independent variables are functions of the strain factor μ and, as μ changes, the entire system (III-1) changes.

To investigate the use of this solution procedure, it was applied to a nonlinear plate problem for which the exact solution [16] could be obtained. The problem consisted of a plate with

$$
\begin{aligned}
a &= 2.92'' \\
b &= 2.92'' \\
h &= 0.112'' \\
d_1 &= 0.01 \\
d_2 &= 0.0 \\
E &= .44 \times 10^6 \text{ psi (Plexiglas)}
\end{aligned}
$$

Initially the program was started with $\mu_o = 0.0004$ and $X_o = \left[0.0, 0.0, 0.0, 0.0, 0.008, 0.0\right]^T$. Iterations were run for k varying from 1 to 40 until a final value of X_{040} was obtained such that $\left|X_{040} - X_{039}\right| < 1 \times 10^{-5}$. This degree of accuracy was very satisfactory for a range of X values encountered. Next a new value of $\mu_1 = u_o +$ 0.000005 was assumed along with X_{040} as the new starting point and 40 new iterations were run and the process continued.

The method outlined was successful over the range of μ values less than μ_{cr}. However, as the nonlinearities due to large deflection theory began to be more pronounced, the computer results started to deviate from the true path and continued to give values of X that resembled the solution one would obtain by using small deflection theory as seen in Figure III-1. At this stage the increments in μ were reduced from 0.000005 to 0.000001. This produced improved values of X and results adhered to the exact solution over a slightly larger interval. It then flattened out and diverged again. It was obvious that some of the partials in Equation (III-9) were becoming so large that the convergence criterion was not met and so the values of X diverged rapidly.

Another attempt to remedy this difficulty was to redefine the nondimensional variables so that the absolute values of the first partials of $F_i(X)$ with respect to x_j were reduced to meet the requirement that

$$\sum_{j=1}^{6} \left| \frac{\partial F_i(X)}{\partial x_i} \right| \leq \zeta \leq 1.$$

This was not successful; i.e., the curve never rose above the μ_{cr} boundary. Because of these results, the iterative scheme was abandoned and a perturbation technique which is described in the next section was developed.

A Perturbation Procedure

In the perturbation method the independent variables x_1, x_2, x_3, x_4, x_5 and x_6 are expressed as power series of a quantity ϵ, called

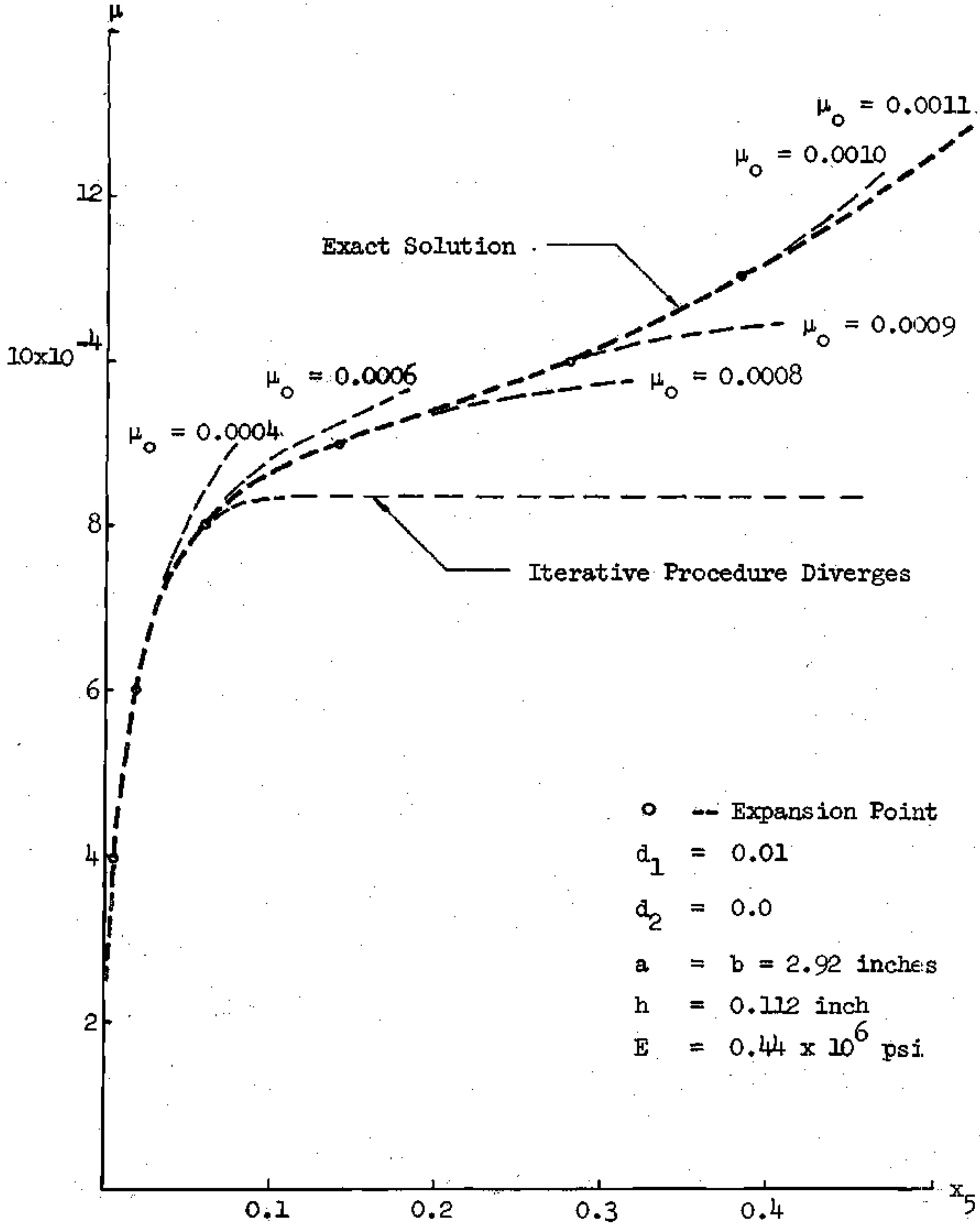

Figure III-1. Strain Versus Transverse Deflection the perturbation parameter; that is,

$$x_i = x_{io} + \epsilon x_{i1} + \epsilon^2 x_{i2} + \ldots \epsilon^5 x_{i5} \qquad \text{(III-11)}$$

or

$$x_i = \sum_{k=o}^{5} \epsilon^k x_{ik}$$

where the perturbation parameter is chosen to be $\epsilon = \mu - \mu_o$ (The μ_o is a point around which a Taylor series expansion is made. Note that the series is truncated after six terms.)

It is important to observe that for the indicated expansions to be valid, all derivatives of the functions x_i with respect to μ must be bounded. By way of analogy, the function $f(x) = x^{\frac{1}{2}}$ cannot, for example, be expanded in powers of x about $x = 0$. For most of the studies described herein on imperfect plates, this requirement was satisfied. In cases where it was not satisfied, an alternative solution procedure was used. This issue is discussed in greater detail in Chapter IV.

The system of nonlinear equations is then rewritten in terms of the sum above. Next the values of x_{ik} are determined by collecting the like powers of ϵ's in the following manner

$$\alpha_{jo}\epsilon^o + \alpha_{j1}\epsilon + \alpha_{j2}\epsilon^2 + \alpha_{j3}\epsilon^3 + \ldots \alpha_{j5}\epsilon^5 = 0, \quad j = 1,\ldots,6 \qquad \text{(III-12)}$$

where the α_{jk}'s are functions of x_{ik}'s. Since ϵ, ϵ^2, ϵ^3 etc. are linearly independent, it follows that

$$\alpha_{jo} = \alpha_{j1} = \alpha_{j2} = \alpha_{j3} = \ldots = \alpha_{j5} = 0 \qquad \text{(III-13)}$$

This requirement yields a set of linear inhomogeneous equations in x_{ik} which can be solved by known "linear algebra" techniques.

In the indicated manner each of the six nonlinear equations is successfully reduced to a system of equations as shown in Appendix D. Writing these in matrix form, we first start by using $\mu_o = 0.0$, and

$$X_o = \left[x_{10}, x_{20}, x_{30}, x_{40}, x_{50}, x_{60}\right]^T = \left[0, 0, 0, 0, 0, 0\right]^T$$

and solve

$$\bar{A}\bar{X}_{i1} = \bar{B}_{i1} \qquad \text{(III-14)}$$

for $\bar{X}_{i1}$, where the real matrix $\bar{A}$ is given in Appendix D. This provides the solution for

$$\bar{X}_{i1} = \left[x_{11}, x_{21}, x_{31}, x_{41}, x_{51}, x_{61}\right]^T .$$

These values, in turn, can be used to express $\bar{B}_{i2}$ in terms of known quantities in the equation.

$$\bar{A}\bar{X}_{i2} = \bar{B}_{i2} \qquad \text{(III-15)}$$

and the values of $\bar{X}_{i2}$ determined. This procedure is continued until all $\bar{X}_{ik}$ are calculated.

The procedure outlined provides a description of the variable x_i in terms of the end-shortening variable μ. Although the resulting expressions could, in theory, be used to describe the entire range of the behavior of interest, it early became clear that this would require a very large number of terms in the sum of Equation (III-11). To avoid this, the solution about $\mu_o = 0$ was used to obtain a continued solution about a small value of $\mu_o > 0$. In Equation (III-11) the values of x_{io} correspond to the values obtained from the solution about $\mu_o = 0$ evaluated at $\mu_o > 0$. The process described above was then repeated to generate a solution about the new value of μ_o.

By the method of solution used, the functions x_i were developed in the segment fashion indicated. The size of the segments will be noted for each of the solutions obtained. Note that within each segment, a sum of six terms was used.

To check the perturbation procedure, the problem cited earlier (see Figure III-1) was analyzed by use of the perturbation method. Results for solutions expanded about six values of μ_o (six segments) are presented in Figure III-1.

The functions were first expanded about $\mu_o = 0.0$ and the first portion of the curve was observed to coincide with the true curve for all values of $\mu_o < 0.0005$. To provide an accurate continuation the function was expanded about $\mu_o = 0.0004$ for the second segment. The computer was then allowed to calculate until $\mu_o = 0.0006$ was reached. A new expansion of the function was developed and a new segment of the curve was obtained until $\mu_o = 0.0008$. This expansion procedure was then repeated three more times. In Figure III-1, therefore, we see six segments of a curve that coincide with the true curve.

The final program was written such that μ_o increments were reduced to 0.000005 so as to obtain unquestionably precise values of X for our final plots. Note this is substantially smaller than the increments used for the results presented in Figure III-1.

In Figure III-2 a comparison is made between a six term expansion and a four term expansion of x_i (refer to Equation III-11). The increments in μ were the same. Obviously, even using a relatively small scale one can detect a diviation of the four term expansion from the six term expansion. The six term approximation with increments of size 0.000005 was therefore used in all of the subsequent calculations.

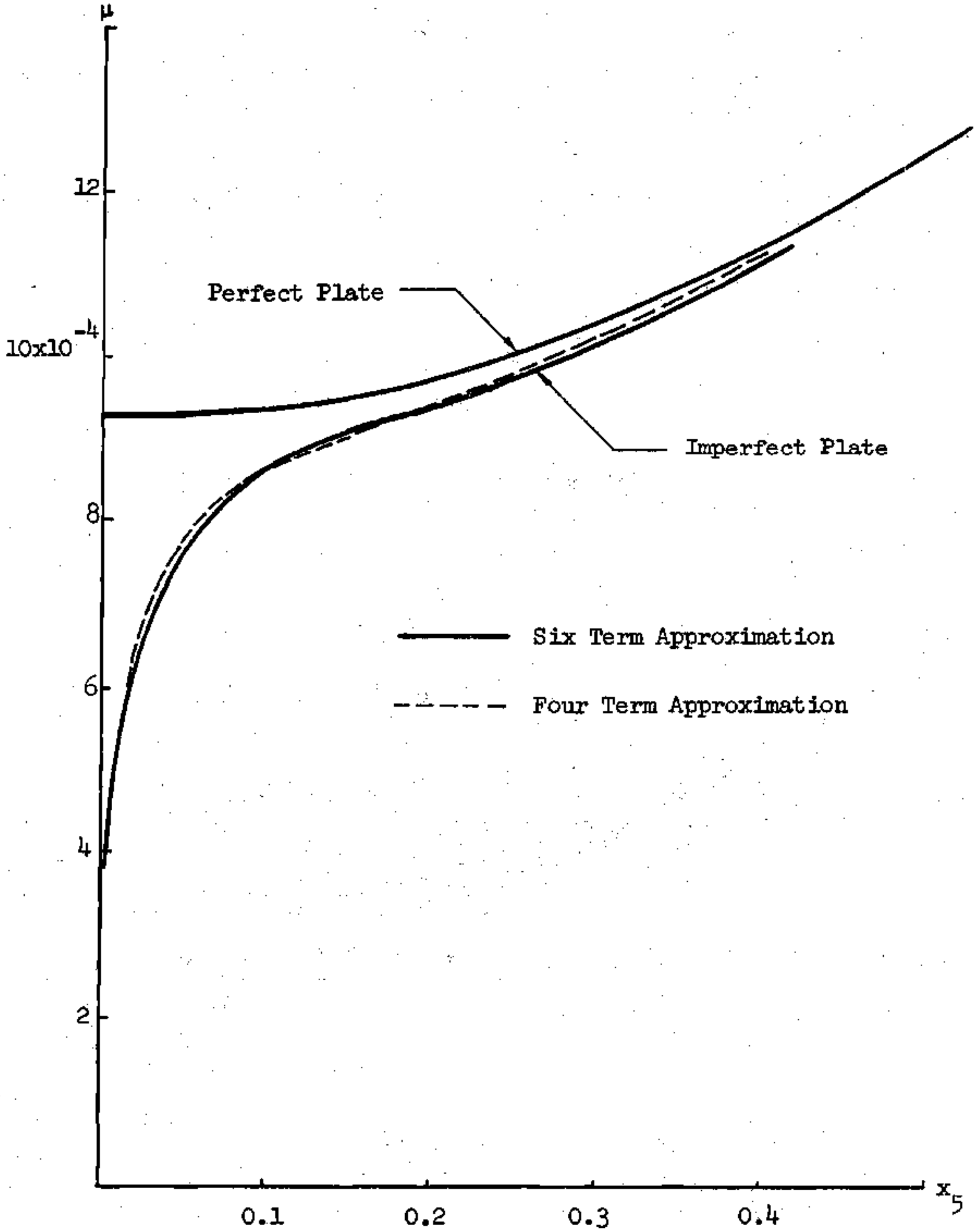

Figure III-2. Strain Versus Transverse Deflection

CHAPTER IV

DISCUSSION OF RESULTS

Introduction

Buckling Analysis

The buckling load, or the critical end shortening strain μ_{cr} of a hinged flat rectangular plate may be determined by performing a linear stability analysis. The results of this analysis may be summarized by plots of $k(r)$ versus the aspect ratio r as used in the equation $\mu_{cr} = \pi^2 h^2 k(r)/48b^2$. (For the derivation of $k(r)$ see Appendix F.)

In Figure IV-1, $m = 1$ corresponds to a deflection mode with a one half-sine wave in the y direction and one half-sine wave in the x direction of Figure II-2. In the present work this mode is identified as the variable x_5. Likewise $m = 2$ corresponds to a deflection mode with a two half-sine wave in the y direction and a one half-sine wave in the x direction. In the present work this mode is identified as the variable x_6. A plate with an aspect ratio $r = r_1$ will buckle in a half-sine wave configuration ($m = 1$) because the associated curve provides the smallest value of $k(r)$. The strain at which this buckling will occur will be $\mu_1 = \pi^2 h^2 k(r_1)/48b^2$. On the other hand, if $r = r_2$, it would appear that the plate may buckle in the y direction in either a half-sine wave, two half-sine waves, or some coupled combination under the critical load.

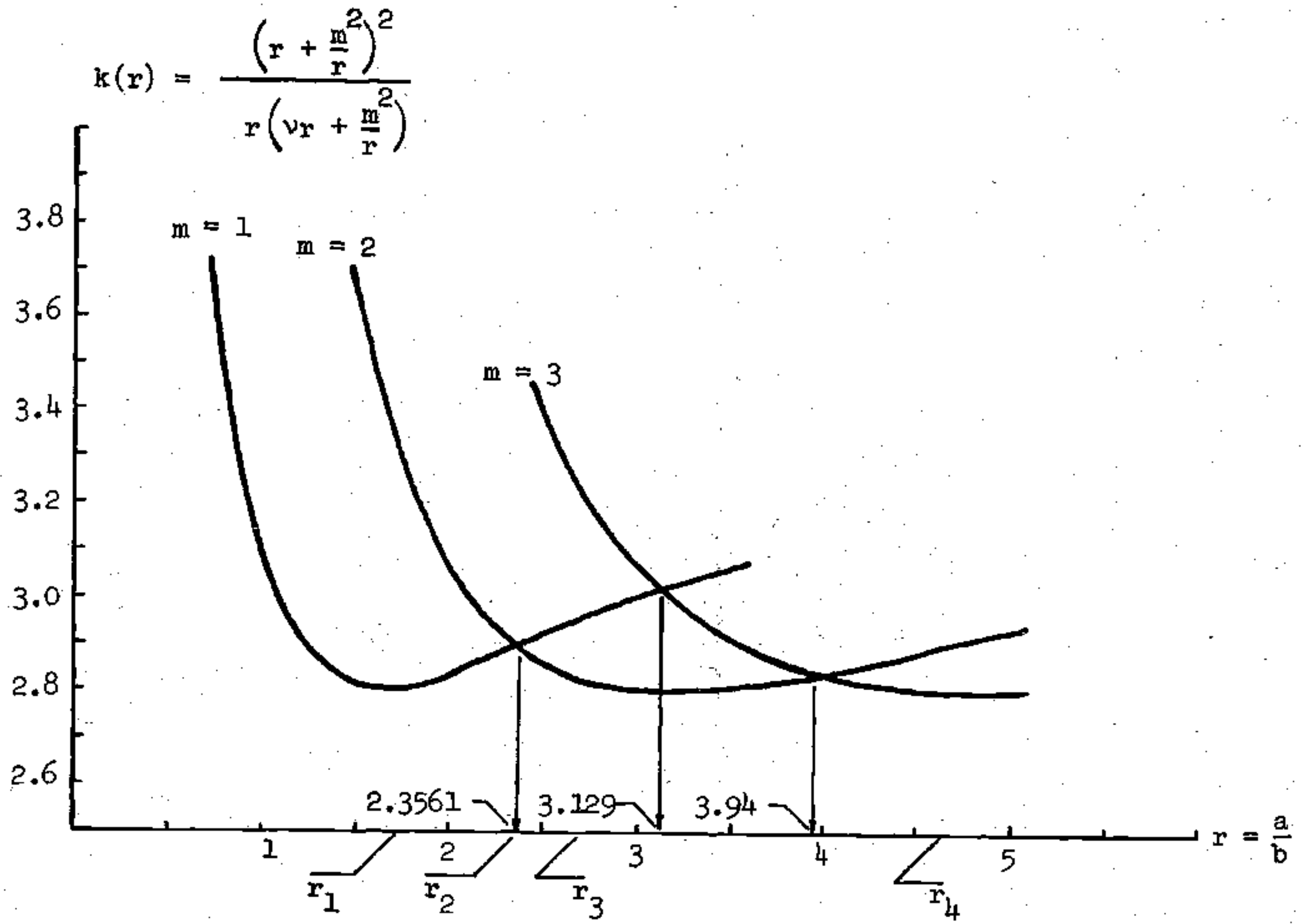

Figure IV-1. Buckling Parameter Versus Aspect Ratio

If the given plate has an aspect ratio $r = r_3$, then it will buckle in a two half-sine wave configuration, because the curve corresponding to r_3 has $m = 2$.

Summarizing, the linearized plate behavior may be deduced by reference to the portion of curve which is appropriate for the given aspect ratio r. These results are valid only if the plate is perfectly flat and only the value of μ_{cr} is obtained; i.e., the value of strain at which a bifurcation from the flat form becomes possible.

Postbuckling Analysis

Supple [11] first considered perfect systems whose deformation may be completely described by two generalized coordinates u_1 and u_2 and whose fundamental equilibrium path is coincident with the load axis, i.e., $u_1 = 0$ and $u_2 = 0$. This means there will be no nonzero u_1 and u_2 values until departures from the fundamental state occur at points of bifurcation (See Figures IV-2 and IV-3 for the perfect case. Note that his u_1 corresponds to x_5 and u_2 to x_6, and the load variable Λ corresponds to μ in the present work.)

Supple started his analysis by expressing the total potential energy V of the system as an even function of u_1 and u_2. He also introduced the effect of initial imperfections ϵ_1 and ϵ_2 associated with u_1 and u_2 respectively, such that when the loading Λ is zero $u_1 = \epsilon_1$ and $u_2 = \epsilon_2$*, and expressed the total potential energy of

* Note that his ϵ_1 and ϵ_2 correspond to d_1 and d_2 respectively of the present work with the modification that in the latter the elastic deflections x_5 and x_6 are measured from d_1 and d_2 respectively.

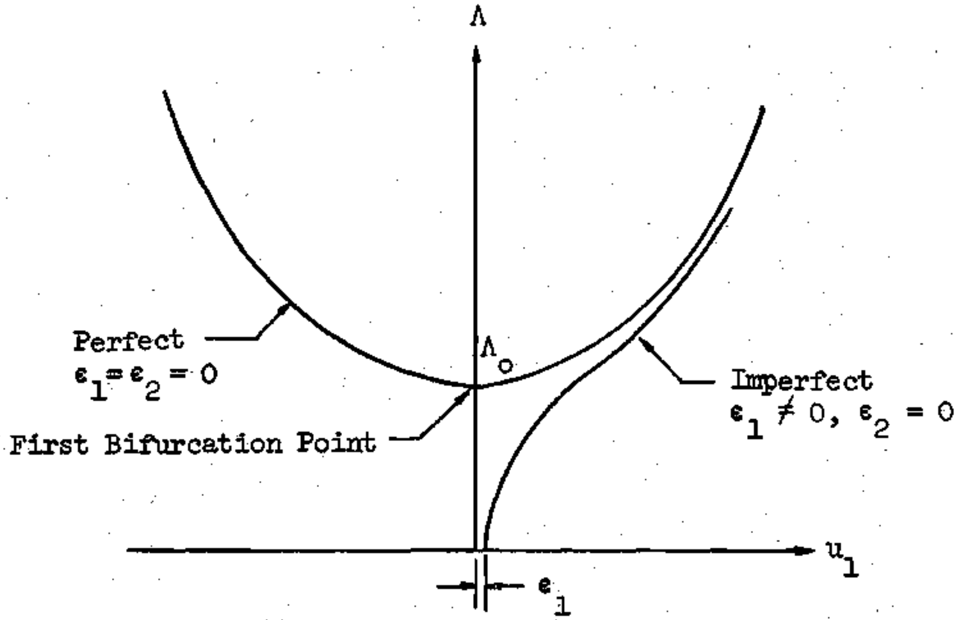

Figure IV-2. Equilibrium Branches in Λ-u_1 Plane

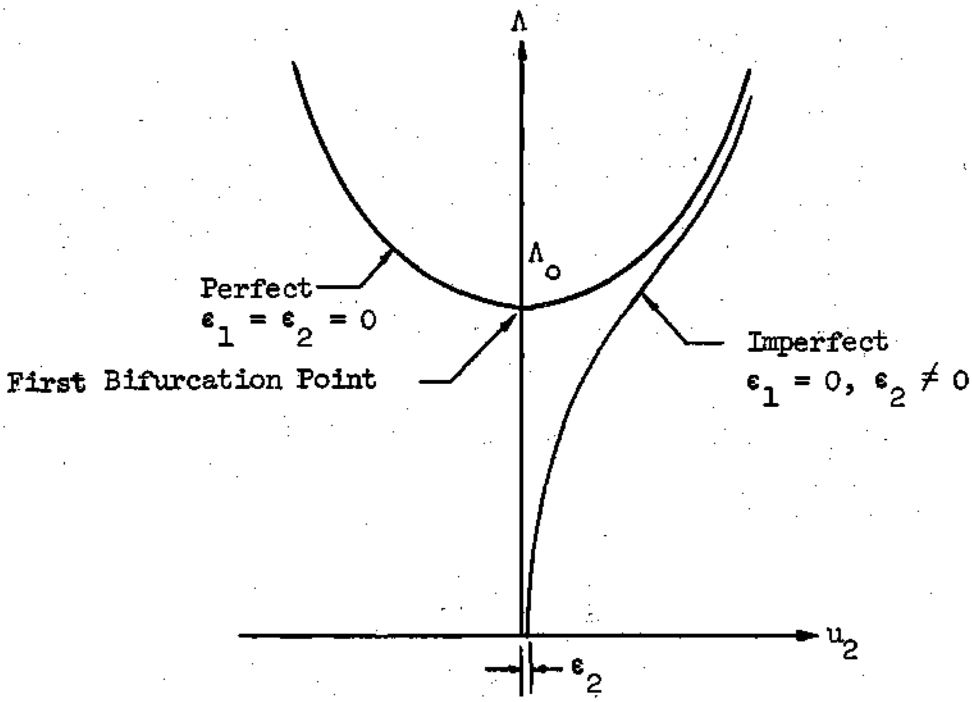

Figure IV-3. Equilibrium Branches in Λ-u_2 Plane the imperfect structural system in a region about $\Lambda = \Lambda_o$ by defining a new variable, λ, such that $\Lambda = \Lambda_o + \lambda$. He then expressed V in a power series in the variables u_1, u_2, ϵ_1, ϵ_2 and λ. By truncating the series and setting $\partial V/\partial u_1$ and $\partial V/\partial u_2$ to zero, he obtained two simultaneous equations which defined the state of static equilibrium. The resulting approximate equilibrium equations were presented in the form

$$V_{1\epsilon_1}\epsilon_1 + \frac{1}{6}\left(V_{1111}\, u_1^3 + 3V_{1122}\, u_1 u_2^2\right) + \lambda\, V'_{11}\, u_1 = 0 \qquad \text{(IV-1)}$$

$$V_{2\epsilon_2}\,\epsilon_2 + \frac{1}{6}\left(V_{2222}\, u_2^3 + 3V_{1122}\, u_1^2 u_2\right) + \left(\lambda - \Delta\lambda\right)V'_{22}\, u_2 = 0 \qquad \text{(IV-2)}$$

where

$$\Delta\lambda = - \frac{V_{22}}{V'_{22}} .$$

Note that a numerical subscript on V denotes partial differentiation with respect to the generalized coordinate, a subscript $\epsilon_i (i = 1,2)$ on V denotes partial differentiation with respect to ϵ_i and a prime on V represents partial differentiation with respect to Λ. All derivatives were evaluated at $\Lambda = \Lambda_o$, and $u_1 = u_2 = \epsilon_1 = \epsilon_2 = 0$.

The Perfect Systems

The postbuckling behavior of the perfect systems can be studied by setting $\epsilon_1 = \epsilon_2 = 0$ in the Equations (IV-1) and (IV-2). They then reduce to the form

$$u_1 \left[e_1 \, u_1^2 + g_1 \, u_2^2 - \lambda \, p_1 \right] = 0 \qquad \text{(IV-3)}$$

$$u_2 \left[e_2 \, u_1^2 + g_2 \, u_2^2 - \lambda \, p_2 + p_3 \right] = 0 \qquad \text{(IV-4)}$$

where e_i, g_i and p_i are resulting quantities which are functions of the derivatives of V.

Equations (IV-3) and (IV-4) have a geometric interpretations; i.e., in a u_1, u_2 and Λ ($\Lambda = \Lambda_o + \lambda$) space, these equations represent curved surfaces. If uncoupled behavior such that $u_2 = 0$ and $u_1 \neq 0$ occurs, then a nontrivial solution is generated from Equation (IV-3).

$$e_1 \, u_1^2 - \lambda \, p_1 = 0 \qquad \text{(IV-5)}$$

geometrically this is the trace of the corresponding surface on the $\Lambda - u_1$ plane of Figure IV-2.

Similarly, if $u_1 = 0$ and $u_2 \neq 0$, a nontrivial solution is generated from Equation (IV-4) as

$$g_2 \, u_2^2 - \lambda \, p_2 + p_3 = 0 \qquad \text{(IV-6)}$$

This is the trace pictured in Figure IV-3. It should be observed that this latter state may not be stable.

If both $u_1 \neq 0$ and $u_2 \neq 0$, the nontrivial state will be coupled; i.e., both Equations (IV-3) and (IV-4) must be satisfied. In geometric terms, this coupled solution would correspond to the intersection of the two surfaces(defined by Equations (IV-3) and (IV-4). It would, then, be a space curve.

Clearly, graphical representation of uncoupled states is easily depicted. Coupled, on the other hand, are not easily visualized in graphic form. Some of the features can be examined, however, by considering projections of the space curve on the coordinate planes. Supple, for example, has considered projections on the $u_1 - u_2$ plane, and he has developed a classification scheme for the various types of behavior which may be encountered. Mathematically, this procedure may be developed by eliminating λ from Equations (IV-3) and (IV-4). The resulting equation in u_1 and u_2 may then be identified as the projection of the space curve on the $u_1 - u_2$ plane.

After the perfect structure buckles and enters the postbuckling state, such that $u_1 \neq 0$, then the bracketed quantity of Equation (IV-3) must be zero; that is

$$e_1 u_1^2 + g_1 u_2^2 - \lambda p_1 = 0 \tag{IV-7}$$

Similarly if the structure buckles such that $u_2 \neq 0$, then from Equation (IV-4) obviously

$$e_2 u_1^2 + g_2 u_2^2 - \lambda p_2 + p_3 = 0 \tag{IV-8}$$

Elimination of λ from Equations (IV-7) and (IV-8) results in

$$\lambda = \frac{1}{p_1}\left(e_1\, u_1^2 + g_1\, u_2^2\right) = \frac{1}{p_2}\left(e_2\, u_1^2 + g_2\, u_2^2 + p_3\right) \qquad \text{(IV-9)}$$

which after rearranging will yield

$$\left(\frac{1}{p_1}\, e_1 - \frac{1}{p_2}\, e_2\right) u_1^2 + \left(\frac{1}{p_1}\, g_1 - \frac{1}{p_2}\, g_2\right) u_2^2 - \frac{p_3}{p_2} = 0 \qquad \text{(IV-10)}$$

Defining

$$\bar{e} = \left(\frac{1}{p_1}\, e_1 - \frac{1}{p_2}\, e_2\right), \qquad \text{(IV-11)}$$

and

$$\bar{g} = \left(\frac{1}{p_1}\, g_1 - \frac{1}{p_2}\, g_2\right) \qquad \text{(IV-12)}$$

$$\bar{p} = \frac{p_3}{p_2} \qquad \text{(IV-13)}$$

Equation (IV-10) can be expressed simply as

$$\bar{e}\, u_1^2 + \bar{g}\, u_2^2 = \bar{p} \qquad \text{(IV-14)}$$

If the structure analyzed is such that the constants $\bar{e}$, $\bar{g}$ and $\bar{p}$ are positive, then the postbuckling behavior of the structure depicted on the $u_1 - u_2$ plane will be an ellipse shown as type I in Figure IV-4.

If $\bar{e} \neq 0$, $\bar{g} = 0$ and $\bar{p} = 0$ the resulting equation represents the u_2 axis $(u_1 = 0)$.

Similarly, if $\bar{e} = 0$, $\bar{g} \neq 0$ and $\bar{p} = 0$ the resulting equation

Stable Equilibrium Path .... Unstable Equilibrium Path

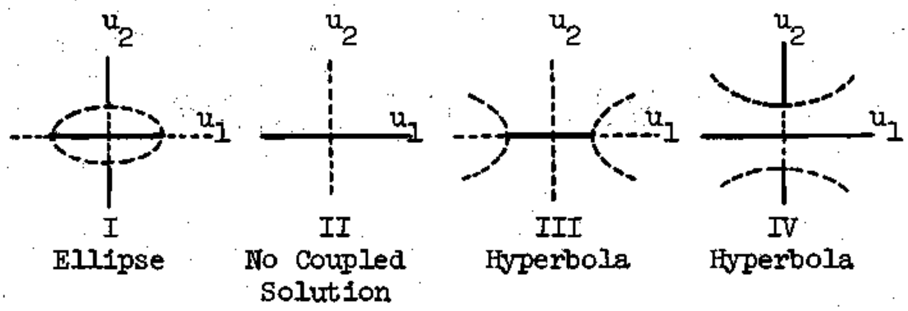

Figure IV-4. Forms of Coupled Postbuckling for Ideal Structural Systems (After Supple [11].)

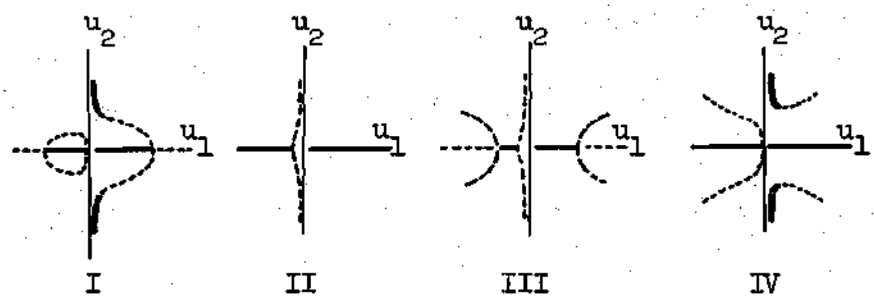

Figure IV-5. Forms of Postbuckling Equilibrium Paths for Structural Systems with Imperfections ϵ_1 (After Supple [11].)

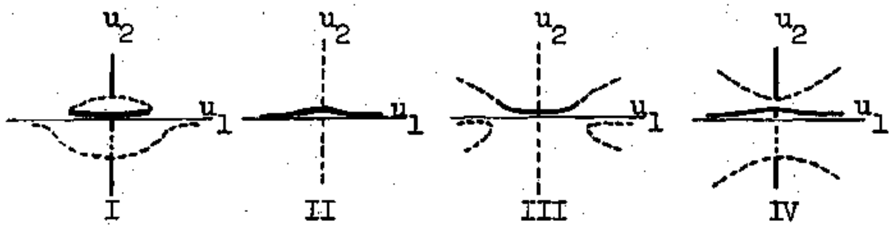

Figure IV-6. Forms of Postbuckling Equilibrium Paths for Structural Systems with Imperfections ϵ_2 (After Supple [11].)

represents the u_1 axis ($u_2 = 0$). These latter two possibilities are depicted as type II in Figure IV-4.

Another possibility is when $\bar{e} > 0$, $g < 0$ and $\bar{p} > 0$; then a hyperbola crossing the u_1 axis will appear on the $u_1 - u_2$ plane. If the structure is such that $\bar{e} < 0$, $\bar{g} > 0$ and $\bar{p} > 0$ the hyperbola crosses the u_2 axis; the last two cases are shown in types III and IV in Figure IV-4.

Summarizing these observations, Supple categorized four types of perfect structures whose postbuckling behavior can be traced on the $u_1 - u_2$ plane as shown in Figure IV-4. Note that the solid lines were found to represent stable branches, while the dashed lines represent unstable ones.

The loaded structure may pass through three possible stages as follows:

a) Upon the application of the load, the variable Λ starts from zero and increases positively until the value $\Lambda = \Lambda_o$, at which point the first bifurcation point is reached. Throughout this increase, the structure exhibits a response for which $u_1 = u_2 = 0$ as seen in Figure IV-2. In Figure IV-4 this corresponds to the point on the origin indicating the so called fundamental state.

b) As the load increases the structure buckles. For example, if $u_1 \neq 0$ and $u_2 = 0$ (a so called primary, uncoupled mode of buckling) the resulting behavior is depicted in Figure IV-4 by the solid line along the u_1 axis.

c) For loads greater than Λ_o, there can exist other stable equilibrium branches which corresponds to a secondary mode of buckling as seen on the u_2 axis of types I and IV of Figure IV-4. Note that these are not directly accessible from the primary mode.

Imperfect Systems

When initial imperfections ϵ_1 and ϵ_2 are present in the system, then the behavior of the structure will be governed by the Equations (IV-1) and (IV-2).

As for perfect systems both uncoupled and coupled behavior is possible. For example, uncoupled responses can develop for either $\epsilon_1 \neq 0$, $\epsilon_2 = 0$ and $u_2 = 0$ or $\epsilon_1 = 0$, $\epsilon_2 \neq 0$ and $u_1 = 0$. These are depicted in Figures IV-2 and IV-3, respectively.

For coupled behavior it is again convenient to represent the behavior on a u_1 versus u_2 plot. That is, the projection of the intersection of the surfaces described by Equations (IV-1) and (IV-2). Cases of basic interest and those for which $\epsilon_1 \neq 0$, $\epsilon_2 = 0$, $u_1 \neq 0$, and $u_2 \neq 0$, or alternatively, $\epsilon_1 = 0$, $\epsilon_2 \neq 0$, $u_1 \neq 0$ and $u_2 \neq 0$.

The variety of possibilities for imperfect systems which correspond to the perfect types of Figure IV-4 are shown in Figures IV-5 and IV-6. An examination of these graphs reveals that stable bifurcation from an uncoupled equilibrium branch to a coupled branch can occur in each of the four types depicted in Figure IV-6. Such bifurcations are not observed in the cases presented in Figure IV-5.

The difference in the behaviors noted above may be related to the nature of the imperfection. Two possibilities may occur.

a) The uncoupled behavior is developed (for example, with $\epsilon_1 \neq 0$, $\epsilon_2 = 0$, $u_1 \neq 0$ and $u_2 = 0$) in cases for which deflection occurs in the lower mode. That is, the buckling load for the mode associated with u_1 is smaller than that for u_2. Figure IV-5 depicts this type of behavior. Note that the coupled branches are not accessible from the natural loading path.

b) The uncoupled behavior is developed (for example, with $\epsilon_1 = 0$, $\epsilon_2 \neq 0$, $u_1 = 0$ and $u_2 \neq 0$) in cases for which deflection occurs in the upper mode. That is, the buckling load for the mode associated with u_2 is greater than that for u_1. Figure IV-6 depicts the type of behavior for this case. Note that bifurcation from the natural loading path leads to coupled behavior.

The various cases treated in the previous sections were for ideal structures; either they were perfect, i.e., $\epsilon_1 = 0$, $\epsilon_2 = 0$ or selectively allowed to possess a prescribed imperfection such that either $\epsilon_1 \neq 0$ and $\epsilon_2 = 0$ or $\epsilon_1 = 0$ and $\epsilon_2 \neq 0$. In real systems, however, an ideal structure with no imperfection would be impossible. In fact, it is realistic to expect that components of both modes of imperfection would be present in the given structure simultaneously. One component may be small, but it is unlikely to be completely absent. Consequently, the emphasis in the work described here was devoted to the analysis of those types of structures for which both imperfections ϵ_1 and ϵ_2 are present in varying degrees.

Presentation of Results

Analytical Alternatives

The imperfect plate problems considered here (see Figure II-2) with $d_1 \neq 0$ and $d_2 \neq 0$ were solved entirely by the use of the perturbation technique described in Chapter III, where all six variables $x_1, x_2, \ldots, x_6$ were expanded as powers of $\epsilon = \mu - \mu_o$, and the six nonlinear equations were reduced to a system of linear equations.

For the special cases of imperfection with $d_1 \neq 0$ and $d_2 = 0$ or with $d_1 = 0$ and $d_2 \neq 0$, however, the perturbation technique was found to be inapplicable. The reason being; the transverse deflection x_6, for example, was expressed in powers of ϵ. Consequently, the derivatives of x_6 with respect to ϵ had to be finite for the expansion to be valid. This requirement was not, of course, satisfied for the perfect system at a point of bifurcation. It was also not satisfied for a case when bifurcation from an uncoupled, upper mode to a coupled behavior occurred. In this latter case, only an imperfection of the upper mode form was, of course, present.

To eliminate these difficulties, an algebraic procedure, similar to that used by Supple was adopted. The solution of the problem then did not depend on the existence of the cited derivatives.

An alternative solution approach would appear to be to express the displacements u and v in terms of w (see Appendix G), and then to solve the resulting partial differential equations. An examination of this approach was made but since solution techniques could not be developed work was discontinued.

The technique used eventually was, to express the unknowns x_1, x_2, x_3 and x_4, the coefficients of the in-plane displacements, in terms of x_5 and x_6, the out-of-plane displacements. By this procedure the six nonlinear equations in six unknowns were reduced to two nonlinear equations in the two unknowns x_5 and x_6. The procedure used is described below.

The first four Equations (C-1) to (C-4) in Appendix C are linear in x_1, x_2, x_3 and x_4. They can, therefore, be easily solved in terms of x_5 and x_6 through the use of Cramer's rule to yield the following:

$$
\begin{aligned}
x_1 &= x_1(x_5, x_6) \\
x_2 &= x_2(x_5, x_6) \\
x_3 &= x_3(x_5, x_6) \\
x_4 &= x_4(x_5, x_6)
\end{aligned}
\qquad \text{(IV-15)}
$$

These, when substituted in Equations (C-5) and (C-6) of Appendix C, yield

$$
\begin{aligned}
&\mu C_{50} + \mu C_{55M}\, x_5 + k_{13}\, x_5 + k_{14}\, x_6 + k_{15}\, x_5\, x_6 \qquad \text{(IV-16)} \\
&\quad + k_{16}\, x_5^2 + k_{17}\, x_6^2 + k_{18}\, x_5\, x_6^2 + k_{19}\, x_5^3 = 0
\end{aligned}
$$

and

$$
k_{21}\, x_6 + \mu C_{66M}\, x_6 + k_{22}\, x_5\, x_6 + k_{23}\, x_5^2\, x_6 + k_{24}\, x_6^3 = 0 \qquad \text{(IV-17)}
$$

respectively, where the k_i are functions of $C_{ijp\ell}$, some of which contain the imperfection terms d_1 and d_2.

The strain quantity μ in Equation (IV-16) was then expressed in terms of the variables k_i, x_5 and x_6 and when equated to the μ of the Equation (IV-17), the resulting equation becomes

$$\bar{k}_1 x_5 + \bar{k}_2 x_5^2 + \bar{k}_3 x_6^2 + \bar{k}_4 x_5 x_6^2 + \bar{k}_5 x_5^3 = 0 \qquad \text{(IV-18)}$$

Collecting like powers of x_6, the latter becomes

$$\bar{k}_6 x_6^2 + \bar{k}_7 = 0 \qquad \text{(IV-19)}$$

where $\bar{k}_6$ and $\bar{k}_7$ are functions of x_5, d_1, d_2 and all pertinent properties of the plate.

Equation (IV-19) was then easily solved for x_6 to yield

$$x_6 = \sqrt{-\frac{\bar{k}_7}{\bar{k}_6}} \qquad \text{(IV-20)}$$

where various values of x_5, d_1, d_2, etc., were assumed and the corresponding x_6 was evaluated.

The Perfect Plate

The plate stability problem analyzed here was described in Chapter II. The results of a linear buckling analysis of the problem are summarized in Figure IV-1. In the discussion which follows, the mode associated with the lowest curve for a given aspect ratio will be described as the lower mode. The next higher curve will be described as the upper mode.

For a perfect plate whose aspect ratio $r_1 < 2.3561$ the lower mode corresponds to $m = 1$ on the graph of Figure IV-1, and it has a half-sine wave deflected shape in the direction of loading.

The upper mode of the same plate has a two half-sine wave configuration corresponding to $m = 2$. The corresponding critical load depends on the $k(r_1)$ of the upper curve.

If, on the other hand the aspect ratio has a value $3.129 > r_3 > 2.3561$, (see Figure IV-1) then the lower mode of buckling of the plate is given by $m = 2$, and hence the lower mode will be a two half-sine wave configuration. The upper mode will be given by either $m = 1$ or $m = 3$.

The strain μ versus the transverse deflection curves of a perfect plate are shown in Figures IV-7 and IV-8.

If the form of presentation used by Supple (see Figure IV-4) is utilized here, the results of the current studies can be presented as shown in Figures IV-9 and IV-10. The curves representing coupled behavior (i.e., both $x_5 \neq 0$ and $x_6 \neq 0$) have been obtained by the algebraic elimination technique described previously in this chapter.

In Figure IV-9, which is for $r < 2.3561$, the trace of the loading path is represented by the heavy line coinciding with the x_5 axis.* This, of course, is an uncoupled behavior in the lower mode.

* An elastic modulus of $E = 10.5 \times 10^6$ psi (Aluminum) and a Poisson's ratio of $\nu = 0.3$ were used for all of the computations described in this section.

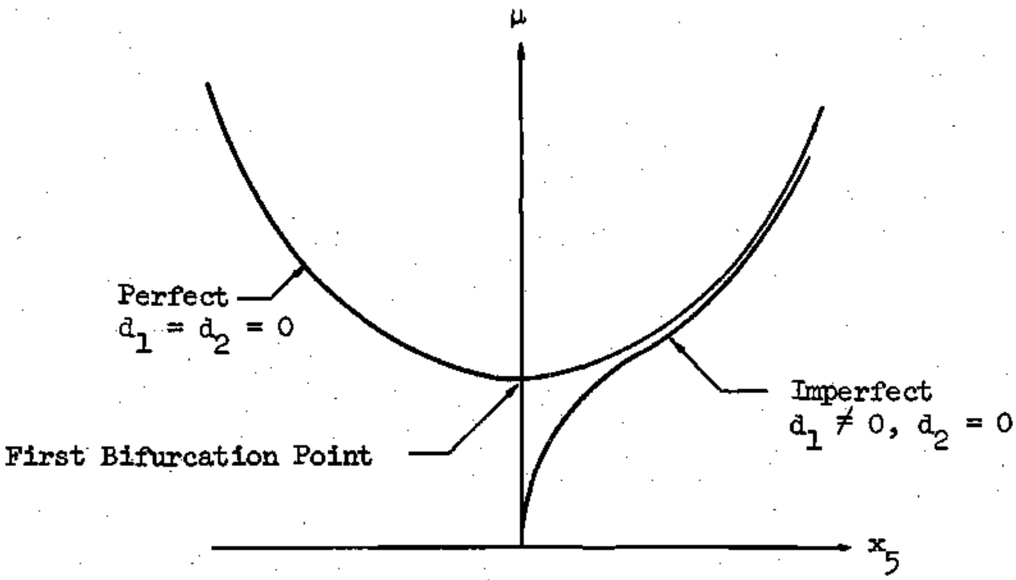

Figure IV-7. Equilibrium Branches in μ - x_5 Plane

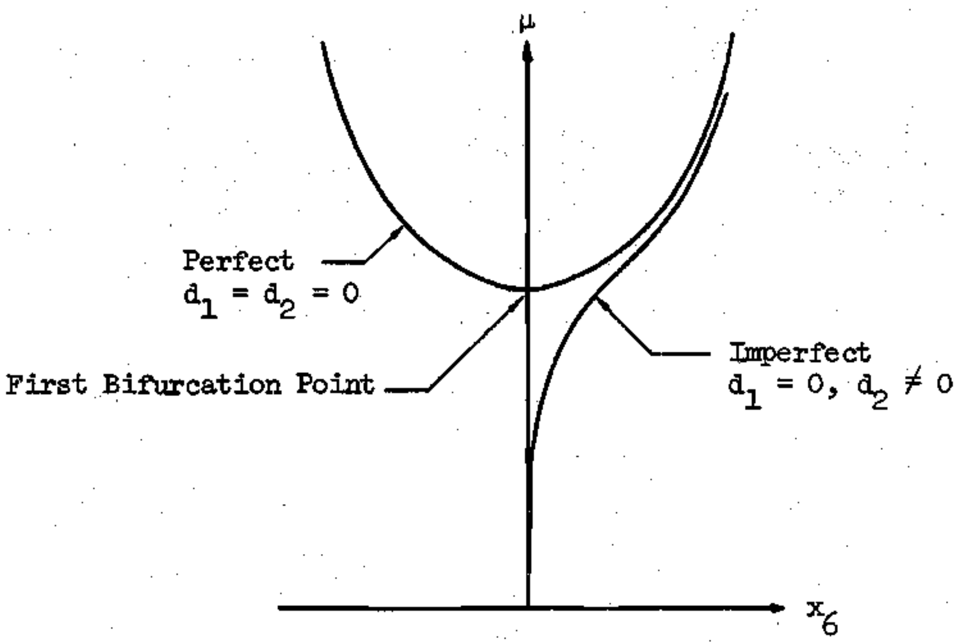

Figure IV-8. Equilibrium Branches in μ - x_6 Plane

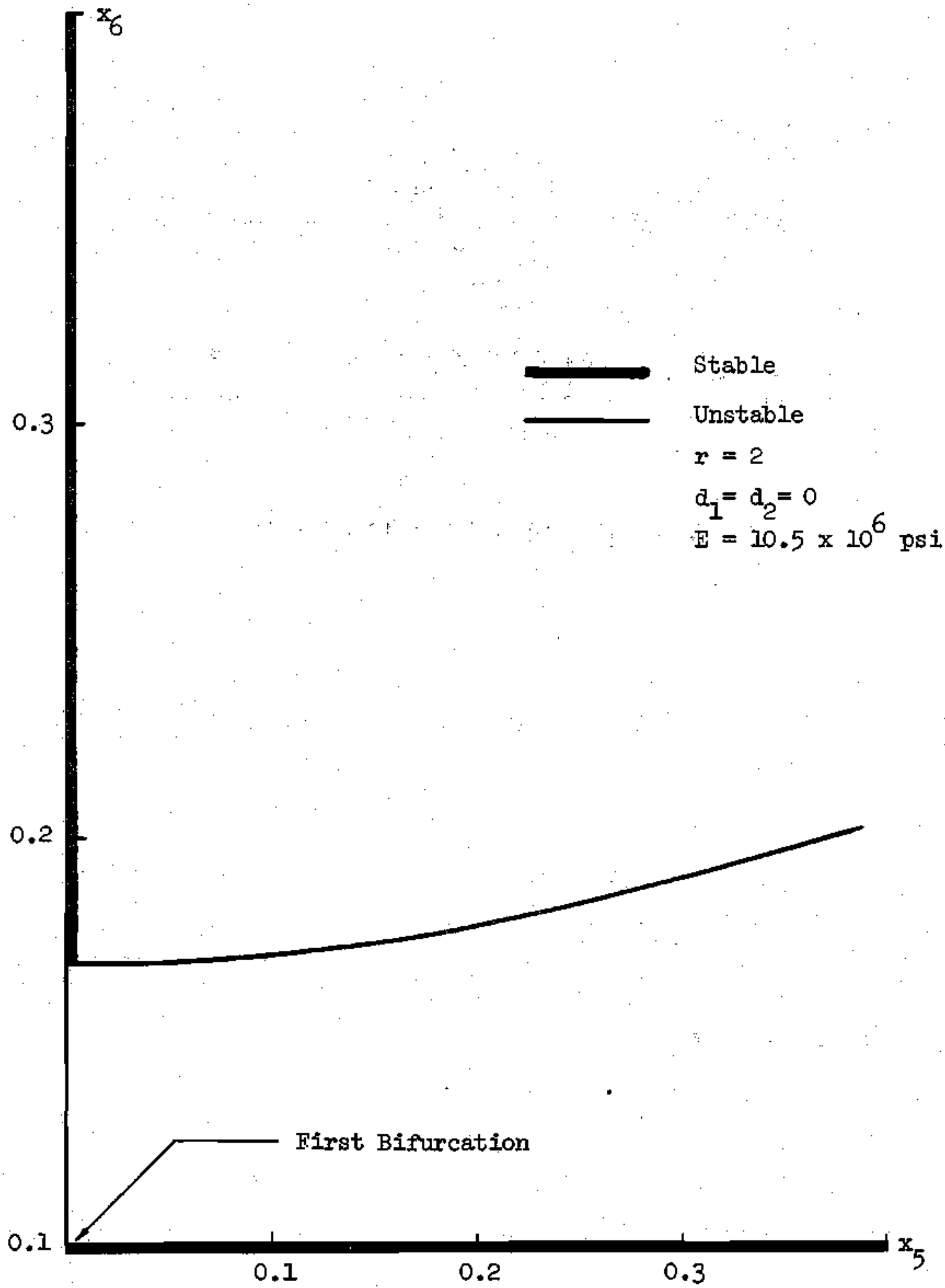

Figure IV-9. x_6 Versus x_5 Diagram for Perfect Plate with $r = 2$

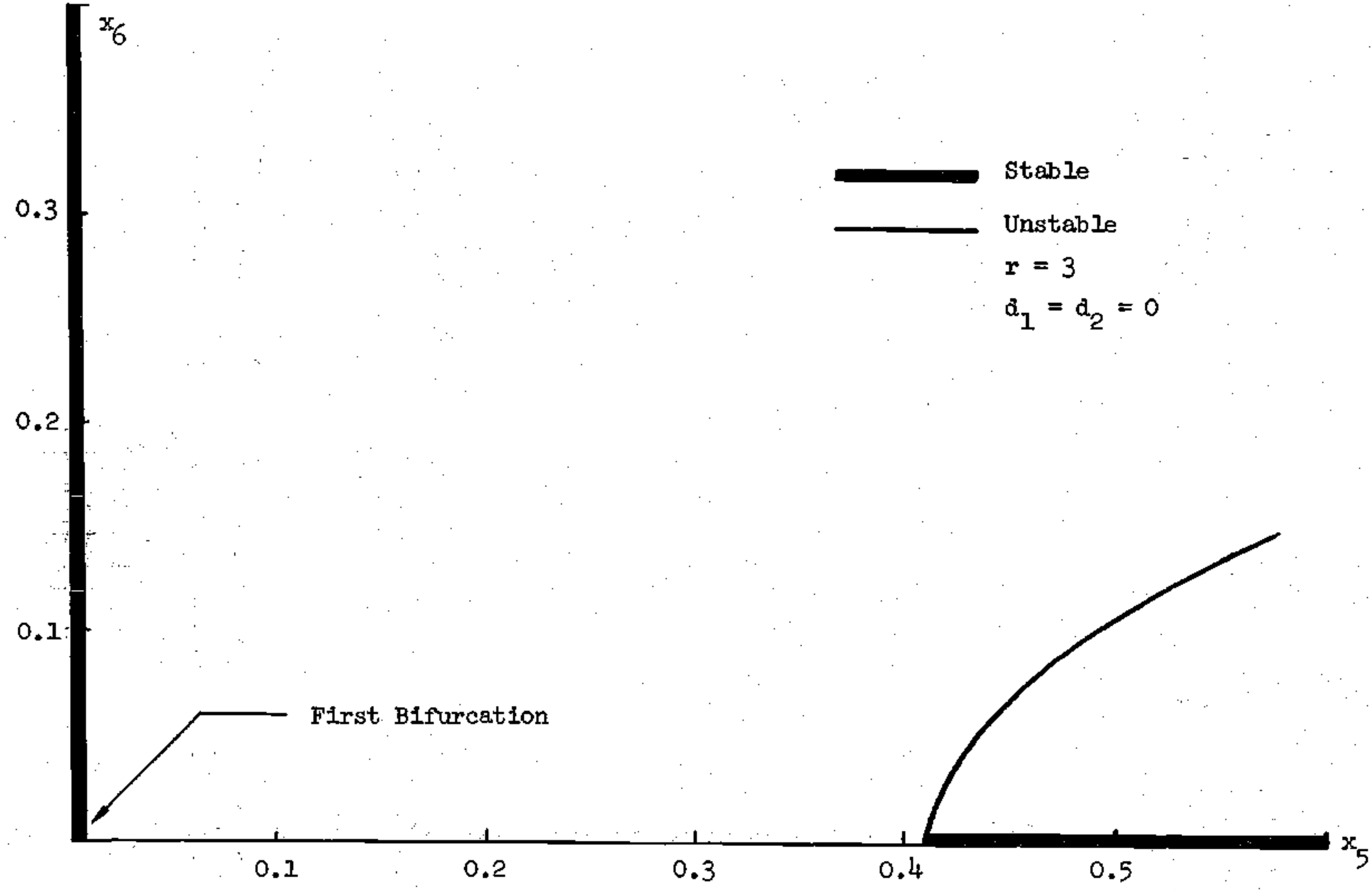

Figure IV-10. x_6 Versus x_5 Diagram for Perfect Plate with $r = 3$

Another equilibrium branch for this perfect structure is a hyperboilic curve bifurcating from the x_6 axis [11]. However, this branch is not stable and it is not accessible from the lower mode (x_5 axis) under natural loading conditions. In terms of the classification scheme proposed by Supple [11], the results presented here for $r < 2.3561$ corresponds to the type IV behavior shown in Figure IV-4.

If the aspect ratio of the plate is $3.129 > r > 2.3561$ then the trace of the loading path is represented by the heavy line coinciding with the x_6 axis. This, obviously is an uncoupled behavior in the lower mode as seen in Figure IV-10.

The other equilibrium branch for the plate whose $3.129 > r > 2.3561$ is the curve bifurcating from the x_5 axis. This coupled branch however, is not a stable one, and is not accessible from the lower mode (x_6 axis) under natural loading conditions. Relating to Supple's* classification scheme it also corresponds to the type IV behavior shown in Figure IV-6.

In conclusion, the stable equilibrium branch of the perfect plate studied will be uncoupled. The unstable equilibrium branch however, will be coupled. The latter will bifurcate from the x_6 axis if $r < 2.3561$, and from the x_5 axis if $3.129 > r > 2.3561$.

---

* Note that Supple uses u_2 exclusively to designate the upper mode. He therefore uses u_1 for the lower mode. Consequently, his u_2 corresponds to x_5, and his u_1 corresponds to x_6 in the present work for plates whose $3.129 > r > 2.3561$. For $r < 2.3561$ the correspondance is reversed.

Imperfection In One Mode

If the plate has an imperfection of the form $d_1 \neq 0$ and $d_2 = 0$, then its compressive load-deflection behavior will be different from that of the perfect case.

For the type of imperfection cited above, a plate with an $r < 2.3561$ will immediately deflect in a one half-sine configuration under the smallest compressive loading. This behavior is exhibited in a μ versus x_5 relation in Figure IV-7. Using Supple's form of representation, the trace of the loading path will be the heavy line coinciding with the x_5 axis shown in Figure IV-11. This is obviously an uncoupled behavior in the lower mode.

Another equilibrium branch for this type of imperfection is the upper curve shown in Figure IV-11. Note that this curve represents a coupled mode of deflection. The heavy portion of the curve represents a stable configuration. This branch however, is not accessible from the uncoupled one (x_5 axis) under natural loading conditions. In terms of Supple's [11] classification scheme, the results presented here for $r < 2.3561$ correspond to type IV behavior shown in Figure IV-5.

As explained previously, if a given flat plate has an $3.129 > r > 2.3561$ then the lower mode of deflection will be the two half-sine wave configuration. However, the plate under consideration possesses an imperfection of the form $d_1 \neq 0$ and $d_2 = 0$, which is of the same general shape as the upper mode of deflection. Consequently, at the initial stages of loading, the plate will be biased to deflect in the shape associated with the upper mode.

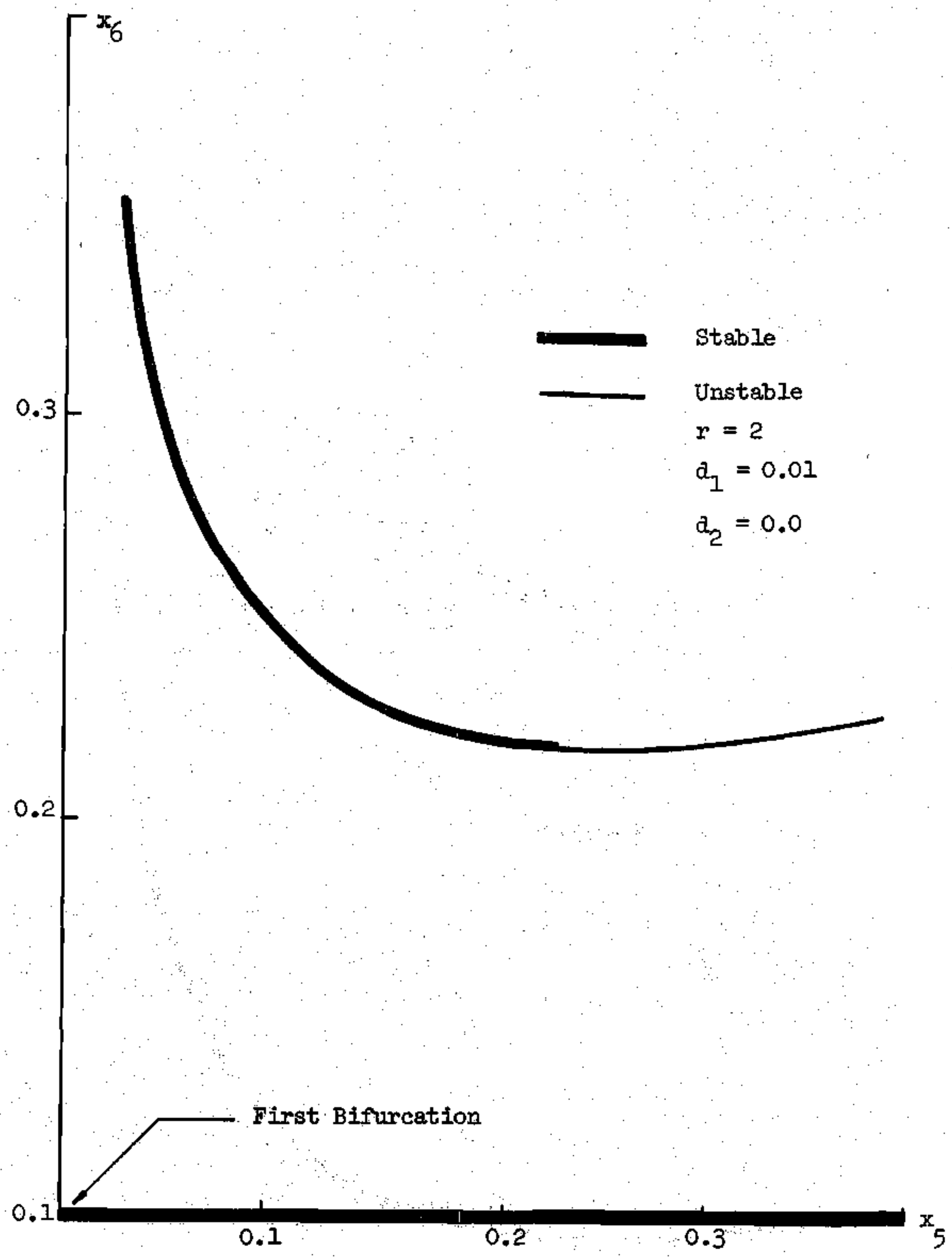

Figure IV-11. x_6 Versus x_5 Diagram for Imperfect Plate with $r = 2$

Using Supple's scheme of representation, the loading path of this imperfect plate will initially coincide with the x_5 axis as demonstrated by the heavy line in Figure IV-12. However, when a specific value of μ is reached it bifurcates into the coupled mode of behavior indicated. Another equilibrium branch representing a coupled mode, is seen to bifurcate from the x_5 axis. It should be pointed out though, that this is an unstable branch.

The two points on the x_5 axis where bifurcation of the equilibrium branches takes place may be brought close to each other until they coincide. This can be accomplished by holding r constant at 3.0 and increasing d_1 to 0.0105 as seen in Figure IV-13. This represents a trifurcation condition where the behavior is not unique. The plate would have three possible equilibrium branches. However, it may be expected to follow a branch or branches which are stable.

For certain values of r and d_1 the coupled equilibrium branches of Figure IV-12 may be joined into a single continuous curve detached from the x_5 axis. This can be realized by holding the aspect ratio constant and increasing the amplitude of imperfection. For example, it was found that for $r = 3$ and $d_1 = 0.015$ the coupled equilibrium branches join into the single continuous curve presented in Figure IV-14. This behavior indicates that it is possible for the plate to remain in the half-sine wave mode if the d_1 imperfection is sufficiently large. Clearly then, the existence of a bifurcation response depends not only on the aspect ratio, but also upon the value of the imperfection.

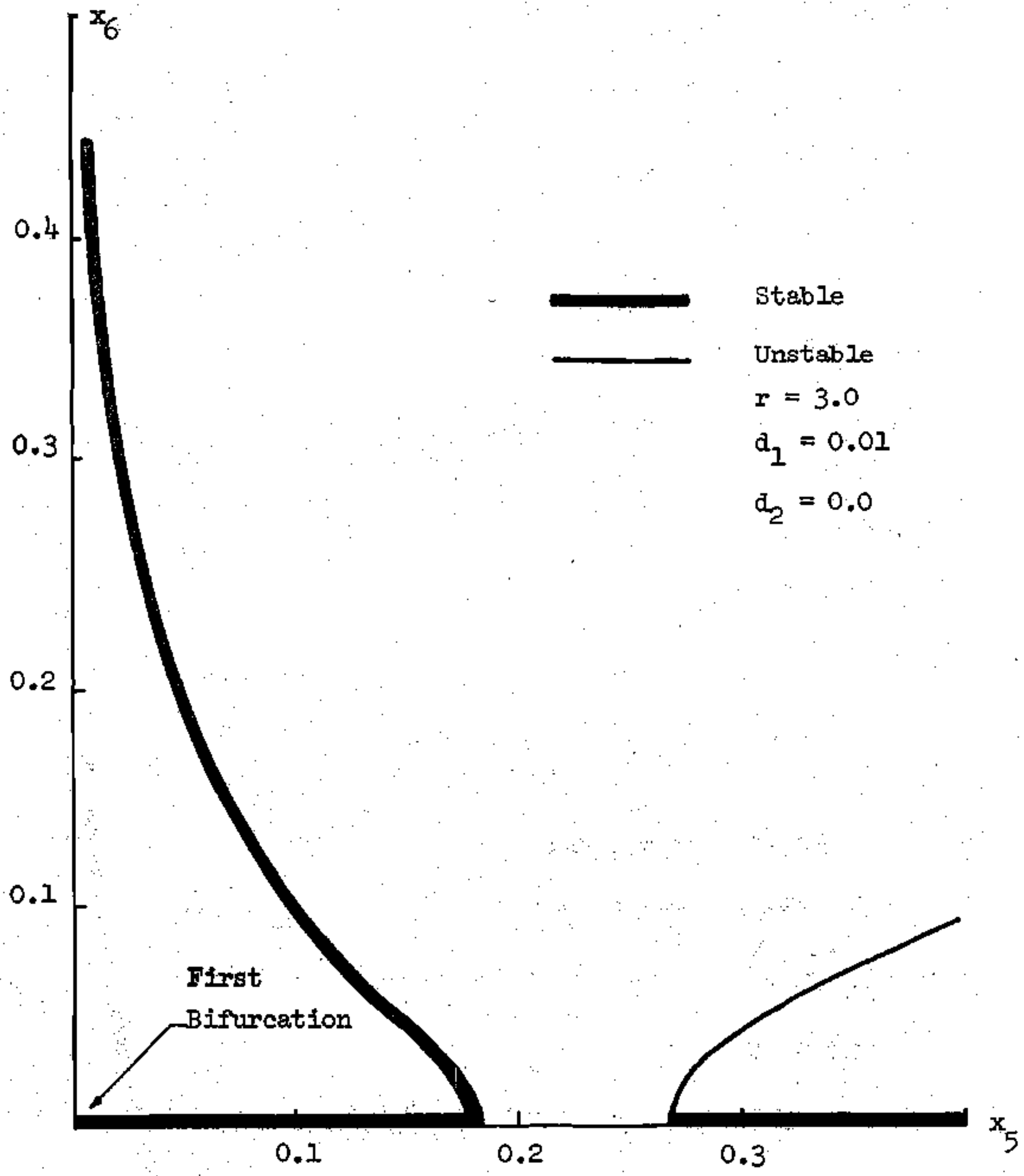

Figure IV-12. x_6 Versus x_5 Diagram for Imperfect Plate with $r = 3$

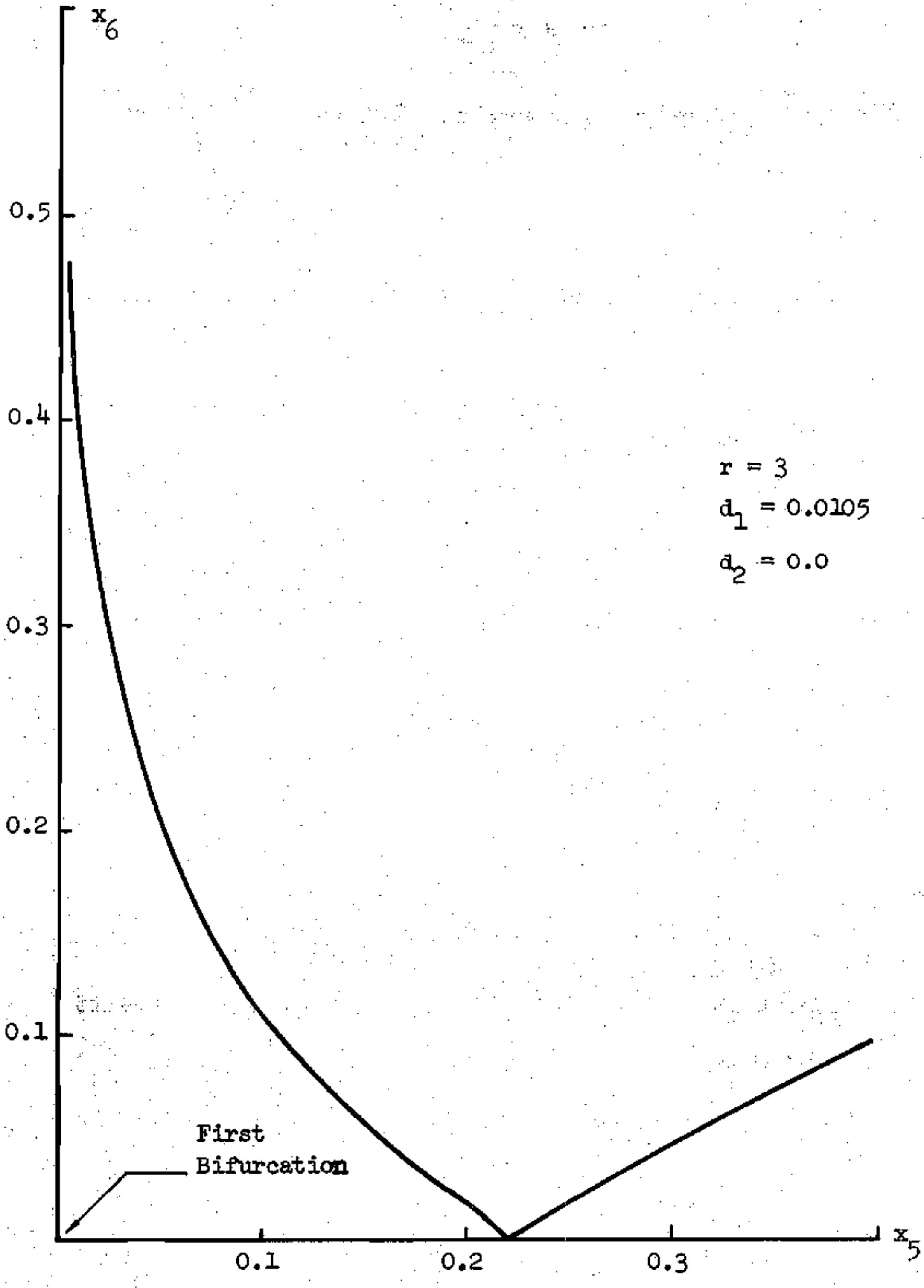

Figure IV-13. x_6 Versus x_5 Diagram for Imperfect Plate with $r = 3$

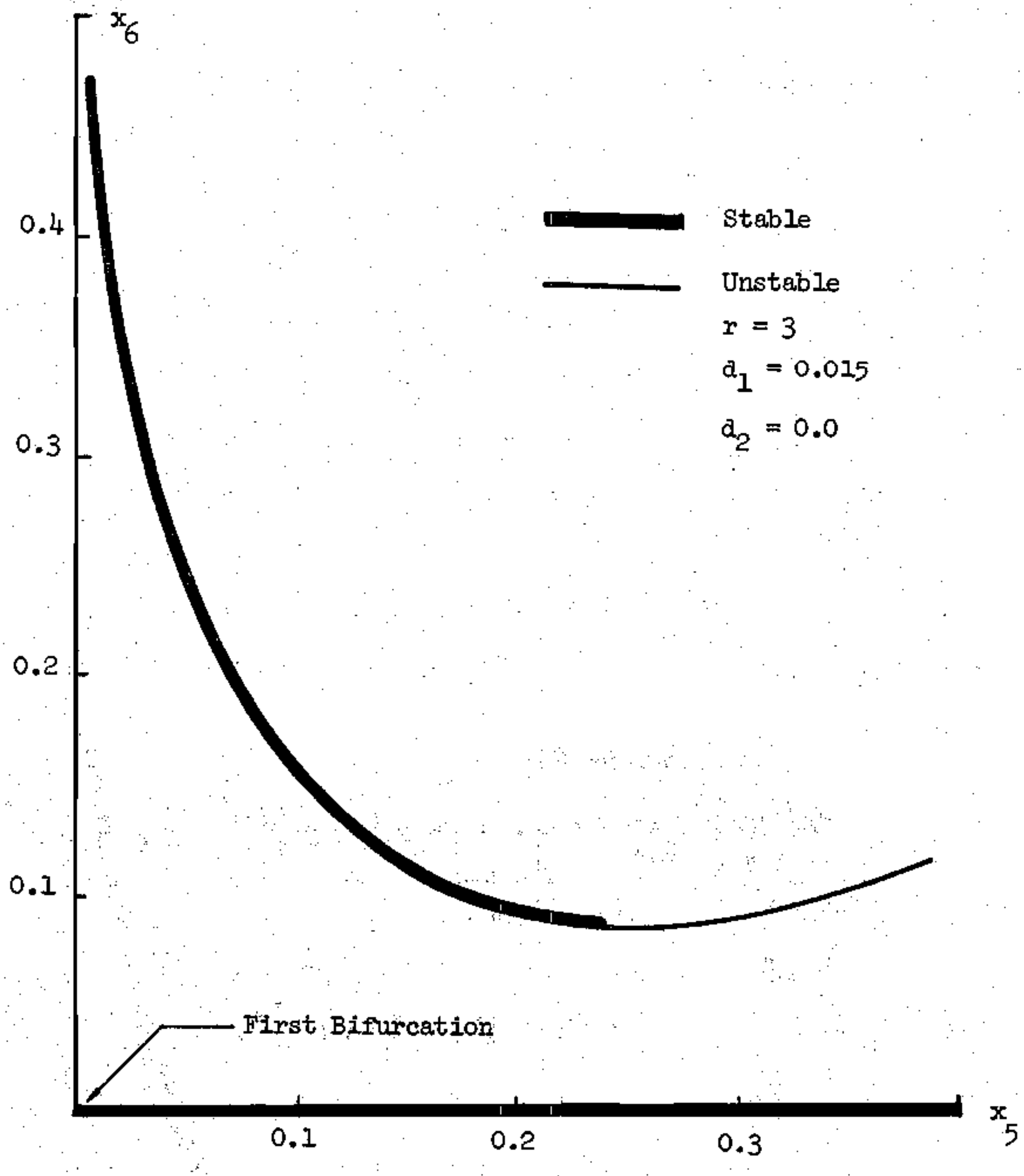

Figure IV-14. x_6 Versus x_5 Diagram for Imperfect Plate with $r = 3$

A review of the case for which $d_1 = 0$ and $d_2 \neq 0$ reveals that although the behavior described above may be observed, the details are reversed. That is, bifurcation from an uncoupled path occurs below a critical value of aspect ratio as seen in Figures IV-15 and IV-16.

Summarizing, a coupled mode of deflection of an imperfect plate for which $d_1 \neq 0$, $d_2 = 0$ and $r < 2.3561$ will not develop by bifurcation from the natural loading path (see the uncoupled mode in Figure IV-11). However, under suitable combinations of imperfection and aspect ratio $3.129 > r > 2.3561$, bifurcation from an uncoupled mode is possible.

<u>Imperfection In Two Modes</u>

The systems discussed previously have either been perfect or had a prescribed imperfection in one mode. The modal composition characteristics of these idealized structures subjected to compressive loads were studied in detail.

In this section systems possessing a more general form of imperfection will be analyzed and discussed. To investigate the behavior of such systems, plates with imperfections of the form $d_1 \neq 0$ and $d_2 \neq 0$ are considered. By including both imperfections simultaneously, a more realistic model is attained. One component may be small, but it is not likely to be completely absent. The objective of this work then, is to study the various deflection responses of such structures under various combinations of the aspect ratio, and differing amplitudes of imperfection. For all of the results presented in this section on the cases of $d_1 \neq 0$ and $d_2 \neq 0$ the perturbation method described previously was

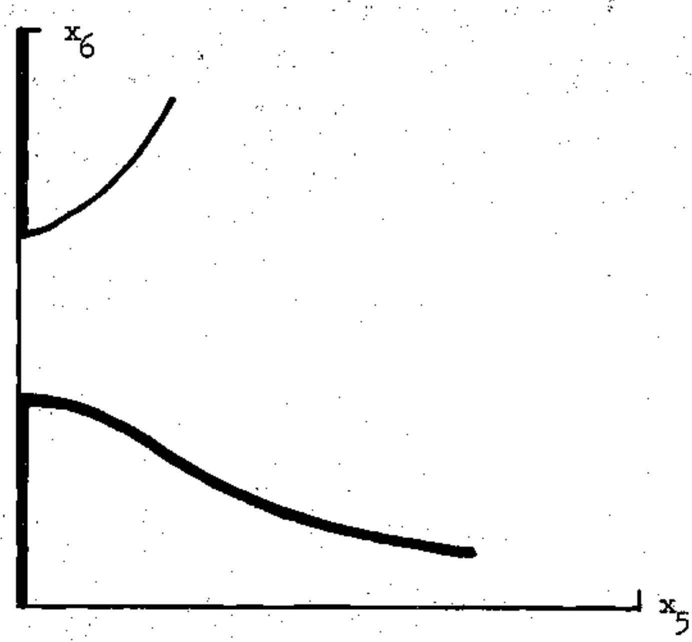

Figure IV-15. x_6 Versus x_5 Diagram for Imperfect Plate with $r < 2.3561$, $d_1 = 0$, $d_2 \neq 0$

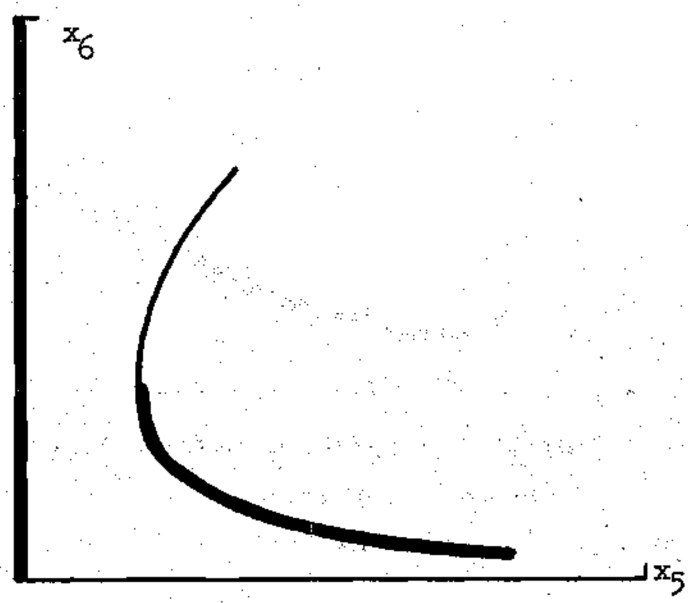

Figure IV-16. x_6 Versus x_5 Diagram for Imperfect Plate with $3.129 > r > 2.3561$ $d_1 = 0$, $d_2 \neq 0$

used (see Chapter III). Note that for all of these computations six term approximations based on a μ increment of 5×10^{-6} were used.

It is clear that an imperfect plate of the type considered would undergo a transverse deflection upon the initial application of compressive loading. This is a contrast to the perfect case for which no deflection occurs prior to the attainment of the critical load.

The behavior of interest was investigated by determining the effect of changes of the aspect ratio of a plate for a given set of initial imperfections. To this end, initial imperfections of $d_1 = 0.01$ and $d_2 = 0.01$ were initially chosen, and the aspect ratio was varied between 1.0 and 3.0. The results of the calculations are presented in the x_5 versus x_6 graph shown in Figure IV-17.

Note that in all cases examined the behavior was coupled; i.e., as the load was applied, the plate deflected such that both $x_5 \neq 0$ and $x_6 \neq 0$. The variation in behavior as r increases is interesting. For $r = 1.0$ the plate deflects primarily in a one half-sine mode. Though the two half-sine wave component is present, it is small and ultimately decreases as μ increases. This behavior is not surprising since $r = 1.0 < 2.3561$.

Similar conclusions were reached by Shigeru Nakagiri [17] who studied square plates subjected to prescribed end loading.

A plate with an aspect ratio = 2.00 still exhibits a dominant x_5 component. However, for $r = 2.1$ there is a dramatic change in the composition of the deflection pattern of the plate. In fact it may be seen that ultimately, loading increases are accompanied by

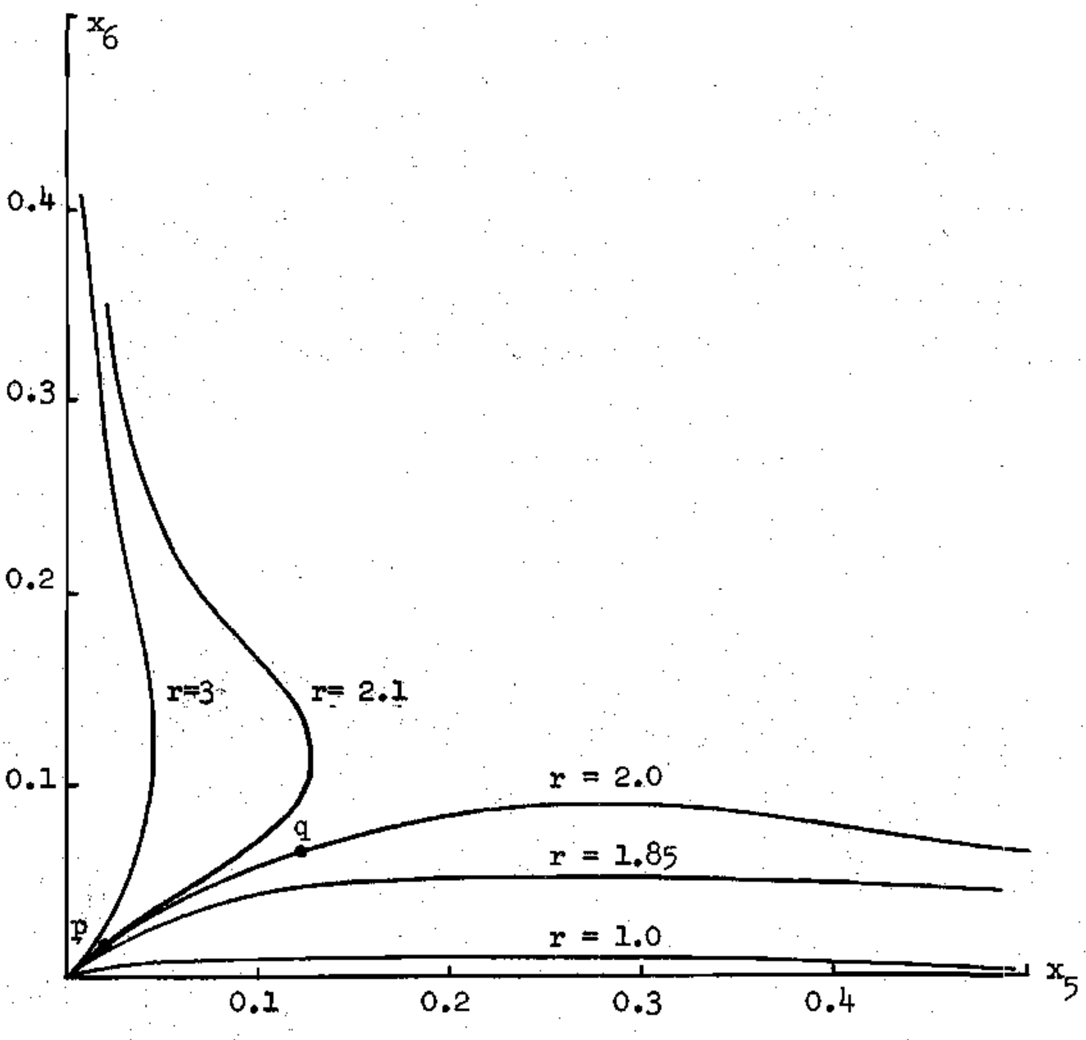

Figure IV-17. Effect of Aspect Ratio on x_6 Versus x_5 Diagram for $d_1 = d_2 = 0.01$

decreases in x_5 component while x_6 component continues to increase.

The sudden change in the modal composition can be illustrated by plots of deflection along a longitudinal line in the plate $[w_o(0,y) + w(0,y)]$. Data corresponding to four stages of loading are shown in Figures IV-18 and IV-19. The first drawing in Figure IV-18 demonstrates the unloaded ($\mu = 0.00$) state of the plate with $r = 2.0$, $d_1 = 0.01$, $d_2 = 0.01$. The second and the third cross-sections show the plate under a loading of $\mu = 0.00015$ and $\mu = 0.00023$ respectively. It can be shown that the plate has almost equal amplitudes of one half-sine, and two half-sine wave components present. These correspond to points p and q on the curves of Figure IV-17. As the loading μ increases, however, the x_5 component becomes predominant, and at $\mu = 0.00035$, the plate shows very little trace of the x_6 component.

Similar data for $r = 2.1$ have been plotted in Figure IV-19. A comparison of the results of Figures IV-18 and IV-19 reveals that for smaller μ between 0.00 and 0.00023 the general deflected shape of the plate with $r = 2.1$ resembles strongly to the previous case ($r = 2.0$). As the loading μ is increased from 0.00023 to 0.00035, however, the plate changes its shape quite suddenly. The x_5 component is decreased and the x_6 component becomes dominant. Thus, for a given imperfection, a very small change in r can result in drastic changes in the deflected shape as loading proceeds.

A measure of the "suddenness" of the changes in the coupled modes of these plates for various aspect ratios may also be defined with the help of Figure IV-20. To facilitate the discussion, the new parameter

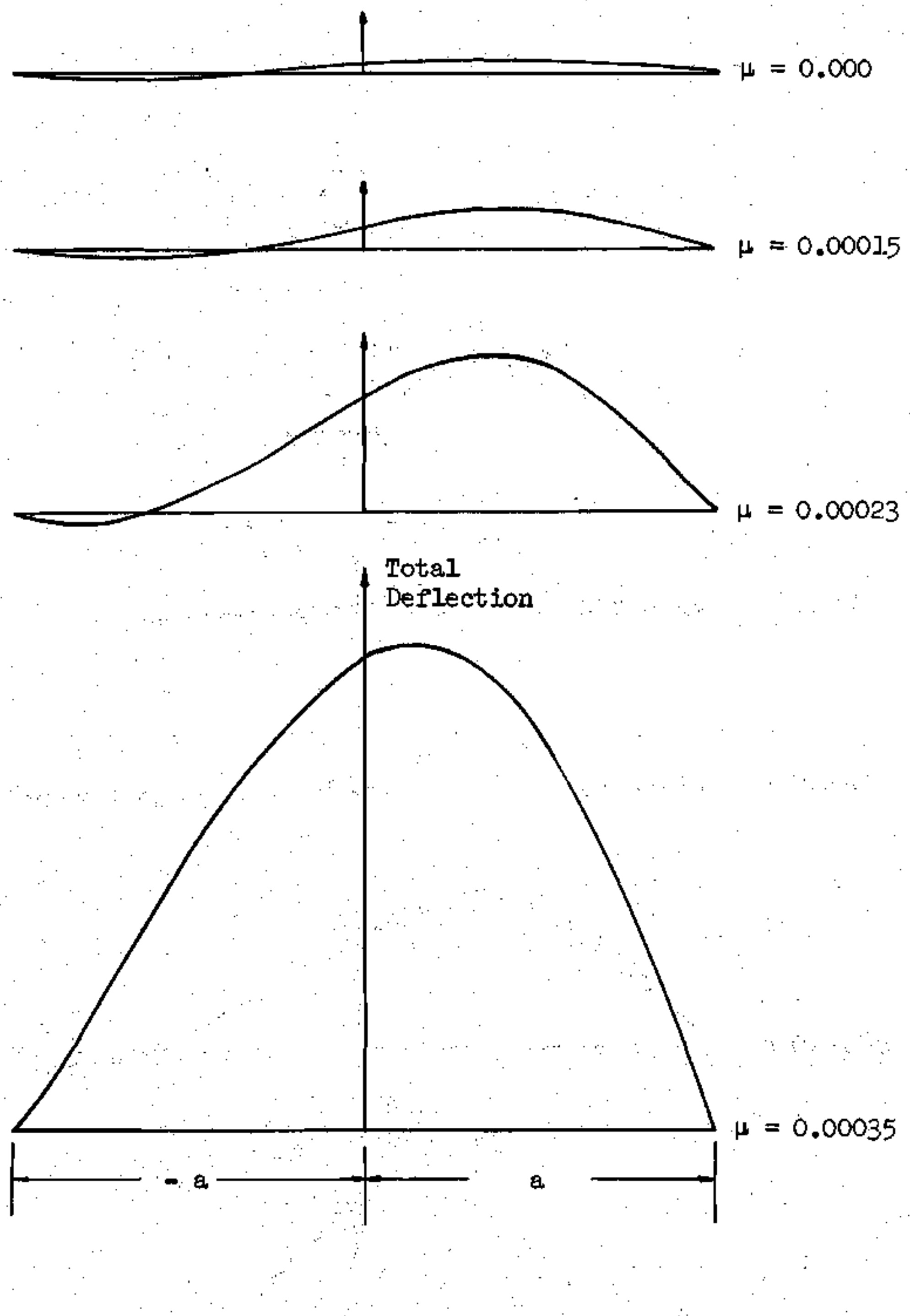

Figure IV-18. Deflection Profiles for $d_1 = d_2 = 0.01$, $r = 2.00$

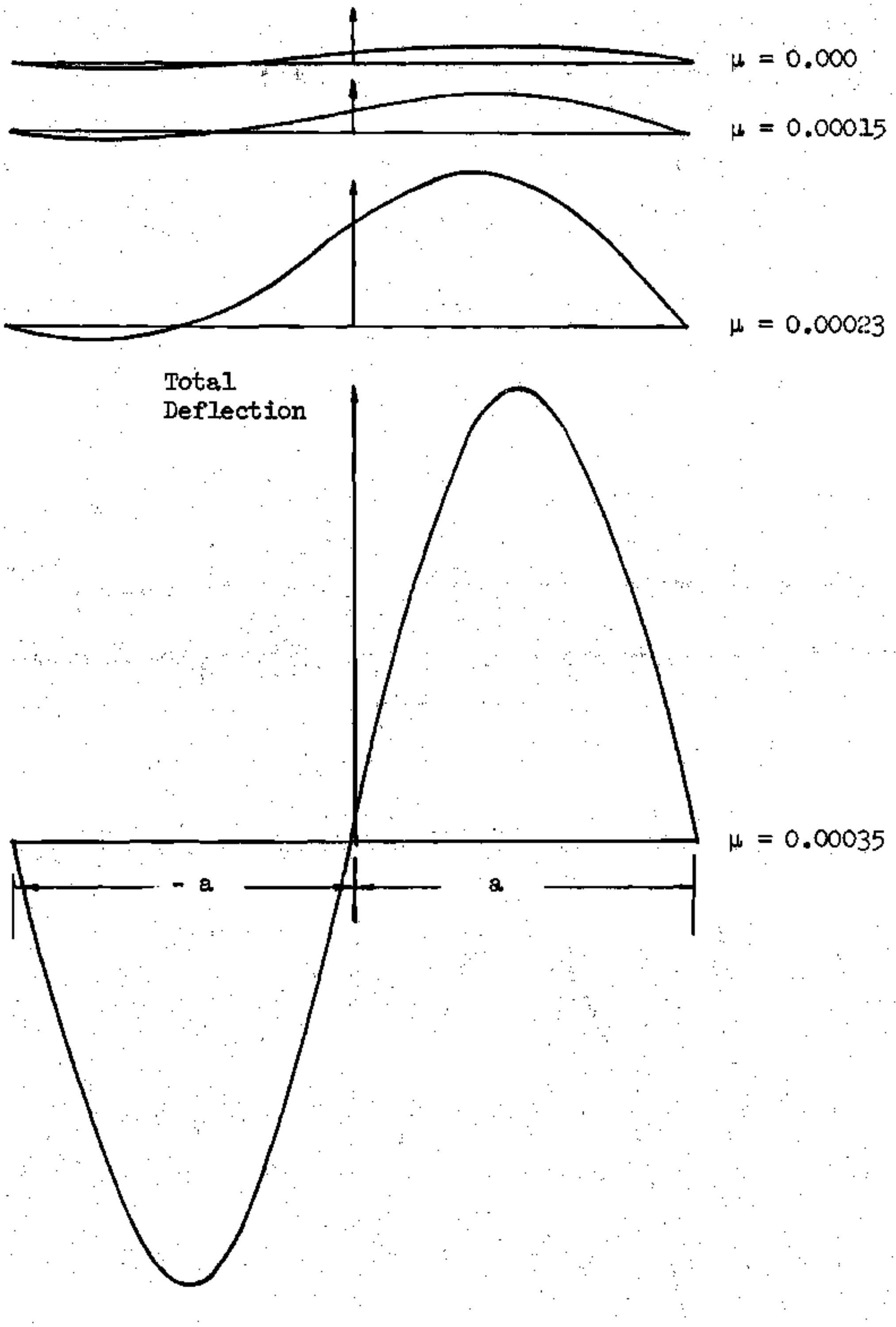

Figure IV-19. Deflection Profiles for $d_1 = d_2 = 0.01$, $r = 2.10$

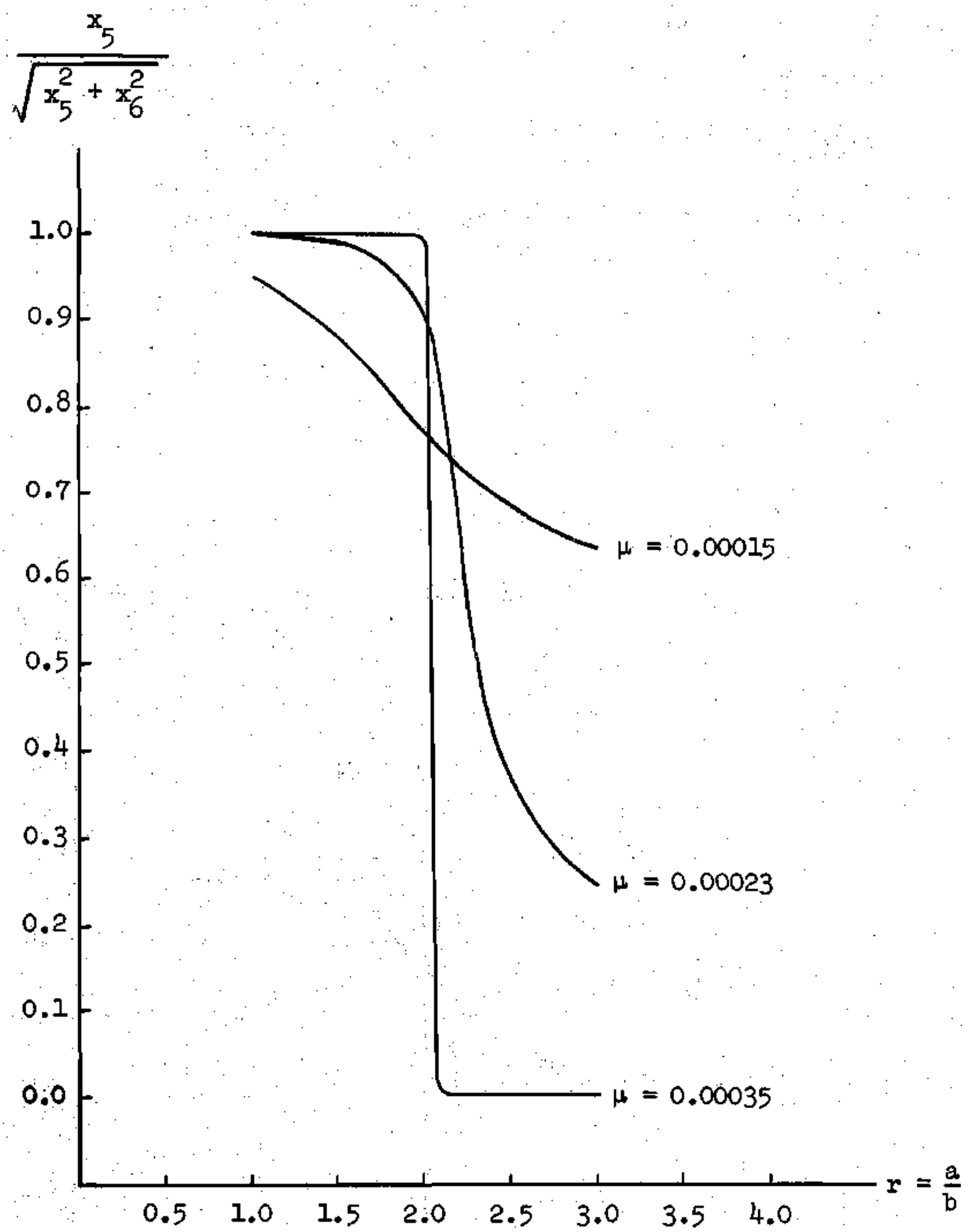

Figure IV-20. Deflection Parameter Versus Aspect Ratio for $d_1 = 0.01$, $d_2 = 0.01$

$\sqrt{x_5^2 + x_6^2}$ is introduced. This provides a measure of the "overall" deflection magnitude of the plate in terms of the components x_5 or x_6. Now, formation of the ratio $x_5 \Big/ \sqrt{x_5^2 + x_6^2}$ gives an indication of the content of the mode x_5. Note that the ratio $x_5 \Big/ \sqrt{x_5^2 + x_6^2} < 1$ when coupling is present.

In Figure IV-20 a plot of $x_5 \Big/ \sqrt{x_5^2 + x_6^2}$ versus the aspect ratio r is shown for different values of μ. The curve with a moderate slope throughout corresponds to $\mu = 0.00015$. This indicates that as the aspect ratio is increased from $r = 1.0$ to $r = 3$, the $x_5 \Big/ \sqrt{x_5^2 + x_6^2}$ quantity reduces at a small rate; i.e., the plate exhibits a coupled mode of deflection in which the half-sine wave mode is larger throughout. (The ratio is greater than 0.6 in the given range.)

The curve corresponding to $\mu = 0.00023$ ($\mu = 0.000233655$ is the critical strain of a flat plate with $r = 2$) shows that the change in the $x_5 \Big/ \sqrt{x_5^2 + x_6^2}$ quantity is in the vicinity of $r = 2$. This indicates that as r varies from 1.5 to 2.5, the deflected shape of the plate changes from a predominantly half-sine wave configuration to a two half-sine wave configuration.

The most dramatic change occurs under the loading $\mu = 0.00035$, note the precipitous drop of the curve for a small increase of the aspect ratio of 2.0.

The example illustrated in the preceding was concerned with plates whose imperfections d_1 and d_2 were equal. Generally, a given plate may well possess imperfections of varying orders of magnitude. To study such cases, calculations were made for plates whose imperfections d_1 and d_2 were unequal. By holding a given set of imperfections constant and varying the aspect ratio the modal composition was studied and graphs were drawn on the $x_5 - x_6$ plane seen in Figures IV-21 and IV-22. Note that in all of the cases studied, the behavior was coupled.

In Figure IV-21 the imperfection $d_1 \gg d_2$. As a consequence, in the initial stages of loading, the plates develop a modal composition such that the x_5 mode (associated with the d_1 imperfection) tends to dominate for the range $2 < r < 3$. The influence of the imperfection d_1 is especially appreciated in the light of the modal composition of the plate whose $r = 2.55$, where the x_5 component dominates throughout. For at this aspect ratio, the loading path of a corresponding flat plate would coincide with the x_6 axis.

In Figure IV-21 there is a separation of behavior regions depicted by dashed curve* which Supple has called the locus of imperfections [12]. The curves that lie above the separation ultimately exhibit a dominant x_6 component. It also was found that numerically unstable** results were obtained in the vicinity of the locus imperfections. Note that this type of behavior is clearly described in Figure IV-20.

---

* The dashed curve shown is not a result of computation.

** Within the range of values of aspect ratio where transition from dominance of one mode to another occurs, relatively large changes in x_5 or x_6 can be expected to occur with a small increase in μ. It follows that the derivatives of x_5 or x_6 with respect to μ would then be large. It is not, then, surprising that numerical instabilities are observed when computations within this range are attempted with the perturbation solution procedure used.

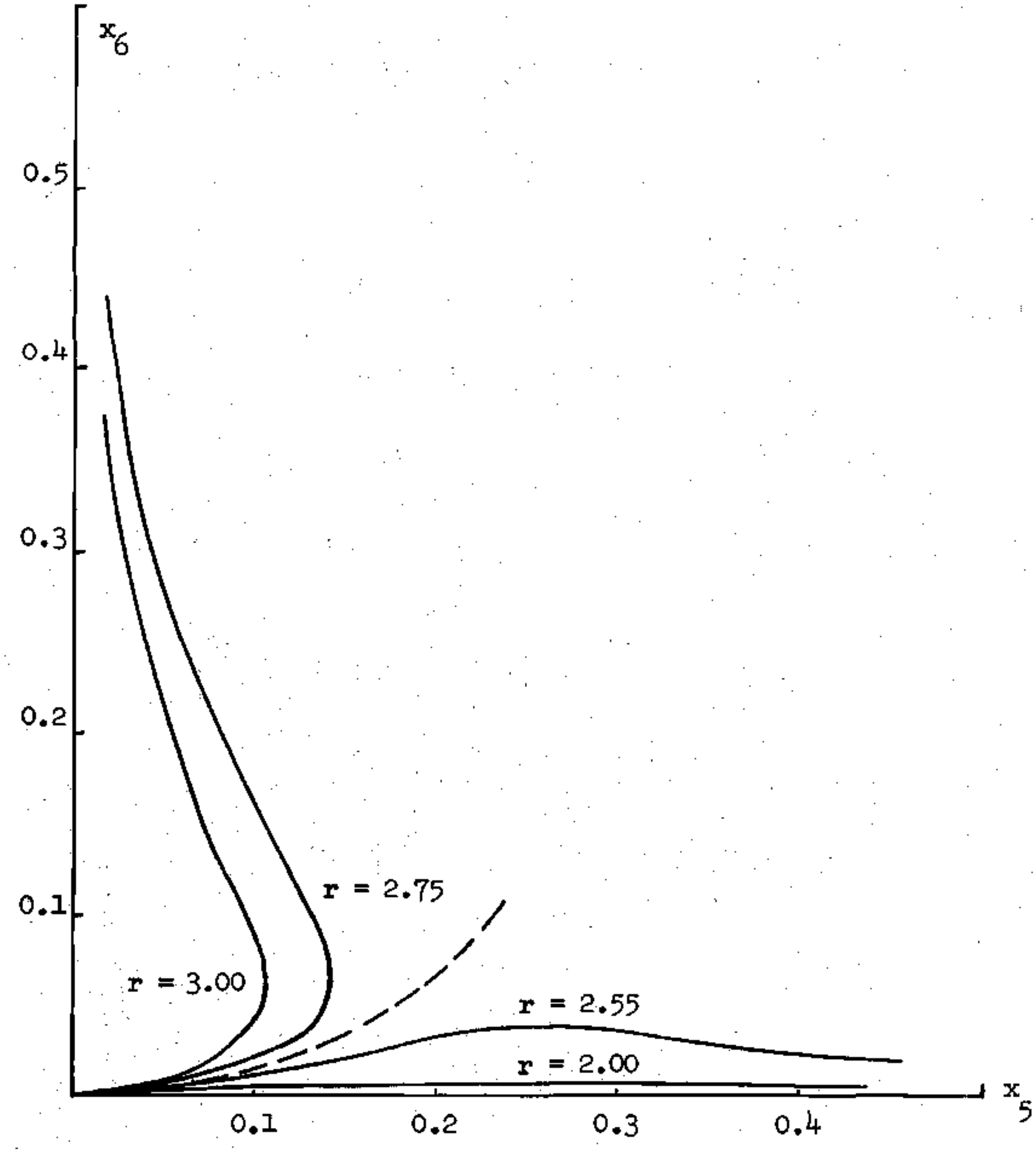

Figure IV-21. Effect of Aspect Ratio on x_6 Versus x_5 Diagram for $d_1 = 0.01$, $d_2 = 0.001$

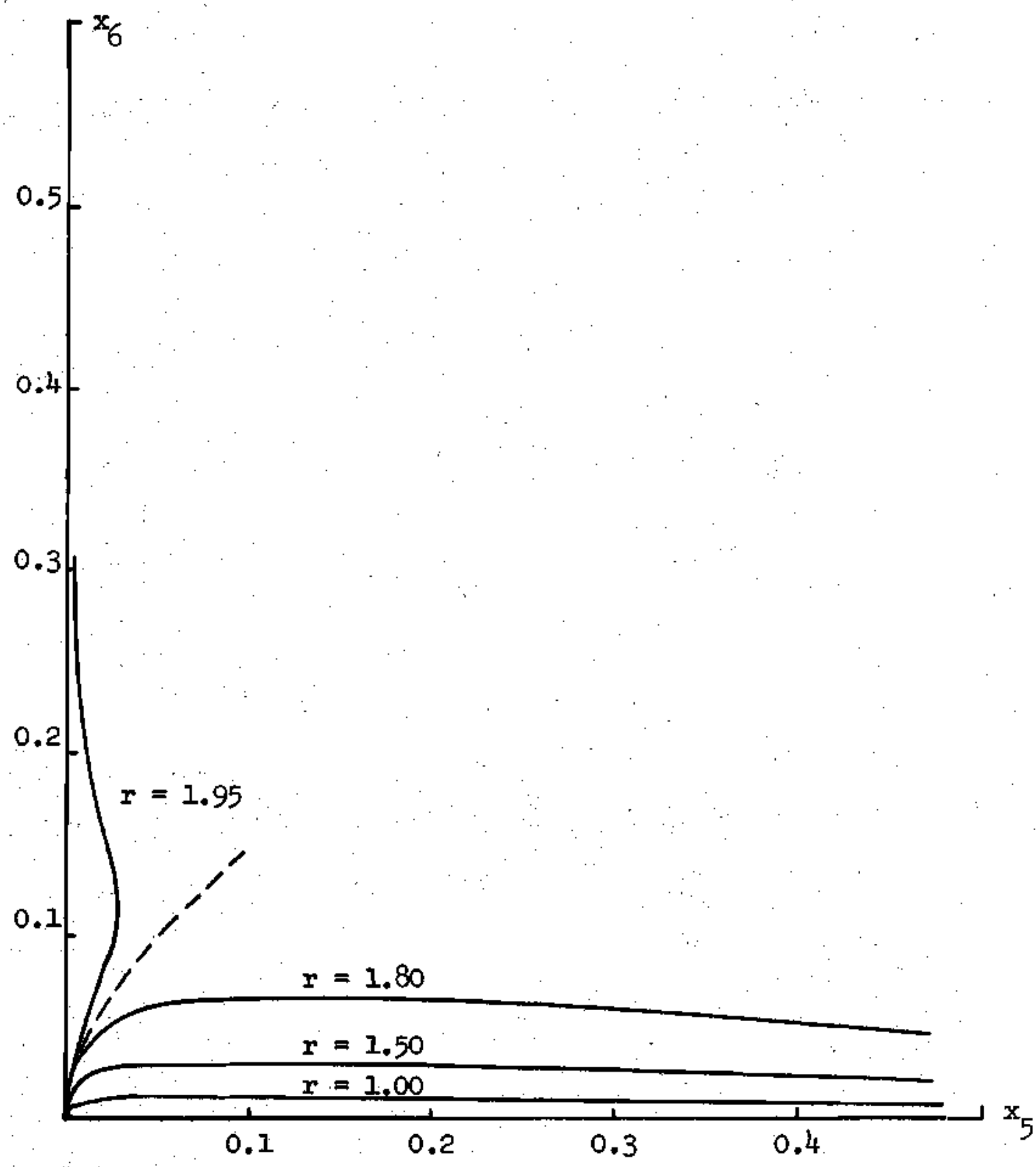

Figure IV-22. Effect of Aspect Ratio on x_6 Versus x_5 Diagram for $d_1 = 0.001$, $d_2 = 0.01$

In Figure IV-22, the order of the imperfections is reversed, i.e., $d_2 \gg d_1$ and the locus of imperfections is biased towards the x_6 axis. This indicates that at the initial stages of loading, the plates deflect and attain a modal shape with a more pronounced x_6 component. Here again, the importance of the imperfection should be emphasized vis a vis the modal composition of the plate whose $r = 1.95$. This plate would have had a loading path coincident with the x_5 axis, had it not been for the presence of a dominant d_2 imperfection.

In conclusion it would be plausible to expect that, at least in the initial stages of loading the modal composition of plates would be decided by the preponderance of a particular form of imperfection.

The observed sensitivity of modal composition to aspect ratio value is of interest in terms of its possible implication in the interpretation of experimental results. In a plate experiment the control of the boundary conditions is difficult. In fact development of uniform conditions of hinged edge support on four edges is very difficult to achieve. Further, as loading proceeds, and the plate deflects it is probable that the boundary conditions will be altered from those present at the start of the test. If this occurs, the effective dimensions of the plate may be changed and this in turn means that the effective aspect ratio may change. Since a change of aspect ratio of the order of several percent may occur, it follows that sudden changes in modal composition may occur if the initial value of aspect ratio is close to a critical value(in Figure IV-20, the plate with $d_1 = d_2 = 0.01$ has a critical value of $r = 2.05$).

Although there may be a temptation to identify such an observed sudden change as a bifurcation behavior, this would not, of course, be correct. It would, in the case cited be due to changes in the boundary conditions.

In the analysis of deflection of plates it was observed that, the imperfections d_1 and d_2 play a vital role in the determination of the modal composition. Hence, in the subsequent pages, attention is focused upon the direct effect of variations of imperfections on the deflection shapes of the plate.

To isolate the problem from other considerations, the aspect ratio was held constant at $r = 2.0$. Variations of imperfection were assigned consistently by letting $d_1 = 0.01$ throughout and changing d_2 from 0.001 to 0.05. The results of these calculations are presented in the x_5 versus x_6 graph shown in Figure IV-23.

Note again that in all of the cases studied, the behavior was coupled. The variation in behavior as d_2 increases is clear. For $d_1 = 0.01$ and $d_2 = 0.001$ the plate deflects in a very pronounced one half-sine wave shape as μ increases. This is reasonable, since d_1 imperfection (a half-sine wave shape) is much larger than the d_2 (two half-sine wave shape) imperfection.

The plate with a $d_1 = 0.01$ and $d_2 = 0.01$ still exhibits a dominant x_5 component. However, for $d_1 = 0.01$ and $d_2 = 0.02$ there is an abrupt change in the composition of the deflection pattern of the plate. Examining the curves for $d_1 = 0.01$ and $d_2 \geq 0.02$ it is clear that loading increases are accompanied by ultimate decreases in the x_5 component and increases of the x_6 component. This behavior indicates

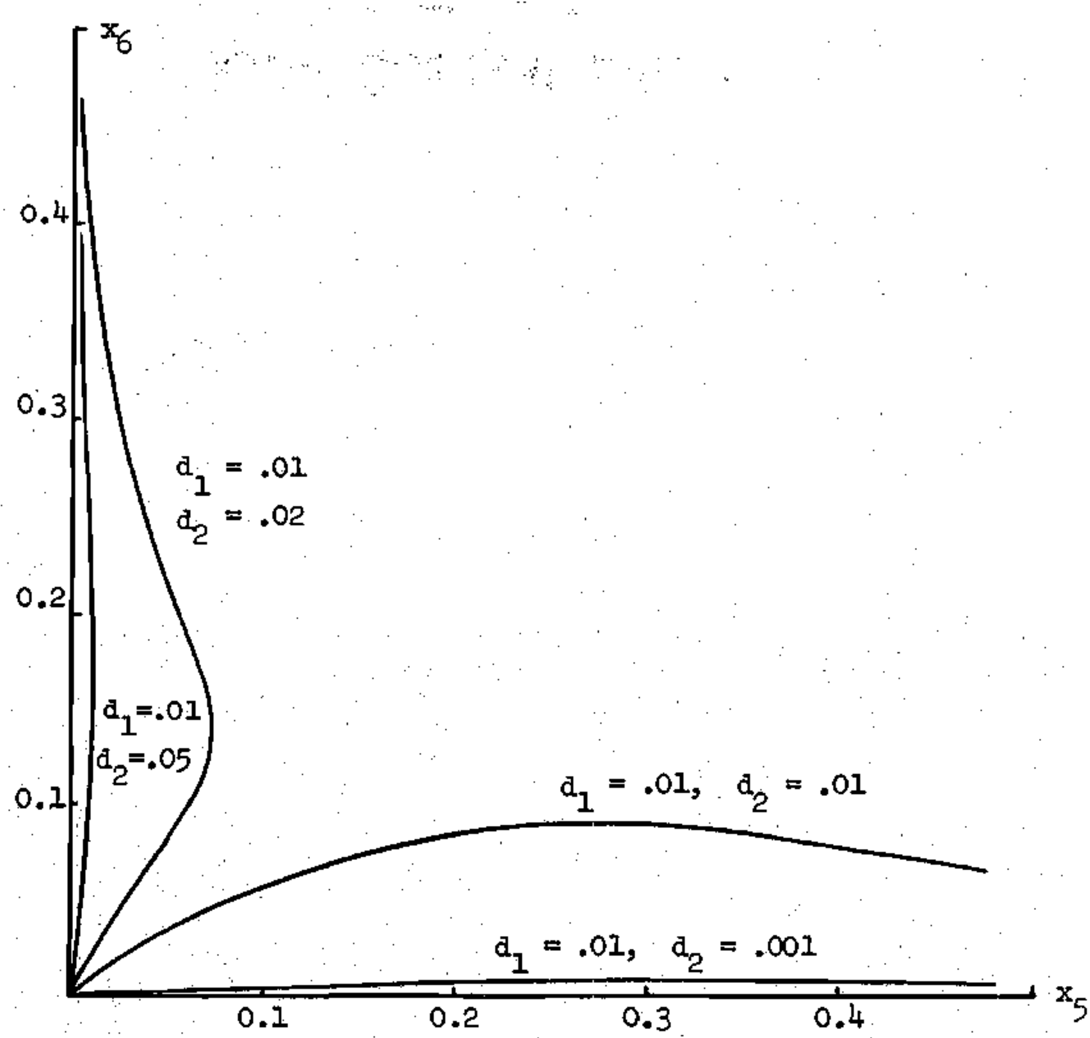

Figure IV-23. Effect of Imperfection on x_6 Versus x_5 Diagram for $r = 2$.

that it is possible for a plate with $r = 2$ to develop a deflection configuration in which the two half-sine wave mode dominates if d_2 is sufficiently large. The above numerical experiments emphasize again the fact that the phenomenon of changes in deflection pattern depends not only on the aspect ratio, but also upon the values of the imperfections.

It would also be interesting to examine the effect of changes in the imperfections of a plate whose aspect ratio > 2.3561. To that end a study was conducted for a plate for which $r = 3.0$, $d_1 = 0.01$ and $d_2 = 0.05$. Holding r and d_1 fixed the imperfection d_2 was reduced successively from 0.05 to zero. The results are presented in the $x_5 - x_6$ graphs shown in Figure IV-24.

It is not surprising that the plate with an aspect ratio > 2.3561 and a $d_2 = 0.05$ has a pronounced x_6 component. Note also that as d_2 is reduced to zero, the behavior of the plate is still coupled, and deflects with increasing x_6 component as the loading progresses. Furthermore, in the limit as $d_2 \rightarrow 0$ the graphs clearly indicate that a plate with both $d_1 \neq 0$ and $d_2 \neq 0$ conforms with the results obtained (see Figure IV-12) for a plate (with $d_2 = 0$) through the algebraic technique.

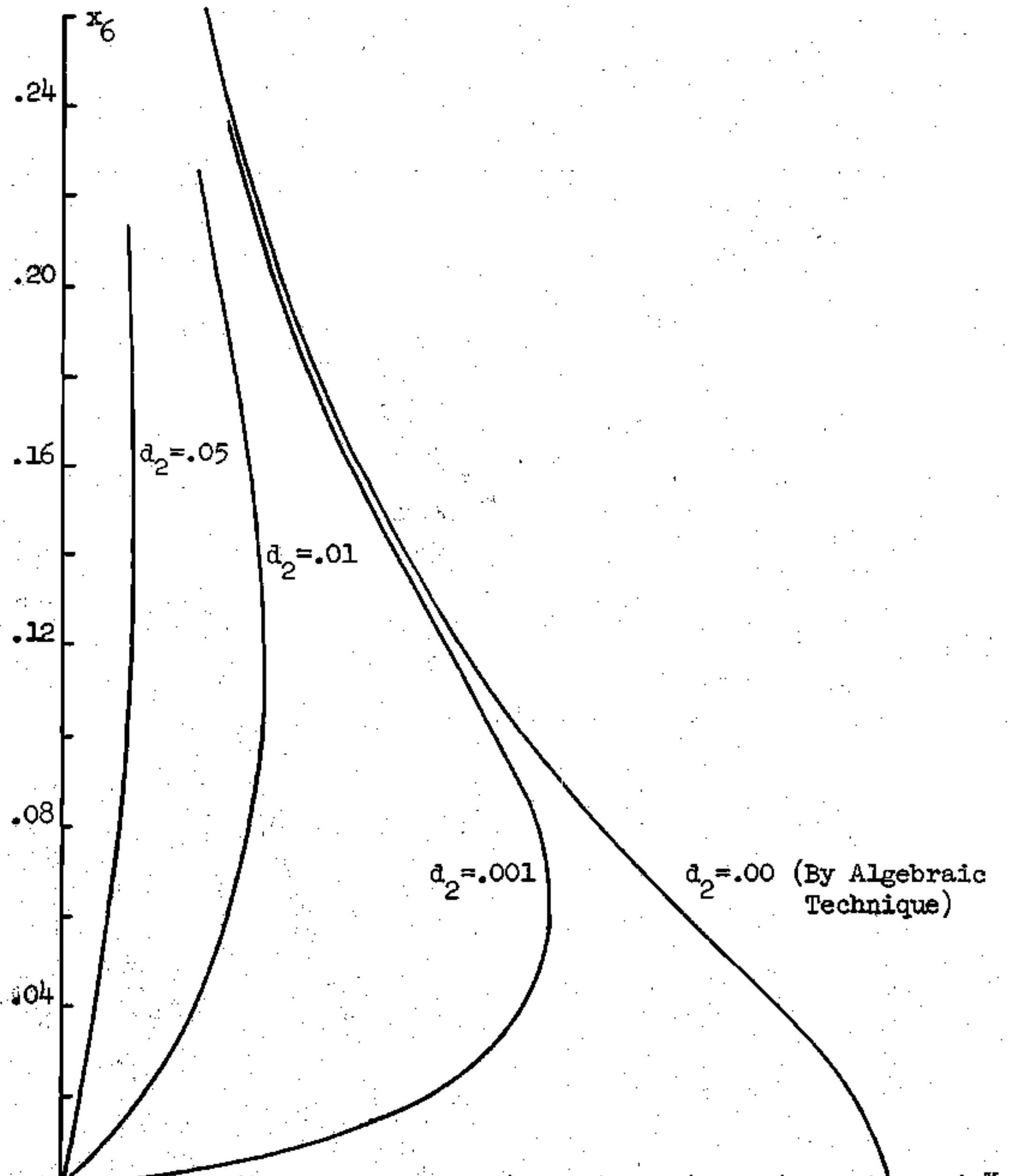

Figure IV-24. Effect of Imperfection on x_6 Versus x_5 Diagram for d_1 = .01, r = 3

CHAPTER V

CONCLUSIONS

The objective of this research was to examine the effect of aspect ratio and prescribed initial imperfections on the modal composition of an elastic plate subjected to compressive loading. The analysis of the problem was developed by deriving the associated total potential energy functional of the system. The Ritz approximation technique was then used to obtain a set of nonlinear equations that defined equilibrium configurations. A perturbation solution procedure was then adopted to solve these equations for various aspect ratios and imperfections. In some instances singularities inherent to the problem precluded the use of the perturbation method. These obstacles were circumvented by seeking recourse to an alternate solution technique. This consisted of an algebraic approach in which the equations were reduced to a manageable form by an elimination procedure.

The data generated were presented by use of a representation used by Supple [11]. This consists of describing the modal composition in terms of two degrees of freedom. In the present work the corresponding variables were designated as x_5 and x_6 and they described the magnitudes of the modal components of the transverse deflection of the plate. The resulting curves indicated the variation in modal composition during the loading history.

A perfectly flat plate subjected to compressive loads was first examined. It was found that, for an aspect ratio below a certain transition value, the natural loading path was an uncoupled mode represented by a line coincident with the x_5 axis. A coupled path was found to develop by bifurcation from the x_6 axis. It was not, however, accessible from the natural loading path.

A similar plate with an aspect ratio greater than the transition value was then examined, and it was found that its modal behavior was the same as the previous case with the roles of the x_5 and the x_6 variables reversed.

A different plate problem with an imperfection denoted by d_1 resembling the x_5 mode was then analyzed. It was observed that for an aspect ratio below a transition value the natural loading path was an uncoupled mode coinciding with the x_5 axis. A coupled mode was also observed to be present. It did not form by bifurcation and it was not accessible from the natural loading path.

The plate with the d_1 present had a different modal behavior for an aspect ratio greater than the transition value. A coupled mode bifurcating from the natural loading path (x_5 axis for this case) was observed to develop. The curve corresponding to this path became detached from the natural loading path for large values of d_1, however.

The main purpose of this research was to study plates with both imperfections d_1 and d_2 (the latter resembling the x_6 modal shape) present in varying degrees. It was determined that under a compressive loading, the modal composition behavior of the plate depended on changes of the aspect ratio when $d_1 = d_2$. For a transitional range of values of the aspect ratio, the compressed plate changed its modal composition from a predominantly x_5 mode, to one of x_6.

Numerical experiments were also conducted to study plates whose imperfection $d_1 \gg d_2$. The results show that for the range of aspect ratios studied, the plates initially tended to develop a modal composition such that the x_5 mode (resembling the d_1 imperfection) was dominant. Computations were also performed on plates with imperfection $d_2 \gg d_1$. During the initial stages of loading, the plates developed a modal composition with a pronounced x_6 component (resembling the d_2 imperfection). As loading was increased, the aspect ratio considerations controlled the modal composition behavior, i.e., for high aspect ratios the x_6 component became larger, while for low aspect ratios the x_5 component became dominant.

Similar experiments were also conducted by holding the aspect ratio fixed and changing the imperfections. The results of these experiments indicate that plates will initially deflect with a pronounced x_6 component if $d_2 \gg d_1$, and deflect in a dominant x_5 component if $d_1 \gg d_2$.

A general conclusion reached therefore was: the relative magnitude of imperfections present controls the modal composition of plates during the early stages of loading. Ultimately, as the loading increases, the plates with a high aspect ratio will tend to develop a modal composition that has a more pronounced x_6 component. It was shown that plates with a low aspect ratio will exhibit a modal composition that has a larger x_5 component.

CHAPTER VI

RECOMMENDATIONS FOR FUTURE RESEARCH

The modal coupling behavior of elastic rectangular plates possessing a prescribed imperfection and various aspect ratios were studied. A more thorough understanding of this behavior would be attained through extensions of the present work. Recommendations for future research in this field are suggested in the itemized discussion as follows:

1. The boundary conditions of the problem studied were simply supported. This is not a prevalant condition for such structures. A more realistic model could be envisioned if one is to allow some form of constraint at the boundaries. These changes would appreciably alter the modal behavior, and may elucidate the behavior further.

2. Changing the boundary conditions would also necessitate changes in the displacement functions selected. While it is true that an approximate solution can be obtained by the use of six displacement functions, it is strongly recommended that more functions be included to allow more degrees of freedom. A perturbation method similar to the one used in this research would be recommended, especially if a great number of degrees of freedom are allowed for the system. The unknowns are calculated simultaneously by this method, and, generally, it is easily adaptable for the computer.

3. The problem of selection of the deflection functions is further compounded by the nature of the prescribed imperfections. When displacements of more degrees of freedom, as noted in item 2 above, are considered, then additional corresponding imperfection modes should also be included.

4. It would be interesting to set up an experimental program to test various specimens to verify the results of this research. Special attention should be directed towards developing controlled conditions which makes it possible to observe the effect of changes in boundary conditions during tests.

5. In the research that was conducted it was discovered that there sometimes was no access from the natural loading path to other stable branches. It would be of interest to investigate the possibility of a dynamic transverse disturbance causing the structure to jump from the equilibrium branch associated with the natural loading path to a branch which is, under static conditions, inaccessible.

6. Plates having a variable thickness, having an anisotropy, or even subjected to temperature gradients could also be investigated. The extent to which these changes would effect the modal coupling behavior would be of practical interest.

APPENDIX A

TOTAL POTENTIAL ENERGY

From Chapter III the total potential energy $\bar{\Pi}$ can be expressed in the form

$$\bar{\Pi} = \int_{-a}^{a}\int_{-b}^{b} \frac{Eh}{2(1-\nu^2)} \left\{\bar{\epsilon}_x^{o\,2} + \bar{\epsilon}_y^{o\,2} + 2\,\nu\bar{\epsilon}_x^o\bar{\epsilon}_y^o + \frac{1}{2}\,(1-\nu)\bar{\gamma}_{xy}^2\right\} d\bar{x}d\bar{y} \tag{A-1}$$

$$+ \int_{-a}^{a}\int_{-b}^{b} \frac{D}{2}\left\{\left(\frac{\partial^2\bar{w}}{\partial\bar{x}^2} + \frac{\partial^2\bar{w}}{\partial\bar{y}^2}\right)^2 - 2(1-\nu)\left[\frac{\partial^2\bar{w}}{\partial\bar{x}^2}\;\frac{\partial^2\bar{w}}{\partial\bar{y}^2} - \left(\frac{\partial^2\bar{w}}{\partial\bar{x}\partial\bar{y}}\right)^2\right]\right\} d\bar{x}d\bar{y}\ ^*$$

Using nondimensionalization parameters defined by

$$x = \frac{\bar{x}}{b}\,,\quad y = \frac{\bar{y}}{a}\,,\quad z = \frac{\bar{z}}{h}\,,\quad w = \frac{\bar{w}}{h}\,,\quad u = \frac{\bar{u}}{\eta}\,,\quad v = \frac{\bar{v}}{\eta} \tag{A-2}$$

$$\Pi = \int_{-1}^{1}\int_{-1}^{1} \left\{\bar{\epsilon}_x^{o\,2} + \bar{\epsilon}_y^{o\,2} + 2\,\nu\bar{\epsilon}_x^o\bar{\epsilon}_y^o + D_2\,\bar{\gamma}_{xy}^{o\,2}\right\} dxdy \tag{A-3}$$

$$+ \frac{D_3}{D_1}\int_{-1}^{1}\int_{-1}^{1}\left\{\left(\frac{h}{b^2}\;\frac{\partial^2 w}{\partial x^2} + \frac{h}{a^2}\;\frac{\partial^2 w}{\partial y^2}\right)^2 - D_4\left[\frac{h^2}{a^2h^2}\;\frac{\partial^2 w}{\partial x^2}\;\frac{\partial^2 w}{\partial y^2}\right.\right.$$

$$\left.\left. - \left(\frac{h}{ab}\;\frac{\partial^2 w}{\partial x\partial y}\right)^2\right]\right\} dxdy$$

---

* Quantities with a bar on top are dimensional.

where

$$D_1 = \frac{Eh}{2(1-\nu^2)}$$

$$D_2 = \frac{1}{2}(1-\nu)$$

$$D_3 = \frac{D}{2} = \frac{Eh^3}{24(1-\nu^2)} \tag{A-4}$$

$$D_4 = 2(1-\nu)$$

$$\frac{D_3}{D_1} = \frac{h^2}{12}$$

Expressing the strains $\bar{\epsilon}_x^o$, $\bar{\epsilon}_y^o$ and $\bar{\gamma}_{xy}^o$ through the displacement functions as defined in Chapter II

$$\begin{aligned} u &= a_i X_i \\ v &= b_i \Psi_i - \mu y \\ w &= c_i \phi_i \\ w_o &= d_i \phi_i \end{aligned} \tag{A-5}$$

$$\bar{\epsilon}_x^o = \frac{\partial \bar{u}}{\partial \bar{x}} + \frac{1}{2}\left\{\frac{\partial}{\partial \bar{x}}\left(\bar{w}_o + \bar{w}\right)\right\}^2 - \frac{1}{2}\left(\frac{\partial \bar{w}}{\partial \bar{x}}\right)^2 \tag{A-6}$$

$$= \left(\frac{\eta}{b}\right)\frac{\partial u}{\partial x} + \frac{1}{2}\left\{\left(\frac{h}{b}\right)\frac{\partial}{\partial x}\left(w_o + w\right)\right\}^2 - \frac{1}{2}\left\{\left(\frac{h}{b}\right)\frac{\partial w_o}{\partial x}\right\}^2$$

$$= \left(\frac{\eta}{b}\right) a_i \chi_{i,x} + \frac{1}{2}\left\{\left(\frac{h}{b}\right)\left(d_i + c_i\right)\phi_{i,x}\right\}^2 - \frac{1}{2}\left\{\left(\frac{h}{b}\right) d_i \phi_{i,x}\right\}^2$$

$$= \left(\frac{\eta}{b}\right) a_i \chi_{i,x} + \frac{1}{2}\ \frac{h^2}{b^2}\left(2\ c_i d_j + c_i c_j\right)\phi_{i,x}\ \phi_{j,x}$$

$$\bar{\epsilon}_x^{o\,2} = \left(\frac{\eta^2}{b^2}\right) a_i a_j \chi_{i,x} \chi_{j,x} \tag{A-7}$$

$$+ \frac{1}{4}\ \frac{h^4}{b^4}\left(2\ c_i d_i + c_i c_j\right)\left(2\ c_m d_n + c_m c_n\right)\phi_{i,x}\phi_{j,x}\phi_{m,x}\phi_{n,x}$$

$$+ \left(\frac{\eta h^2}{b^3}\right)\left(2\ c_i d_i + c_i c_j\right) a_m\ \chi_{m,x}\ \phi_{i,x}\ \phi_{j,x}$$

$$\bar{\epsilon}_y^o = \frac{\partial \bar{v}}{\partial \bar{y}} + \frac{1}{2}\left\{\frac{\partial}{\partial \bar{y}}\left(\bar{w}_o + \bar{w}\right)\right\}^2 - \frac{1}{2}\left(\frac{\partial \bar{w}_o}{\partial \bar{y}}\right)^2 \tag{A-8}$$

$$= \left(\frac{\eta}{a}\right)\frac{\partial v}{\partial y} + \frac{1}{2}\left\{\frac{h}{a}\left(d_i + c_i\right)\phi_{i,y}\right\}^2 - \frac{1}{2}\left\{\frac{h}{a} d_i \phi_{i,y}\right\}^2$$

$$= \left(\frac{\eta}{a}\right) b_i \Psi_{i,y} - \left(\frac{\eta\mu}{a}\right) + \frac{1}{2}\ \frac{h^2}{a^2}\left(2\ c_i d_j + c_i c_j\right)\phi_{i,y}\phi_{j,y}$$

$$\bar{\epsilon}_y^{o\,2} = \frac{\eta^2}{a^2} b_i b_j \Psi_{i,y}\Psi_{j,y} + \frac{\eta^2\mu^2}{a^2} \tag{A-9}$$

$$+ \frac{1}{4}\ \frac{h^4}{a^4}\left(2\ c_i d_j + c_i c_j\right)\left(2\ c_m d_n + c_m c_n\right)\phi_{i,y}\phi_{j,y}\phi_{m,y}\phi_{n,y}$$

$$- \frac{2\eta^2\mu}{a^2} b_i \Psi_{i,y} + \frac{\eta h^2}{a^3}\left(2\ c_i d_j + c_i c_j\right) b_m \Psi_{m,y}\phi_{i,y}\phi_{j,y}$$

$$- \frac{\eta h^2 \mu}{a^2}\left(2\ c_i d_j + c_i c_j\right)\phi_{i,y}\ \phi_{j,y}$$

$$\bar{\epsilon}_x^o \, \bar{\epsilon}_y^o = \left(\frac{\eta^2}{ab}\right) a_i b_i \chi_{i,x} \Psi_{j,y} - \left(\frac{\eta^2 \mu}{ab}\right) a_i \chi_{i,x} \tag{A-10}$$

$$+ \frac{\eta h^2}{2a^2 b} \left(2\, c_i d_j + c_i c_j\right) a_m \chi_{m,x} \phi_{i,y} \phi_{j,y}$$

$$+ \frac{\eta h^2}{2ab} \left(2\, c_i d_j + c_i c_j\right) b_m \Psi_{m,y} \phi_{i,x} \phi_{j,x}$$

$$- \frac{\eta \mu h^2}{2ab^2} \left(2\, c_i d_j + c_i c_j\right) \phi_{i,x}\, \phi_{j,x}$$

$$+ \frac{1}{4} \, \frac{h^4}{a^2 b^2} \left(2\, c_i d_j + c_i c_j\right)\left(2\, c_m d_n + c_m c_n\right) \phi_{i,x} \phi_{j,x} \phi_{m,y} \phi_{n,y}$$

$$\bar{\gamma}_{xy}^o = \left(\frac{\eta}{a}\right) \frac{\partial u}{\partial y} + \left(\frac{\eta}{b}\right) \frac{\partial v}{\partial x} + \frac{h}{b} \, \frac{\partial}{\partial x} \left(w_o + w\right) \frac{h}{a} \frac{\partial}{\partial y} \left(w_o + w\right) \tag{A-11}$$

$$- \frac{h}{b} \, \frac{\partial w_o}{\partial x} \, \frac{h}{a} \, \frac{\partial w_o}{\partial y}$$

$$= \left(\frac{\eta}{a}\right) a_i \chi_{i,y} + \left(\frac{\eta}{b}\right) b_i \Psi_{i,x} + \frac{h^2}{ab} \left(2\, d_i c_j + c_i c_j\right) \phi_{i,x} \phi_{j,y}$$

$$\bar{\gamma}_{xy}^{o\,2} = \left(\frac{\eta^2}{a^2}\right) a_i a_j \chi_{i,y} \chi_{j,y} + \left(\frac{\eta^2}{b^2}\right)^2 b_i b_j \Psi_{i,x} \Psi_{j,x} \tag{A-12}$$

$$+ \left(\frac{h^4}{a^2 b^2}\right)\left(2\ d_i c_i + c_i c_j\right)\left(2\ d_m c_n + c_m c_n\right) \phi_{i,x} \phi_{j,y} \phi_{m,x} \phi_{n,y}$$

$$+ \left(\frac{2\eta^2}{ab}\right) a_i b_m \chi_{i,y} \Psi_{m,x} + \left(\frac{2\eta h^2}{a^2 b}\right)\left(2\ d_i c_j + c_i c_j\right) a_m \chi_{m,y} \phi_{i,x} \phi_{j,y}$$

$$+ \left(\frac{2\eta h^2}{ab^2}\right)\left(2\ d_i c_j + c_i c_j\right) b_m \Psi_{m,x} \phi_{i,x} \phi_{j,y}$$

$$\left\{\frac{\partial^2 \bar{w}}{\partial \bar{x}^2} + \frac{\partial^2 \bar{w}}{\partial \bar{y}^2}\right\}^2 = \left\{\frac{h}{b^2} \frac{\partial^2 w}{\partial x^2} + \frac{h}{a^2} \frac{\partial^2 w}{\partial y^2}\right\}^2 \tag{A-13}$$

$$= \left\{\frac{h}{b^2} c_i \phi_{i,xx} + \frac{h}{a^2} c_i \phi_{i,yy}\right\}^2$$

$$= \frac{h^2}{b^4} c_i c_j \phi_{i,xx} \phi_{j,xx} + \frac{h^2}{a^4} c_i c_j \phi_{i,yy} \phi_{j,yy}$$

$$+ \left(\frac{2h^2}{a^2 b^2}\right) c_i c_j \phi_{i,xx} \phi_{j,yy}$$

$$\left\{\frac{\partial^2 \bar{w}}{\partial \bar{x}^2} \frac{\partial^2 \bar{w}}{\partial \bar{y}^2} - \left(\frac{\partial^2 \bar{w}}{\partial \bar{x} \partial \bar{y}}\right)^2\right\} = \left\{\frac{h}{b^2} \frac{\partial^2 w}{\partial x^2} \cdot \frac{h}{a^2} \frac{\partial^2 w}{\partial y^2} - \left(\frac{h}{ab} \frac{\partial^2 w}{\partial x \partial y}\right)^2\right\} \tag{A-14}$$

$$= \frac{h^2}{a^2 b^2} c_i \phi_{i,xx} c_j \phi_{j,yy} - \left(\frac{h^2}{a^2 b^2}\right) c_i c_j \phi_{i,xy} \phi_{j,xy}$$

Substitution of (A-4) to (A-14) into (A-3) gives the total potential Π in terms of the generalized displacements.

APPENDIX B

THE RITZ PROCEDURE

To find the equilibrium state, we extremize Π through the Ritz procedure by taking partials with respect to a_i, b_i and c_i as follows.

$$\frac{\partial \Pi}{\partial a_r} = 0 \quad r = 1, 2$$

$$\frac{\partial \Pi}{\partial b_r} = 0 \tag{B-1}$$

$$\frac{\partial \Pi}{\partial c_r} = 0$$

$$\frac{\partial \Pi}{\partial a_r} = \frac{\partial}{\partial a_r} \int_{-1}^{1} \int_{-1}^{1} \left\{ \bar{\epsilon}_x^{o^2} + \bar{\epsilon}_y^{o^2} + \ldots \right\} dxdy \tag{B-2}$$

$$= \int_{-1}^{1} \int_{-1}^{1} \left\{ \frac{\partial}{\partial a_r} \left(\bar{\epsilon}_x^o\right)^2 + \frac{\partial}{\partial a_r} \left(\bar{\epsilon}_y^o\right)^2 + \ldots \right\} dxdy$$

where $\bar{\epsilon}_x^o$, $\bar{\epsilon}_y^o$, ... are derived in Appendix A.

$$\frac{\partial}{\partial a_r}\left(\bar{\varepsilon}^{o^2}_x\right) = 2\ \bar{\varepsilon}^o_x \cdot \frac{\partial \bar{\varepsilon}^o_x}{\partial a_r} \tag{B-3}$$

$$= 2\ \bar{\varepsilon}^o_x \cdot \frac{\partial}{\partial a_r}\left[\left(\frac{\eta}{b}\right) a_i \chi_{i,x} + \frac{1}{2}\frac{h^2}{b^2}\left(2\ c_i d_j + c_i c_j\right) \phi_{i,j}\phi_{j,x}\right]$$

$$= \left(\frac{2\eta}{b}\right)\ \bar{\varepsilon}^o_x \cdot \frac{\partial a_i}{\partial a_r}\chi_{i,x} = \left(\frac{2\eta}{b}\right)\bar{\varepsilon}^o_x\ \delta_{ir}\ \chi_{i,x} = \left(\frac{2\eta}{b}\right)\bar{\varepsilon}^o_x\ \chi_{r,x}$$

$$= \left(\frac{2\eta}{b}\right)\left[\left(\frac{\eta}{b}\right) a_i \chi_{i,x} + \frac{1}{2}\ \frac{h^2}{b^2}\left(2\ c_i d_j + c_i c_j\right) \phi_{i,x}\phi_{j,x}\right]\chi_{r,x}$$

$$= \left(\frac{2\eta^2}{b^2}\right) a_i \chi_{i,x}\chi_{r,x} + \frac{\eta h^2}{b^3}\left(2\ c_i d_j + c_i c_j\right) \phi_{i,x}\phi_{j,x}\chi_{r,x}$$

$$\frac{\partial\left(\bar{\varepsilon}^{o^2}_y\right)}{\partial a_r} = 0 \tag{B-4}$$

Since $\bar{\varepsilon}^o_y$ is not a function of a_r.

$$\frac{\partial\left(\bar{\epsilon}^o_x\ \bar{\epsilon}^o_y\right)}{\partial a_r} = \bar{\epsilon}^o_x\ \frac{\partial \bar{\epsilon}^o_y}{\partial a_r} + \bar{\epsilon}^o_y\ \frac{\partial \bar{\epsilon}^o_x}{\partial a_r} = \bar{\epsilon}^o_y \left(\frac{\eta}{b}\right) \delta_{ir}\, \chi_{i,x} \tag{B-5}$$

$$= \left(\frac{\eta^2}{ab}\right) b_i \Psi_{i,y} \chi_{r,x} - \left(\frac{\eta^2 \mu}{ab}\right) \chi_{r,x}$$

$$+ \frac{\eta h^2}{2a^2 b} \left(2\ c_i d_j + c_i c_j\right) \phi_{i,y} \phi_{j,y} \chi_{r,x}$$

$$\frac{\partial}{\partial a_r} \left(\bar{\gamma}^o_{xy}\right)^2 = 2\ \bar{\gamma}_{xy}\ \frac{\partial \bar{\gamma}^o_{xy}}{\partial a_r} = 2\ \bar{\gamma}^o_{xy} \left(\frac{\eta}{a}\right) \frac{\partial a_i}{\partial a_r} \chi_{r,y} = \left(\frac{2\eta}{a}\right) \bar{\gamma}^o_{xy}\ \chi_{r,y} \tag{B-6}$$

$$= \frac{2\eta^2}{a^2} a_i\, \chi_{i,y}\, \chi_{r,y} + \left(\frac{2\eta^2}{ab}\right) b_i \Psi_{i,x}\, \chi_{r,y}$$

$$+ \frac{2\eta h^2}{a^2 b} \left(2\ c_i d_j + c_i c_j\right) \phi_{i,x} \phi_{j,y} \chi_{r,y}$$

$$\frac{\partial}{\partial a_r} \left\{\left(\frac{\partial^2 \bar{w}}{\partial \bar{x}^2} + \frac{\partial^2 \bar{w}}{\partial \bar{y}^2}\right)^2 - 2(1-\nu) \left[\frac{\partial^2 \bar{w}}{\partial \bar{x}^2}\ \frac{\partial^2 \bar{w}}{\partial \bar{y}^2} - \left(\frac{\partial^2 \bar{w}}{\partial \bar{x} \partial \bar{y}}\right)^2\right.\right\} = 0 \tag{B-7}$$

Since $\bar{w}$ and its derivatives are not functions of a_r.

$$\frac{\partial}{\partial b_r}\left(\bar{\epsilon}_x^o\right) = 0 \tag{B-8}$$

$$\frac{\partial}{\partial b_r}\left(\bar{\epsilon}_y^o\right)^2 = 2\ \bar{\epsilon}_y^o \cdot \frac{\partial \bar{\epsilon}_y^o}{\partial b_r} = 2\ \bar{\epsilon}_y^o \left(\frac{\eta}{a}\right) \delta_{ir}\ \Psi_{i,y} = 2\ \bar{\epsilon}_y^o \cdot \left(\frac{\eta}{a}\right) \Psi_{r,y} \tag{B-9}$$

$$= \left(\frac{2\eta^2}{a^2}\right) b_i \Psi_{i,y} \Psi_{r,y} - \left(\frac{2\eta^2 \mu}{a^2}\right) \Psi_{r,y}$$

$$+ \left(\frac{\eta h^2}{a^3}\right)\left(2\ c_i d_j + c_i c_j\right) \phi_{i,y} \phi_{j,y} \Psi_{r,y}$$

$$\frac{\partial}{\partial b_r}\left(\bar{\epsilon}_x^o \bar{\epsilon}_y^o\right) = \bar{\epsilon}_x^o \left(\frac{\eta}{a}\right) \delta_{ir}\ \Psi_{i,y} + \bar{\epsilon}_y(o) = \bar{\epsilon}_x^o \left(\frac{\eta}{a}\right) \Psi_{r,y} \tag{B-10}$$

$$= \left(\frac{\eta^2}{ab}\right) a_i X_{i,x} \Psi_{r,y} + \left(\frac{\eta h^2}{2ab^2}\right)\left(2\ c_i d_j + c_i c_j\right) \phi_{i,x} \phi_{j,x} \Psi_{r,y}$$

$$\frac{\partial}{\partial b_r}\left(\bar{\gamma}^{o}_{xy}\right)^2 = 2\bar{\gamma}_{xy} \cdot \frac{\partial \bar{\gamma}_{xy}}{\partial b_r} = 2\bar{\gamma}_{xy}\left(\frac{\eta}{b}\right)\Psi_{r,x} \tag{B-11}$$

$$= \left(\frac{2\eta^2}{ab}\right) a_i \chi_{i,y}\Psi_{r,x} + \left(\frac{2\eta^2}{b^2}\right) b_i \Psi_{i,x}\Psi_{r,x}$$

$$+ \left(\frac{2\eta h^2}{ab^2}\right)\left(2\ c_i d_j + c_i c_j\right) \phi_{i,x}\phi_{j,y}\Psi_{r,x}$$

$$\frac{\partial}{\partial b_r}\ \left\{\left(\frac{\partial^2 \bar{w}}{\partial \bar{x}^2} + \frac{\partial^2 \bar{w}}{\partial \bar{y}^2}\right)^2 - 2(1-\nu)\ \left[\frac{\partial^2 \bar{w}}{\partial \bar{x}^2}\ \frac{\partial^2 \bar{w}}{\partial \bar{y}^2} - \left(\frac{\partial^2 \bar{w}}{\partial \bar{x}\partial \bar{y}}\right)^2\right]\right\} = 0 \tag{B-12}$$

$$\frac{\partial}{\partial c_r}\left(\bar{\epsilon}^{o}_{x}\right)^2 = 2\ \bar{\epsilon}^{o}_{x} \cdot \frac{\partial \bar{\epsilon}^{o}_{x}}{\epsilon c_r} \tag{B-13}$$

$$= \left(\frac{2\eta h^2}{b^3}\right)\left(d_i + c_i\right)\ a_i \chi_{j,x}\phi_{i,x}\phi_{r,x}$$

$$+ \left(\frac{h^4}{b^4}\right)\left(2\ c_i d_j + c_i c_j\right)\left(d_p + c_p\right)\ \phi_{p,x}\phi_{j,x}\phi_{i,x}\phi_{r,x}$$

$$\frac{\partial}{\partial c_r}\left(\bar{\varepsilon}^o_y\right)^2 = 2\ \bar{\varepsilon}^o_y \cdot \frac{\partial \bar{\varepsilon}^o_y}{\partial c_r} \tag{B-14}$$

$$= 2\ \bar{\varepsilon}^o_y \left(\frac{h^2}{2a^2}\right)\left(2\delta_{ir}\ d_j + c_i\delta_{jr} + c_j\delta_{ir}\right)\phi_{i,y}\phi_{j,y}$$

$$= \frac{2\eta h^2}{a^3}\left(d_i + c_i\right) b_j \psi_{j,y}\phi_{i,y}\phi_{r,y} - \frac{2\eta\mu h^2}{a^3} \cdot \left(d_i + c_i\right)\phi_{i,y}\phi_{r,y}$$

$$+ \left(\frac{h^4}{a^4}\right)\left(2c_i d_j + c_i c_j\right)\left(d_p + c_p\right)\phi_{p,y}\phi_{r,y}\phi_{i,y}\phi_{j,y}$$

$$\frac{\partial}{\partial c_r}\left(\bar{\varepsilon}^o_x\ \bar{\varepsilon}^o_y\right) = \bar{\varepsilon}^o_x \frac{\partial \bar{\varepsilon}^o_y}{\partial c_r} + \bar{\varepsilon}^o_y \cdot \frac{\partial \bar{\varepsilon}^o_x}{\partial c_r} \tag{B-15}$$

$$= \frac{\eta h^2}{a^2 b}\left(d_i + c_i\right) a_i \chi_{j,x}\phi_{i,y}\phi_{r,y}$$

$$+ \frac{1}{2}\frac{h^4}{a^2 b^2}\left(2c_i d_j + c_i c_j\right)\left(d_p + c_p\right)\phi_{p,y}\phi_{r,y}\phi_{i,x}\phi_{j,x}$$

$$+ \frac{2h^2}{ab^2}\left(d_i + c_i\right) b_i \psi_{j,y}\phi_{i,x}\phi_{r,x}$$

$$- \frac{2\mu h^2}{ab^2}\left(d_i + c_i\right)\phi_{i,x}\ \phi_{r,x}$$

$$+ \frac{h^4}{2a^2 b^2}\left(2c_i d_j + c_i c_j\right)\left(d_p + c_p\right)\phi_{p,x}\phi_{r,x}\phi_{i,y}\phi_{j,y}$$

$$\frac{\partial}{\partial c_r}\bar{\gamma}^{o^2}_{xy} = 2\bar{\gamma}^{o}_{xy}\cdot\frac{\partial\bar{\gamma}_{xy}}{\partial c_r} \tag{B-16}$$

$$= \frac{2\eta h^2}{a^2 b}\left\{\left(2d_i + c_i\right)a_j\chi_{j,y}\phi_{i,x}\phi_{r,y} + c_i a_j\chi_{j,y}\phi_{i,y}\phi_{r,x}\right\}$$

$$+ \frac{2\eta h^2}{ab^2}\left\{\left(2d_i + c_i\right) b_j\Psi_{j,x}\phi_{i,x}\phi_{r,y} + c_i b_j\Psi_{j,x}\phi_{i,y}\phi_{r,x}\right\}$$

$$+ \frac{2h^4}{a^2b^2}\left\{\left(2d_i c_j + c_i c_j\right)\left(2d_p + c_p\right)\phi_{p,x}\phi_{r,y}\phi_{r,y}\phi_{i,x}\phi_{j,y}\right.$$

$$\left. + \left(2d_i\, c_j + c_i c_j\right)c_p\phi_{p,y}\phi_{r,x}\phi_{i,x}\phi_{j,y}\right\}$$

$$\frac{\partial}{\partial c_r}\left\{\left(\frac{\partial^2\bar{w}}{\partial\bar{x}^2} + \frac{\partial^2\bar{w}}{\partial\bar{y}^2}\right) - D_4\left[\frac{\partial^2\bar{w}}{\partial\bar{x}^2}\;\frac{\partial^2\bar{w}}{\partial\bar{y}^2} - \left(\frac{\partial^2\bar{w}}{\partial\bar{x}\partial\bar{y}}\right)^2\right]\right\} \tag{B-17}$$

$$= \left(\frac{2h^2}{b^4}\right) c_i\,\phi_{i,xx}\phi_{r,xx} + \left(\frac{2h^2}{a^4}\right) c_i\phi_{i,yy}\phi_{r,yy}$$

$$+ \frac{h^2}{a^2b^2}\left(2 - D_4\right) c_i\left(\phi_{i,xx}\,\phi_{r,yy} - \phi_{i,yy}\,\phi_{r,xx}\right)$$

$$+ D_4\left(\frac{2h^2}{a^2b^2}\right) c_i\phi_{i,xy}\phi_{r,xy}$$

APPENDIX C

APPLICATION OF THE RITZ PROCEDURE

Evaluating the partials of Appendix B for i, j, p, r = 1, 2 and setting them equal to zero, i.e.,

$$\frac{\partial\Pi}{\partial a_1} = \frac{\partial\Pi}{\partial a_2} = \frac{\partial\Pi}{\partial b_1} = \frac{\partial\Pi}{\partial b_2} = \frac{\partial\Pi}{\partial c_1} = \frac{\partial\Pi}{\partial c_2} = 0 \quad ,$$

results in expressions of the form below.

$$\frac{\partial\Pi}{\partial a_1} = \int_{-1}^{1}\int_{-1}^{1} \left\{\left(\frac{2\eta^2}{b^2}\right) a_1 \chi_{1,x} \chi_{1,x}\right.$$

$$+ \left(\frac{\eta h^2}{b^3}\right)\left(2c_1 d_1 + c_1 c_1\right) \phi_{1,x} \phi_{1,x} \chi_{1,x}$$

$$\left. + \left(\frac{2\eta^2}{b^2}\right) a_2 \chi_{2,x} \chi_{1,x} \cdots \right\} dxdy = 0$$

where the functions χ_i, Ψ_i, ϕ_i are defined in Chapter II.

After integrating, and evaluating the resulting quantities, six nonlinear equations in the unknowns a_1, a_2, b_1, ..., c_2 are obtained.

These unknowns are then replaced by $x_1, x_2, \ldots, x_6$ respectively (for each of identification in the computer) to yield the following system of equations.

$$\frac{\partial \Pi}{\partial x_1} = 0: \quad c_{11}x_1 + c_{13}x_3 + c_{14}x_4 + c_{15}x_5 + c_{16}x_6 \tag{C-1}$$

$$+ c_{155}x_5^2 + c_{166}x_6^2 = 0$$

$$\frac{\partial \Pi}{\partial x_2} = 0: \quad c_{22}x_2 + c_{25}x_5 + c_{26}x_6 + c_{256}x_5x_6 = 0 \tag{C-2}$$

$$\frac{\partial \Pi}{\partial x_3} = 0: \quad c_{31}x_1 + c_{33}x_3 + c_{35}x_5 + c_{355}x_5^2 = 0 \tag{C-3}$$

$$\frac{\partial \Pi}{\partial x_4} = 0: \quad c_{41}x_1 + c_{44}x_4 + c_{46}x_6 + c_{466}x_6^2 = 0 \tag{C-4}$$

$$\frac{\partial \Pi}{\partial x_5} = 0: \quad c_{51}x_1 + c_{52}x_2 + c_{53}x_3 + \mu c_{55M}x_5 + c_{55}x_5 + c_{56}x_6 \tag{C-5}$$

$$+ c_{515}x_1x_5 + c_{526}x_2x_6 + c_{535}x_3x_5 + c_{556}x_5x_6 + c_{555}x_5^2$$

$$+ c_{566}x_6^2 + c_{5566}x_5x_6^2 + c_{5555}x_5^3 + \mu c_{50} = 0$$

$$\frac{\partial \Pi}{\partial x_6} = 0: \quad c_{61}x_1 + c_{62}x_2 + c_{64}x_4 + c_{65}x_5 + \mu c_{55M}x_6 + c_{66}x_6 \tag{C-6}$$

$$+ c_{616}x_1x_6 + c_{625}x_2x_5 + c_{646}x_4x_6 + c_{656}x_5x_6$$

$$+ c_{6556}x_5^2x_6 + c_{655}x_5^2 + c_{666}x_6^2 + c_{6666}x_6^3 + \mu c_{60} = 0$$

where the c_{ij}, c_{ijk} and $c_{ijk\ell}$ are the known quantities, which depend upon the physical properties of the plate.

APPENDIX D

DERIVATION OF THE PERTURBATION TECHNIQUE

The unknowns x_i, the coefficients of the displacement functions, are expressed in powers of the perturbation parameter ϵ, i.e.,

$$x_i = \sum_{k=o}^{5} x_{ik}\, \epsilon^k \qquad i = 1, 2, \ldots , 6 \tag{D-1}$$

where $\epsilon = \mu - \mu_o$. This form of x_i is then substituted into the six nonlinear Equations (C-1)to(C-6)of Appendix C, and rearranged to yield equations of the form,

$$\sum_{k=o}^{5} \alpha_{jk}\, \epsilon^k = 0, \qquad j = 1,2, \ldots , 6 .$$

Setting $\alpha_{ik} = 0$ will then give six linear equations, one for each of the relations $\frac{\partial \Pi}{\partial x_i} = 0$. As an example, the coefficient of ϵ^3 in equation $\frac{\partial \Pi}{\partial x_2}$ is $(j = 2,\ k = 3)$.

$$\alpha_{23} = c_{22}x_{23} + c_{25}x_{53} + c_{26}x_{63} \tag{D-2}$$

$$+ c_{256}\left(x_{53}x_{60} + x_{52}x_{61} + x_{51}x_{62} + x_{50}x_{63}\right) = 0$$

Assembling all such equations in a matrix of the form $\bar{A}\,\bar{X}_{ik} = \bar{B}_{ik}$, results in elements of the matrix $\bar{A}$, listed below

$$A_{11} = c_{11}$$

$$A_{12} = 0$$

$$A_{13} = c_{13}$$

$$A_{14} = c_{14}$$

$$A_{15} = (c_{15} + 2c_{155}x_{50})$$

$$A_{16} = (c_{16} + 2c_{166}x_{60})$$

$$A_{21} = 0$$

$$A_{22} = c_{22}$$

$$A_{23} = 0$$

$$A_{24} = 0$$

$$A_{25} = (c_{25} + c_{256}x_{60})$$

$$A_{26} = (c_{26} + c_{256}x_{50})$$

$$A_{31} = c_{31}$$

$$A_{32} = 0$$

$$A_{33} = c_{33}$$

$$A_{34} = 0$$

$$A_{35} = (c_{35} + 2c_{355}x_{50})$$

$$A_{36} = 0$$

$$A_{41} = c_{41}$$

$$A_{42} = 0$$

$$A_{43} = 0$$

$$A_{44} = c_{44}$$

$$A_{45} = 0$$

$$A_{46} = (c_{46} + 2c_{466}x_{60})$$

$$A_{51} = (c_{51} + c_{515}x_{50})$$

$$A_{52} = (c_{52} + c_{526}x_{60})$$

$$A_{53} = (c_{53} + c_{535}x_{50})$$

$$A_{54} = 0$$

$$A_{55} = (c_{55} + \mu_o c_{55M} + c_{515}x_{10} + c_{535}x_{30} + c_{556}x_{60}$$

$$+ 2c_{555}x_{50} + c_{5566}x_{60}^2 + 3c_{5555}x_{50}^2)$$

$$A_{56} = (c_{56} + c_{526}x_{20} + c_{556}x_{50} + 2c_{566}x_{60} + 2c_{5566}x_{60}x_{50})$$

$$A_{61} = (c_{61} + c_{616}x_{60})$$

$$A_{62} = (c_{62} + c_{625}x_{50})$$

$$A_{63} = 0$$

$$A_{64} = (c_{64} + c_{646}x_{60})$$

$$A_{65} = (c_{65} + c_{625}x_{20} + c_{656}x_{60} + 2c_{6556}x_{50}x_{60} + 2c_{655}x_{50})$$

$$A_{66} = (c_{66} + \mu_o c_{66M} + c_{616}x_{10} + c_{646}x_{40} + c_{656}x_{50} + c_{6556}x_{50}^2 + 2c_{666}x_{60} + 3c_{6666}x_{60}^2)$$

Some of the column matrices $\overline{B}_{ik}$ are as listed below.

$$B_{11} = 0$$

$$B_{21} = 0$$

$$B_{31} = 0$$

$$B_{41} = 0$$

$$B_{51} = - c_{55M}x_{50} - c_{50}$$

$$B_{61} = - c_{66M}x_{60} - c_{60}$$

$$B_{12} = - c_{155}x_{51}^2 - c_{166}x_{61}^2$$

$$B_{22} = - c_{256}x_{51}x_{61}$$

$$B_{32} = - c_{355}x_{51}^2$$

$$B_{42} = - c_{466}x_{61}^2$$

$$B_{52} = - c_{55M}x_{51} - c_{515}x_{11}x_{51} - c_{526}x_{21}x_{61} - c_{535}x_{31}x_{51}$$

$$- c_{566}x_{51}x_{61} - c_{555}x_{51}^2 - c_{566}x_{61}^2 - c_{5566}x_{61}^2x_{50}$$

$$- c_{5566}x_{60}x_{61}x_{51} - 3c_{5555}x_{50}x_{51}^2$$

$$B_{62} = - c_{66M}x_{61} - c_{616}x_{11}x_{61} - c_{625}x_{21}x_{51} - c_{646}x_{41}x_{61}$$

$$- c_{656}x_{51}x_{61} - c_{6556}x_{51}^2x_{60} - 2c_{6556}x_{50}x_{51}x_{61}$$

$$- c_{655}x_{51}^2 - c_{666}x_{61}^2 - 3c_{6666}x_{60}x_{61}^2$$

Similarly for B_{i3}, B_{i4}, B_{i5} $\qquad i = 1, 2, \ldots, 6$

APPENDIX E

A DIRECT ALGEBRAIC METHOD OF SOLUTION

Equations (C-1) to (C-4) in Appendix C can be written as

$$c_{11}x_1 + c_{13}x_3 + c_{14}x_4 = G_1 \tag{E-1}$$

$$c_{22}x_2 = G_2 \tag{E-2}$$

$$c_{31}x_1 + c_{33}x_3 = G_3 \tag{E-3}$$

$$c_{41}x_1 + c_{44}x_4 = G_4 \tag{E-4}$$

where the G_i are functions of x_5 and x_6 defined by

$$G_1 = -(c_{15}x_5 + c_{16}x_6 + c_{155}x_5^2 + c_{166}x_6^2) \tag{E-5}$$

$$G_2 = -(c_{25}x_5 + c_{26}x_6 + c_{256}x_5x_6) \tag{E-6}$$

$$G_3 = -(c_{35}x_5 + c_{355}x_5^2) \tag{E-7}$$

$$G_4 = -(c_{46}x_5 + c_{466}x_6^2) \tag{E-8}$$

Solving Equations (E-1) to (E-4) in terms of G_i yields

$$x_1 = \frac{G_1 c_{33} c_{44} - G_4 c_{33} c_{14} - G_3 c_{13} c_{44}}{k_1} \tag{E-9}$$

where k_1 is the resulting determinant.

Also observing that G_1, G_4 and G_3 are functions of x_5 and x_6 Equation (E-9) could be expressed as

$$x_1 = k_2 x_5 + k_3 x_5^2 + k_4 x_6^2 \tag{E-10}$$

where the k_2, k_3 and k_4 are the resulting quantities which are functions of $c_{ijk\ell}$. Similarly

$$x_2 = k_5 x_6 + k_6 x_5 x_6 \tag{E-11}$$

$$x_3 = k_7 x_5 + k_8 x_5^2 + k_9 x_6^2 \tag{E-12}$$

$$x_4 = k_{10} x_5 + k_{11} x_5^2 + k_{12} k_6^2 \tag{E-13}$$

Substituting these values of $x_1, \ldots, x_4$ into Equation (C-5) and (C-6) of Appendix C results in,

$$\mu c_{50} + \mu c_{55M} x_5 + k_{13} x_5 + k_{14} x_6 + k_{15} x_5 x_6 + k_{16} x_5^2 \tag{E-14}$$

$$+ k_{17} x_6^2 + k_{18} x_5 x_6^2 + k_{19} x_5^3 = 0$$

and

$$k_{21}x_6 + \mu c_{66M}x_6 + k_{22}x_5x_6 + k_{23}x_5^2x_6 + k_{24}x_6^3 = 0 \qquad \text{(E-15)}$$

respectively.

Equations (E-14) and (E-15) are then rearranged to solve for x_6 in terms of x_5 as explained in Chapter III.

APPENDIX F

THE EIGENVALUE ANALYSIS

The governing equation of the plate in Figure F-1 is

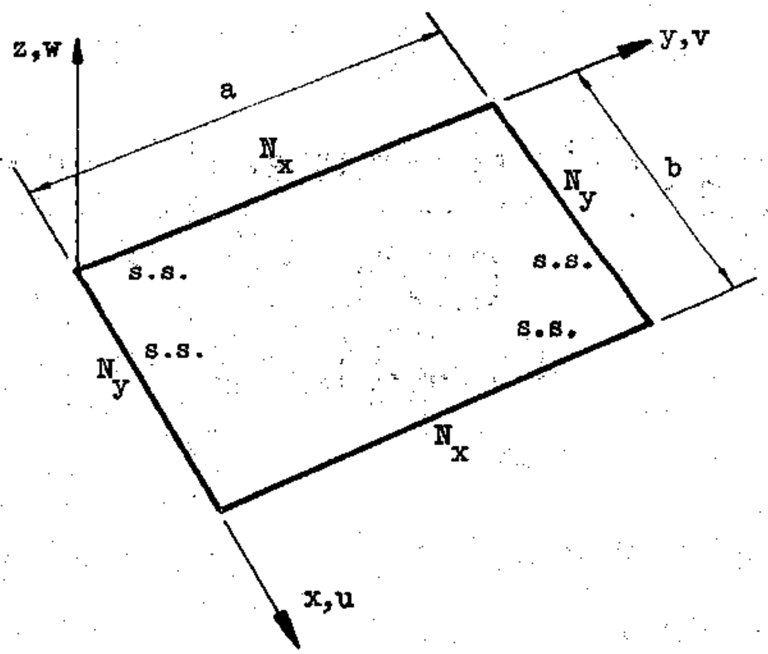

Figure F-1. Plate Under Biaxial Loading

$$\nabla^4 w = \frac{1}{D}\left[N_x \frac{\partial^2 w}{\partial x^2} + N_y \frac{\partial^2 w}{\partial y^2} + 2N_{xy} \frac{\partial^2 w}{\partial x \partial y}\right] \qquad \text{(F-1)}$$

(Note that the plate above has the same boundary condition as the one in Figure II-2), where N_x and N_y are uniformly distributed forces, and $N_{xy} = 0$. For the problem analyzed N_y, N_x could be written as

$$N_y = -N, \quad N_x = -\nu N , \qquad \text{(F-2)}$$

which are the consequences of the prebuckling plane stress solution for the geometric boundary condition problem. Hence Equation (F-1) reduces to

$$D\nabla^4 w + N\left(\nu \frac{\partial^2 w}{\partial x^2} + \frac{\partial^2 w}{\partial y^2}\right) = 0 \qquad \text{(F-3)}$$

The deflection function of the form

$$w_{nm} = c_{mn} \sin \frac{n\pi x}{b} \sin \frac{m\pi y}{a}, \quad n, m = 1,2,3 \ldots \qquad \text{(F-4)}$$

satisfies the simple-supported boundary conditions. Substituting into Equation (F-3) and simplifying, results in

$$\pi^2 D\left(\frac{n^2}{b^2} + \frac{m^2}{a^2}\right)^2 - N\left(\nu \frac{n^2}{b^2} + \frac{m^2}{a^2}\right) = 0 \qquad \text{(F-5)}$$

which is a necessary condition for a nontrivial solution.

Rearranging gives

$$N_{nm} = \frac{\pi^2 D\left(\frac{n^2}{b^2} + \frac{m^2}{a^2}\right)^2}{\left(\nu \frac{n^2}{b^2} + \frac{m^2}{a^2}\right)} \qquad \text{(F-6)}$$

N_{nm} will attain its smallest value when $n = 1$. To prove this, rewrite Equation (F-6) as

$$\frac{N_{nm}}{\pi^2 D} = \frac{\left(\frac{n^2}{b^2} + \frac{m^2}{a^2}\right)^2}{\left(\nu \frac{n^2}{b^2} + \frac{m^2}{a^2}\right)} = \frac{\left(\frac{a}{b} n^2 + \frac{b}{a} m^2\right)^2}{ab\left(\nu \frac{a}{b} n^2 + \frac{b}{a} m^2\right)} \qquad \text{(F-7)}$$

Define the aspect as $r = \frac{a}{b}$, and H_n as

$$H_n = N_{nm}\left(\frac{b^2}{\pi^2 D}\right) = \frac{\left(rn^2 + \frac{m^2}{r}\right)}{r\left(\nu rn^2 + \frac{m^2}{r}\right)} \qquad \text{(F-8)}$$

for $n = 1$

$$H_1 = \frac{\left(r + \frac{m^2}{r}\right)^2}{r\left(\nu r + \frac{m^2}{r}\right)} \qquad \text{(F-9)}$$

for $n = q > 1 \quad q = 2,3,4, \ldots$

$$H_q = \frac{\left(rq^2 + \frac{m^2}{r}\right)^2}{r\left(\nu rq^2 + \frac{m^2}{r}\right)} \qquad \text{(F-10)}$$

$$H_q - H_1 = \nu r^4\left(q^4-q^2\right) + \nu m^4\left(1-q^2\right)+ m^2r^2\left(q^4-1\right) + 2m^4\left(q^2-1\right) \qquad \text{(F-11)}$$

$$= \nu r^4\left(q^4-q^2\right) + m^2r^2\left(q^4-1\right) + m^4\left(q^2-1\right)\left(2-\nu\right) \qquad \text{(F-12)}$$

$H_q - H_1 > 0$ since q is an integer > 1 and $\nu \leq .5$

This implies that the smallest N_{nm} is associated with a deflected shape that has the form of a half-sine wave in a direction perpendicular to the applied loading.

To find the r at which $N_{11} = N_{12}$, use of Equation (F-8) leads to the condition

$$\frac{\left(r + \frac{1}{r}\right)^2}{\left(\nu r + \frac{1}{r}\right)} = \frac{\left(r + \frac{4}{r}\right)^2}{\left(\nu r + \frac{4}{r}\right)} \qquad \text{(F-13)}$$

Solving the above yields $r = 2.3561$ (see Figure IV-1). Equation (F-8) can also be used to find that the r for which $N_{11} = N_{13}$ is $r = 3.129$. Similarly the r for which $N_{12} = N_{13}$ is $r = 3.94$. (See Figure IV-1).

To find the critical strain μ_{cr}, we proceed as follows: The stress-strain relations are

$$\epsilon_x = \frac{1}{E}\left(\sigma_x - \nu\sigma_y\right) \qquad \text{(F-14)}$$

$$\epsilon_y = \frac{1}{E}\left(\sigma_y - \nu\sigma_x\right) \tag{F-15}$$

Before and at buckling $\epsilon_x = 0$. This implies $\sigma_x = \nu\sigma_y$. Substituting in Equation (F-15)

$$\epsilon_y = \mu = \frac{\sigma_y}{E}\left(1 - \nu^2\right) = \frac{N_y}{hE}\left(1 - \nu^2\right) \tag{F-16}$$

From Equation (F-8)

$$N_{cr} = \frac{\pi^2 D}{b^2} \cdot \frac{\left(r + \frac{m^2}{r}\right)^2}{r\left(\nu r + \frac{m^2}{r}\right)} = \frac{\pi^2 D}{b^2}\,k(r)$$

Therefore,

$$\mu_{cr} = \frac{\pi^2 h^2}{12b^2}\;\frac{\left(r + \frac{m^2}{r}\right)^2}{r\left(\nu r + \frac{m^2}{r}\right)} = \frac{\pi^2 h^2}{12b^2}\,k(r) \tag{F-17}$$

For the dimensions of Figure II-2, the strain μ_{cr} will be

$$\mu_{cr} = \frac{\pi^2 h^2}{48b^2}\,k(r) \tag{F-18}$$

APPENDIX G

FURTHER ANALYTICAL ALTERNATIVES

An alternate approach to the procedure used in this thesis would be to express the in-plane displacements u and v in terms of the transverse displacement w. This would, of course, result in a partial differential equation in w.

The governing equations of the plate are

$$\frac{\partial N_x}{\partial x} + \frac{\partial N_{xy}}{\partial y} = 0 \tag{G-1}$$

$$\frac{\partial N_{xy}}{\partial x} + \frac{\partial N_y}{\partial y} = 0 \tag{G-2}$$

$$\nabla^4 w - \frac{1}{D}\left[N_x \frac{\partial^2 w}{\partial x^2} + \frac{\partial^2 w}{\partial y^2} + 2N_{xy} \frac{\partial^2 w}{\partial x \partial y}\right] \tag{G-3}$$

where

$$N_x = \frac{Eh}{1-\nu^2}\left(\epsilon_x + \nu\epsilon_y\right) \tag{G-4}$$

$$N_y = \frac{Eh}{1-\nu^2}\left(\epsilon_y + \nu\epsilon_y\right) \tag{G-5}$$

$$N_{xy} = \frac{Eh}{2(1+\nu)}\,\gamma_{xy} \tag{G-6}$$

Using the values of the strains ϵ_x, ϵ_y and γ_{xy} from Equations (II-1)(II-2) and (II-3), in Equations (G-1) and (G-2) results in

$$k_1\frac{\partial^2 u}{\partial x^2} + k_2\frac{\partial^2 u}{\partial y^2} + k_3\frac{\partial^2 v}{\partial x \partial y} = f(w) \tag{G-7}$$

$$k_2\frac{\partial^2 v}{\partial x^2} + k_1\frac{\partial^2 v}{\partial y^2} + k_3\frac{\partial^2 u}{\partial x \partial y} = g(w) \tag{G-8}$$

respectively, where $f(w)$ and $g(w)$ are functions of w and its derivatives, and

$$k_1 = \frac{Eh}{1-\nu^2}, \quad k_2 = \frac{Eh}{2(1+\nu)}, \quad k_3 = k_1\nu + k_2.$$

Letting

$$P_1 = \frac{\partial u}{\partial x} \qquad Q_1 = \frac{\partial u}{\partial y}, \tag{G-9}$$

$$P_2 = \frac{\partial v}{\partial x} \qquad Q_2 = \frac{\partial v}{\partial y} \tag{G-10}$$

(note that $\frac{\partial P_1}{\partial y} = \frac{\partial Q_1}{\partial x}$ and $\frac{\partial P_2}{\partial y} = \frac{\partial Q_2}{\partial x}$ 0)

Equations (G-7) and (G-8) can be written as

$$k_1 \frac{\partial P_1}{\partial x} + k_2 \frac{\partial Q_1}{\partial y} + k_3 \frac{\partial P_2}{\partial y} = f(w) \tag{G-11}$$

$$k_2 \frac{\partial P_2}{\partial x} + k_1 \frac{\partial Q_2}{\partial y} + k_3 \frac{\partial P_1}{\partial y} = g(w) \tag{G-12}$$

Since $k_1 \neq 0$. $k_2 \neq 0$ we have

$$\frac{\partial P_1}{\partial x} + \frac{k_2}{k_1} \frac{\partial Q_1}{\partial y} + \frac{k_3}{k_1} \frac{\partial P_2}{\partial y} = \frac{f(w)}{k_1} \tag{G-13}$$

$$\frac{\partial P_2}{\partial x} + \frac{k_1}{k_2} \frac{\partial Q_2}{\partial y} + \frac{k_3}{k_2} \frac{\partial P_1}{\partial y} = \frac{g(w)}{k_2} \tag{G-14}$$

$$\frac{\partial Q_1}{\partial x} + 0 - \frac{\partial P_1}{\partial y} = 0 \tag{G-15}$$

$$\frac{\partial Q_2}{\partial x} + 0 - \frac{\partial P_2}{\partial y} = 0 \tag{G-16}$$

Rewriting Equations (G-13) to (G-16) in matrix form results is

$$\frac{\partial}{\partial x}\begin{bmatrix} P_1 \\ P_2 \\ Q_1 \\ Q_2 \end{bmatrix} + \frac{\partial}{\partial y}\begin{bmatrix} 0 & \frac{k_3}{k_1} & \frac{k_2}{k_1} & 0 \\ \frac{k_3}{k_2} & 0 & 0 & \frac{k_1}{k_2} \\ -1 & 0 & 0 & 0 \\ 0 & -1 & 0 & 0 \end{bmatrix}\begin{bmatrix} P_1 \\ P_2 \\ Q_1 \\ Q_2 \end{bmatrix} = \begin{bmatrix} \frac{f(w)}{k_1} \\ \frac{g(w)}{k_2} \\ 0 \\ 0 \end{bmatrix} \qquad \text{(G-17)}$$

The system of Equations (G-17) will be uncoupled if the square matrix can be diagonalized.

Let

$$M = \begin{bmatrix} 0 & \frac{k_3}{k_1} & \frac{k_2}{k_1} & 0 \\ \frac{k_3}{k_1} & 0 & 0 & \frac{k_1}{k_2} \\ -1 & 0 & 0 & 0 \\ 0 & -1 & 0 & 0 \end{bmatrix}$$

The eigenvalues t_i of matrix M can be obtained by setting $|M - tI| = 0$, which results in

$$t^4 + \left(\frac{k_2}{k_1} - \frac{k_3^2}{k_1^2} - \frac{k_1}{k_2}\right) t^2 + 1 = 0 \tag{G-18}$$

whose roots are

$$t_1 = \sqrt{\frac{-k_4 + \sqrt{k_4^2 - 4}}{2}}$$

$$t_2 = \sqrt{\frac{-k_4 - \sqrt{k_4^2 - 4}}{2}}$$

$$t_3 = -\sqrt{\frac{-k_4 + \sqrt{k_4^2 - 4}}{2}} \tag{G-19}$$

$$t_4 = -\sqrt{\frac{-k_4 - \sqrt{k_4^2 - 4}}{2}}$$

where

$$k_4 = \left(\frac{k_2}{k_1} - \frac{k_3^2}{k_1^2} - \frac{k_1}{k_2}\right)$$

The corresponding eigenvectors W_{ik} are determined by solving

$$\left(M - t_i I\right) W_{ik} = 0$$

As an example, the vector W_{1k} can be found by solving the following system of equations

$$- t_1\omega_{11} + \frac{k_3}{k_1}\omega_{12} + \frac{k_2}{k_1}\omega_{13} + 0 = 0$$

$$\frac{k_3}{k_1}\omega_{11} - t_1\omega_{12} + 0 + \frac{k_1}{k_2}\omega_{14} = 0$$

$$- \omega_{11} + 0 - t_1\omega_{13} + 0 = 0 \tag{G-20}$$

$$0 - \omega_{12} + 0 + t_1\omega_{14} = 0$$

which results in

$$W_{1k} = \begin{bmatrix} \omega_{11} \\ \omega_{12} \\ \omega_{13} \\ \omega_{14} \end{bmatrix} = \begin{bmatrix} - t_1\omega_{13} \\ - \frac{k_1}{k_3}\left[t_1^2 + \frac{k_2}{k_1}\right]\omega_{13} \\ \omega_{13} \\ \frac{k_2}{k_1}\left(t_1\omega_{12} - \frac{k_3}{k_1}\omega\right) \end{bmatrix}$$

Similarly W_{2k}, W_{3k} and W_{4k} can be solved to yield the matrix R defined by

$$R = \begin{bmatrix} \uparrow & \uparrow & \uparrow & \uparrow \\ W_{1k} & W_{2k} & W_{3k} & W_{4k} \\ \downarrow & \downarrow & \downarrow & \downarrow \end{bmatrix} \tag{G-21}$$

If the four eigenvectors W_{ik} are linearly independent then Det. $R \neq 0$. consequently, the matrix M can be diagonalized by the operation $R^{-1}M\,R$ resulting in a matrix D [18] . This is a matrix whose diagonal elements are the eigenvalues of M, i.e.,

$$R^{-1}\,M\,R = D = \begin{bmatrix} t_1 & 0 & 0 & 0 \\ 0 & t_2 & 0 & 0 \\ 0 & 0 & t_3 & 0 \\ 0 & 0 & 0 & t_4 \end{bmatrix} \tag{G-22}$$

Premultiplying Equation (G-17) by R^{-1} results in

$$\frac{\partial}{\partial x} R^{-1} \begin{bmatrix} P_1 \\ P_2 \\ Q_1 \\ Q_2 \end{bmatrix} + \frac{\partial}{\partial y} R^{-1} M \begin{bmatrix} P_1 \\ P_2 \\ Q_1 \\ Q_2 \end{bmatrix} = R^{-1} \begin{bmatrix} \frac{f(w)}{k_1} \\ \frac{g(w)}{k_2} \\ 0 \\ 0 \end{bmatrix} \qquad \text{(G-23)}$$

Postmultiplying M above by $R R^{-1}$ will make $R^{-1} MRR^{-1} = DR^{-1}$

Let

$$R^{-1} \begin{bmatrix} P_1 \\ P_2 \\ Q_1 \\ Q_2 \end{bmatrix} = \begin{bmatrix} P_1' \\ P_2' \\ Q_1' \\ Q_2' \end{bmatrix} \qquad \text{(G-24)}$$

then Equation (G-23) becomes

$$\frac{\partial}{\partial x}\begin{bmatrix} P_1' \\ P_2' \\ Q_1' \\ Q_2' \end{bmatrix} + \frac{\partial}{\partial y} D \begin{bmatrix} P_1' \\ P_2' \\ Q_1' \\ Q_2' \end{bmatrix} = R^{-1} \begin{bmatrix} \frac{f(w)}{k_1} \\ \frac{g(w)}{k_1} \\ 0 \\ 0 \end{bmatrix} \qquad \text{(G-25)}$$

Equation (G-25) can be solved for P_1', P_2', Q_1' and Q_2' by the method of characteristics [19], where the independent variables x and y are first transformed through the relation

$$r = ax + y$$

$$s = ax - y$$

where a is a function of k_i . Using the Equation (G-24) the unknowns P_1, P_2, Q_1 and Q_2 are then obtained in terms of $f(w(r,s))$ and $g(w(r,s))$. The resulting expressions are integrated and evaluated so as to satisfy the boundary conditions. This leads to expressions in u and v as functions of w and its derivatives.

The displacements u and v may also be eliminated from Equations (G-1) and (G-2) through an operational procedure. This consists of defining $\frac{\partial}{\partial x} = D_x$ and $\frac{\partial}{\partial y} = D_y$ and rewriting Equation (G-7) and (G-8) as

$$\left(k_1 D_x^2 + k_2 D_y^2\right)u + k_3 D_x D_y v = f(w) \tag{G-26}$$

$$k_3 D_x D_y u + \left(k_2 D_x^2 + k_1 D_y^2\right)v = g(w) \tag{G-27}$$

respectively. The unknown function u can be eliminated by operating on Equation (G-26) with the operator $k_3 D_x D_y$, and operating on Equation (G-27) with the operator $\left(k_1 D_x^2 + k_2 D_y^2\right)$, and subtracting, we obtain

$$\left[k_3^2 D_x^2 D_y^2 - \left(k_1 D_x^2 + k_2 D_y^2\right)\left(k_2 D_x^2 + k_1 D_y^2\right)\right]v \tag{G-28}$$

$$= k_3 D_x D_y f(w) - \left(k_1 D_x^2 + k_2 D_y^2\right) g(w)$$

which can be reduced to

$$k_1 k_2 \frac{\partial^4 v}{\partial x^4} + \left(k_1^2 + k_2^2\right) \frac{\partial^4 v}{\partial x^2 \partial y^2} + k_1 k_2 \frac{\partial^4 v}{\partial y^4} - k_3^2 \frac{\partial^4 v}{\partial x^2 \partial y^2} \tag{G-29}$$

$$= + k_2 \frac{\partial^2 g(w)}{\partial y^2} + k_1 \frac{\partial^2 g(w)}{\partial x^2} - k_3 \frac{\partial^2 f(w)}{\partial x \partial y}$$

Likewise v could be eliminated to obtain

$$k_1k_2 \frac{\partial^4 u}{\partial x^4} + \left(k_1^2 + k_2^2\right) \frac{\partial^4 u}{\partial x^2 \partial y^2} + k_1k_2 \frac{\partial^4 u}{\partial y^4} - k_3^2 \frac{\partial^4 u}{\partial x^2 \partial y^2} \tag{G-30}$$

$$= k_2 \frac{\partial^2 f(w)}{\partial x^2} + k_1 \frac{\partial^2 f(w)}{\partial y^2} - k_3 \frac{\partial^2 g(w)}{\partial x \partial y}$$

A close scrutiny of Equations (G-29) and (G-30) reveals that they are of the biharmonic form, i.e., they can be expressed as

$$k_1k_2\nabla^4 v = \alpha(w) \tag{G-31}$$

$$k_1k_2\nabla^4 u = \beta(w) \tag{G-32}$$

where $\alpha(w)$ and $\beta(w)$ are functions of the derivatives of w. The Equations (G-31) and (G-32) cannot however be used to eliminate the u and the v quantities from Equation (G-3), because, the latter is not biharmonic in u and v. An attempt to eliminate u and v from Equation (G-3) by expressing u and v in series form such as Equations (II-12) and (II-13) will be unsuccessful because Equation (G-3) is nonlinear in $\frac{\partial w}{\partial x}$ and $\frac{\partial w}{\partial y}$.

It may be noted that a perturbation method may be applied directly to the partial differential Equations (G-1), (G-2) and (G-3). This would lead to a system of linear ordinary differential equations which could, at least in theory, be solved successively. That is, the solution from the first set of linear equations could be used to solve the second set, etc. In practice this approach cannot be used as the basis for the development of a sound solution procedure because the solutions to the individual sets of equations are difficult to obtain. If approximation techniques are used to develop solutions, the advantage of the linearization process will be largely lost.

REFERENCES

1. Koiter, W. T., "The Effective Width of Infinitely Long Flat Rectangular Plates Under Various Conditions of End Restraint," National Aeronautical Research Institute, Amsterdam, NLL Report S 287, December, (1943).

2. Koiter, W. T., Dissertation, Delft, Holland (1945).

3. Koiter, W. T., "Introduction to the Postbuckling Behavior of Flat Plates," Colloquium on the Postbuckling Behavior of Plates Used in Metal Structures, University of Liege, Belgium, (1963).

4. Stein, Manuel, "The Phenomenon of Change in Buckle Pattern in Elastic Structures," NASA TR R-39, (1959).

5. Stein, Manuel, "Loads and Deformations of Buckled Rectangular Plates," NASA TR-40 (1959).

6. Hlavacek, I., Acta Tech. CSAV Praha, No. 2 (1962).

7. Augusti, G., Publication No. 172 (Univ. Napoli. Fac. Ing., Instituto Sci. Construz.) (1964).

8. Chilver, A. H., "Coupled Modes of Elastic Buckling," J. Mech. Phys. Solids Vol. 15, pp. 15-28, (1967).

9. Supple, W. J., "Coupled Branching Configurations in the Elastic Buckling of Symmetric Structural Systems," Int. J. Mech. Sci., Vol. 9, pp 97-112, (1967).

10. Supple, W. J. and Chilver, A. H., "Elastic Postbuckling of Compressed Rectangular Flat Plates," Ed. by Chilver, Chatto and Windus (1967).

11. Supple, W. J., "On the Change in Buckle Pattern in Elastic Structures," Int. J. Mech. Sci., Vol. 10, pp 737-745. (1968).

12. Supple, W. J., "Changes of Wave-Form of Plates in the Postbuckling Range," Int. J. Solid Structures, Vol. 6, pp 1243-1258. (1970).

13. Vol'mir, A. S., "Flexible Plates and Shells," Technical Report AFFDL-TR-66-216, p. 14, Wright-Patterson Air Force Base, Ohio, (1967).

14. Timoshenko, S. P. and Gere, J. M., "Theory of Elastic Stability," Second Edition, pp 337-339. McGraw-Hill Book Company, New York (1961).

15. Carnahan, B., Luther, H. A. and Wilkes, J. O., "Applied Numerical Methods," pp 308-309, J. Wiley and Sons, Inc. 1969.

16. Hu, P. C., Lundquist, E. E. Batdorf, S. B., "Effect of Small Deviations from Flatness on Effective Width and Buckling of Plates in Compression," NACA Tech. Note 1124, 1946.

17. Nakagiri, Shigeru, "A Note on the Coupled Buckling Mode of an Elastic Plate with Initial Deflection," Theoretical and Applied Mechanics , Vol. 21, p. 391, Proceedings of the 21st Japan National Congress for Applied Mechanics, 1971, University of Tokio Press.

18. Hilderbrand, Francis B., "Methods of Applied Mathematics," Second Edition. pp 36-39, Prentice-Hall, Inc.

19. Garabedian, P. R., "Partial Differential Equations," John Wiley and Sons, New York (1964).

VITA

Edward Michael Dombourian was born in Cyprus in March, 1938. His elementary and secondary education were obtained in the Armenian Evangelical High School in Beirut, Lebanon. In 1962 he received his B.S. in Civil Engineering from the American University of Beirut and shortly thereafter came to the United States.

Mr. Dombourian obtained an M. S. in Civil Engineering from the Georgia Institute of Technology in 1963 and, after six years employment in consulting work in Atlanta and Los Angeles, his M.S. in Engineering Science and Mechanics, also at Georgia Tech. Subsequent to this, he enrolled in the School of Aerospace Engineering at the same institution and during his studies towards the doctorate taught in the School of Mathematics.

Mr. Dombourian is married to the former Loretta Joan Risinger and has one daughter, Sona Lea.